Durham E-Theses

Models of hierarchical: galaxy formation

Helly, John Christopher

How to cite:

Helly, John Christopher (2003) *Models of hierarchical: galaxy formation*, Durham theses, Durham University. Available at Durham E-Theses Online: http://etheses.dur.ac.uk/4055/

Use policy

Models of Hierarchical

Galaxy Formation

by John Christopher Helly

PhD Thesis, October 2003

Abstract

A semi-analytic galaxy formation model, N-body GALFORM, is developed which uses outputs from an N-body simulation to follow the merger histories of dark matter halos and treats baryonic processes using the semi-analytic model of Cole et al. We find that, apart from limited mass resolution, the only significant differences between this model and the Monte-Carlo based model of Cole et al. are due to known inaccuracies in the distribution of halo progenitor masses in the Monte-Carlo method.

N-body GALFORM is used to compare Smooth Particle Hydrodynamics (SPH) and semi-analytic calculations of radiative cooling in the absence of star formation. We consider two cases: firstly, a simulation of a representative volume of the Universe with relatively poor mass resolution, and, secondly, a high resolution simulation of the formation of a single galaxy. We find good agreement between the models in terms of the mass of gas which cools in each halo, the masses of individual galaxies, and the spatial distribution of the galaxies. The semi-analytic model is then compared with a realistic, high resolution galaxy simulation which includes prescriptions for star formation and feedback. A semi-analytic model *without feedback* is found to best reproduce the masses of the simulated galaxy and its progenitors. This model is used to populate a large volume with semi-analytic galaxies. The resulting luminosity function has an order of magnitude too many galaxies at high and low luminosities.

We conclude that, while SPH and semi-analytic cooling calculations are largely consistent and therefore likely to be reasonably reliable, current numerical models of galaxy formation still contain major uncertainties due to the treatment of feedback, which will lead them to predict very different galaxy populations. Further work is required to find simulation algorithms which can simultaneously produce realistic individual galaxies and a population with reasonable statistical properties.

Models of Hierarchical Galaxy Formation

by John Christopher Helly

A thesis submitted to the University of Durham

in accordance with the regulations for

admittance to the Degree of Doctor of Philosophy.

Department of Physics

University of Durham

October 2003

- 2 JUN 2004

Contents

List of Figures

List of Tables

Declaration

The work described in this thesis was undertaken between 2000 and 2003 while the author was a research student under the supervision of Prof. Carlos Frenk and Dr. Shaun Cole in the Department of Physics at the University of Durham. This work has not been submitted for any other degree at the University of Durham or any other University.

Portions of this work have appeared in the following papers:

- Helly, John C.; Cole, Shaun; Frenk, Carlos S.; Baugh, Carlton M.; Benson, Andrew; Lacey, Cedric, 2003, MNRAS, 338, 903 (Chapter 2)

- Helly, John C.; Cole, Shaun; Frenk, Carlos S.; Baugh, Carlton M.; Benson, Andrew; Lacey, Cedric; Pearce, Frazer R., 2003, MNRAS, 338, 913 (Chapter 3)

The description of the GALFORM semi-analytic model found in Section 1.3 is based on the description which appears in the following paper:

- Cole, Shaun; Lacey, Cedric G.; Baugh, Carlton M.; Frenk, Carlos S., 2000, MNRAS, 319, 168

Acknowledgements

Chapter 1

Introduction

1.1 Background

According to current theories of cosmology, the early universe was extremely hot and dense, and almost entirely homogeneous. However, since the universe as we know it today is far from uniform on small scales, tiny density fluctuations must have been present. As the universe expanded, in accordance with the laws of General Relativity, these fluctuations grew through gravitational instability and eventually collapsed to form galaxies and clusters of galaxies.

This theory, known as the Hot Big Bang, provides the background for modern theories of galaxy formation. In these theories, the mass density of the universe is dominated by invisible, non-baryonic "dark matter", which collapses to create potential wells in which gas may collect and condense to form stars and galaxies.

In this introductory Chapter, we[1] present a short summary of the observational justification for this model. In particular, the evidence supporting the Big Bang and the existence of non-baryonic dark matter is considered. We briefly describe possible origins of the primordial density fluctuations, and the mechanisms which are thought to lead to the formation of structure in the Universe. The development of increasingly sophisticated techniques for modelling the subsequent formation of galaxies is reviewed, and details of the GALFORM semi-analytic model of Cole et al. (2000), which is used extensively in this thesis, are presented.

1.1.1 The Big Bang

Expansion of the Universe

In 1929, Hubble announced his discovery of a linear relationship between the distances to galaxies and the recessional velocities obtained from their redshifts. This relationship is exactly what would be expected in a uniformly expanding universe. Hubble mea-

---

[1]Throughout this thesis I will use the conventional 'we' to refer to the first person.

sured the constant of proportionality between velocity and distance, H_0, to be around $500 \mathrm{kms}^{-1}\mathrm{Mpc}^{-1}$ (Hubble 1929).

Modern measurements of the expansion rate of the universe are made in a number of ways. The relative distances of galaxies may be determined using "standard candles", such as Type Ia supernovae (e.g. Tonry et al. 2003), or by making use of empirical relations between galaxy luminosities and distance independent properties, such as the Tully-Fisher relation which relates luminosity to circular velocity (e.g. Tully & Fisher 1977). Distances to a few nearby galaxies are then required to calibrate the distance scale. These are typically obtained by using Cepheid variable stars as standard candles. See, for example, the recent results from the HST key project (Freedman et al. 2001).

Alternatively, fundamental physics may be used to calculate distances directly, thus avoiding uncertainties in the calibration of the distance scale. For example, distances to Type II supernovae may be obtained by comparing the expansion rate of the supernova envelope determined from its redshift with the increase in size inferred from its temperature and luminosity (e.g. Schmidt et al. 1992). The Sunyaev-Zel'dovich (S-Z) effect, the Compton scattering of microwave background photons by hot electrons in galaxy clusters, provides another direct measure of distance , since the S-Z effect and X-ray emission from the cluster scale differently with the its size and gas density (Birkinshaw 1979). H_0 may also be estimated by measuring the time delay between multiple images of gravitationally lensed objects, because the time delay depends on the angular diameter distance which scales as H_0^{-1}. For a recent example, see Ofek & Maoz (2003).

Recently, observations of the cosmic microwave background made using the Wilkinson Microwave Anisotropy Probe (WMAP, see Bennett et al. 2003) have placed strong constraints on a range of cosmological parameters. Encouragingly, the value of H_0 in the model which best fits the WMAP results is in very good agreement with results from the HST Key Project, which obtained a value for the Hubble constant, expressed in units of $100 \mathrm{kms}^{-1}\mathrm{Mpc}^{-1}$, of $h = 0.72 \pm 0.08$.

The Cosmic Microwave Background

The cosmic microwave background radiation (CMB) was discovered by Penzias and Wilson in 1965. Much of this background radiation lies roughly in the wavelength range from fractions of millimeters to tens of centimeters and it is almost entirely isotropic, suggesting that it may uniformly fill the universe. Observations made with the Cosmic Microwave Background Explorer (COBE) satellite, launched in 1989, have shown that the

CMB spectrum is that of a black body with a temperature of 2.7 K (Mather et al. 1994). COBE mapped the entire sky with a spatial resolution of 7-10 degrees and found only very small fluctuations in temperature, of the order of one part in 10^5 (Bennett et al. 1996).

It is difficult to see how such a radiation field could arise in the Universe as it is today. Instead, the CMB is thought to have originated just after the Big Bang when the temperature of the Universe dropped enough to allow the recombination of protons and electrons. From this point onwards, photons were no longer able to interact with the baryons and propagated freely through space. The expansion of the Universe has since reduced the temperature of the radiation spectrum, but its black body shape has been preserved. Hence the detection of the CMB is a strong indication that the Universe was once much hotter and denser than it is now, in agreement with the Big Bang theory.

Big Bang Nucleosynthesis

In the 1950's and 60's it was thought that elements heavier than Hydrogen may all have been produced as a by-product of stellar evolution (e.g. Burbidge et al. 1957). However, the observed masses and luminosities of galaxies indicate that if this were the only mechanism, Helium would make up 1-4% of the baryonic mass of the Universe, rather than about 25% as is observed. Hence, some other means of Helium production is required. The Big Bang provides ideal conditions for this to happen in the early Universe.

At the time when Big Bang nucleosynthesis is thought to occur, the Universe contains large numbers of photons but far fewer baryons. The exact ratio of photons to baryons is not known precisely, and in fact this is the only free parameter in the theory of nucleosynthesis. Weak reactions keep the neutron to proton ratio at its equilibrium value until neutrinos decouple. Subsequently, the neutron abundance falls as the neutrons decay. Deuterium production has begun, but the high photon density and the low binding energy of deuterium means that heavier nuclei are only produced when the temperature falls further. There follows a short period during which heavier elements are created, which ends when the temperature falls to the point where Coulomb repulsion prevents nuclear reactions. The limited time available and the absence of stable nuclei with atomic masses of five or eight mean that only lighter species (deuterium, helium, lithium and beryllium) are created. Heavier elements can only be produced later, in the interiors of stars (e.g. Wagoner et al. 1967).

Standard Big Bang Nucleosynthesis predicts the abundances of these elements as a function of the photon to baryon ratio, which is closely related to the baryon density.

Observational constraints on light element abundances (for example, by measuring the deuterium abundance from absorption in high redshift clouds) mean that this can be used to constrain the baryon density parameter, Ω_b, to the range $\Omega_b h^2 = 0.005 - 0.022$ (Kurki-Suonio 2002). However, there are are uncertainties in these measurements due to the effects of stellar populations on light element abundances.

1.1.2 Inflation

While the observations described above support the Big Bang theory, several problems remain. One of these is the horizon problem. The microwave background shows that the universe is extremely isotropic on large scales — the temperature of the radiation in completely different directions differs by only one part in 10^5. However, in the standard Big Bang theory these photons would have been emitted from regions too widely separated to be in causal contact at the time of recombination. These regions could therefore never have been in thermal equilibrium.

The second problem is known as the flatness problem. In the standard Big Bang model, the density of the Universe rapidly evolves away from the critical density required to eventually halt the expansion of the Universe. Observations indicate that the current density is of the order of the critical density, which would require extremely fine tuning in the early Universe.

Finally, Grand Unified Theories (GUTs) predict the existence of magnetic monopoles, which are not observed and which, in the standard Big Bang model, would contribute sufficient density to cause the Universe to have re-collapsed long before the present day. In the 1980's, Alan Guth proposed a possible resolution to all three of these problems in the form of a period of rapid, exponential expansion very early in the history of the Universe (Guth 1981). This solves the horizon problem by expanding initially causally connected regions to sizes greater than the present horizon. During inflation, the density of the Universe is driven towards the critical density, so that a flat universe is expected, and the density of magnetic monopoles is diluted down to a negligibly small value.

As well as solving a number of problems with the standard Big Bang theory, inflation conveniently provides a mechanism to generate the primordial density fluctuations which are needed if structure is to form in the Universe. These fluctuations originate from quantum fluctuations of the same scalar field which provides the vacuum energy to drive the rapid expansion.

1.1.3 Dark Matter

In the 1920's Hubble made the first attempt to calculate the mass density of the Universe. This was done by counting the number of visible galaxies and estimating the masses of individual galaxies by considering the potential required to contain their constituent gas and stars (Hubble 1926).

However, it soon became apparent that significant amounts of mass were being missed in this accounting. The first such estimates were made by Zwicky (1933) and Smith (1936). The observed velocity dispersions of galaxies in clusters indicated total cluster masses an order of magnitude greater than the mass of the visible galaxies. Later, X-ray observations revealed the presence of a hot, diffuse intracluster medium contributing a quantity of mass similar to that of the luminous galaxies, but this still left the majority of the mass in galaxy clusters unaccounted for.

Evidence for the existence of dark matter in smaller systems was found in the 1970's, when the rotation curves of spiral galaxies were shown to remain constant out to larger radii than would be expected if the visible stars and gas constituted the entire mass of the galaxy (e.g. Faber & Gallagher 1979). Nucleosynthesis places a strong constraint on the mean density of baryonic material in the Universe which is around an order of magnitude lower than the mass density inferred from studies of cluster dynamics and galaxy rotation curves. The majority of the dark matter must therefore be non-baryonic. Fortunately, particle physics provides several possible candidate dark matter particles.

Each of these candidates may be classified as 'hot' (for example, massive neutrinos) or 'cold' dark matter (perhaps Weakly Interacting Massive Particles, WIMPs) depending on whether they move relativistically or non-relativistically when they decouple from the radiation field in the early Universe. This distinction has important consequences for the formation of large scale structure, as will be seen in the next section.

1.1.4 Formation of Large Scale Structure

It has long been known that in an otherwise homogeneous universe, primordial density perturbations would be amplified by gravitational instability — this behaviour was first investigated by Lifshitz (1946). The presence of structure in the local Universe suggests that the primordial perturbations must have existed, and inflation provides a possible mechanism to generate them, but the subsequent evolution of these perturbations depends strongly on the nature of the dark matter which contributes the majority of the mass

density of the Universe.

Bond et al. (1980) considered a Hot Dark Matter (HDM) model in which the mass density of the Universe was dominated by massive neutrinos. They found that free streaming of the HDM particles erases density perturbations smaller than a characteristic mass which is a function of the particle mass. This mass is quite high — for a neutrino mass of 30eV, perturbations less massive than $4 \times 10^{15} h^{-1} M_\odot$ are suppressed. White et al. (1983) used numerical N-body simulations to show that massive, pancake-like structures were the first objects to form in such a model. Galaxies could then only form through the subsequent fragmentation of these "pancakes".

Cold Dark Matter (CDM) particles are non-relativistic in the early Universe, and, in models where the mass density is dominated by CDM, structure is able to form on much smaller scales at early times. In this picture, low mass objects form first and grow through mergers to form more massive objects. Davis et al. (1985) used N-body techniques to simulate this process, and found that a model with a low density parameter, $\Omega = 0.2$, appeared to best match the observed galaxy distribution if the galaxies traced the underlying dark matter distribution. However, they noted that this might not be the case, and found that a "biased" model with $\Omega = 1$, in which galaxies were assumed to be associated with peaks in the initial density distribution, was consistent with observations.

The hierarchical Cold Dark Matter scenario is now favoured, since on large scales the mass distribution seen in CDM simulations appears similar to that in the real Universe. For example, White et al. (1987) demonstrated that CDM N-body simulations were able to reproduce the observed abundance of galaxy clusters and produced filaments and voids similar to those observed.

More recent evidence in favour of CDM has come from large scale galaxy redshift surveys and improved observations of the microwave background. Redshift surveys provide detailed information on the present day, large scale distribution of galaxies which may be compared with models of structure and galaxy formation. For example, the 2dF Galaxy Redshift Survey (Colless & the 2dFGRS team 2003, preprint (astro-ph/0306581)) obtained reliable redshifts for over 200,000 galaxies. These data may, amongst other things, be used to determine galaxy clustering properties on scales as large as $300 h^{-1} Mpc$, to constrain the density and spatial distribution of dark matter, and to directly measure the galaxy bias parameter.

An alternative approach is to use detailed measurements of the CMB to find out about conditions in the early Universe. The WMAP satellite has improved on the measurements

taken by COBE by mapping the microwave background with greatly improved angular resolution (Bennett et al. 2003). This has allowed a determination of the power spectrum of the CMB temperature anisotropy down to smaller scales than was previously possible. The WMAP results are entirely consistent with the Big Bang theory and inflation and, when used in combination with other CMB observations and the 2dF survey, place tight constraints on the cosmological parameters.

It now appears that the background cosmological model and the origin of large scale structure may be reasonably well understood. However, these processes alone cannot account for the galaxy populations we see today. In the next section, we summarise the development of current, hierarchical, models of galaxy formation.

1.2   Theories of Galaxy Formation

The baryonic material which makes up the galaxies we observe in the Universe today behaves quite differently from the dark matter. While on very large scales its distribution is likely to follow that of the dark matter, on smaller scales hydrodynamic processes such as shock heating and radiative cooling will become important. Rees & Ostriker (1977), Binney (1977) and Silk (1977) first recognised that radiative cooling would have significant consequences for galaxy formation. On small (i.e. galactic or sub-galactic) scales, and in the absence of any form of heating, gas in a virialised halo will quickly radiate away its thermal energy. This results in a loss of pressure support, and the gas will collapse to the centre of the halo.

White & Rees (1978) suggested a model in which galaxies formed in this way at the centres of hierarchically assembled dark matter halos. It was realised that dissipation would allow the galaxies to become sufficiently concentrated to survive mergers between halos, thereby accounting for the observed groups and clusters of galaxies. By considering the rate at which gas would be able to cool in a dark matter halo, White & Rees (1978) were able to obtain a galaxy luminosity function with approximately the correct shape.

Later, Cole (1991) developed a Monte-Carlo model, based on extensions to Press-Schechter theory (Press & Schechter 1974) developed by Bond et al. (1991) and Bower (1991), to investigate the radiative cooling of gas in dark matter halos. It was found that some form of heating, perhaps by supernovae, was required to prevent the cooling of a large fraction of the gas at high redshift. White & Frenk (1991) obtained similar results with their model, and were also able to show that mergers between galaxies were

necessary to avoid an overabundance of faint objects. At the same time, Lacey & Silk (1991) adopted a slightly different approach, associating galaxies with peaks in the linear density field and assuming that star formation was induced by tidal interactions. This model also included the effects of radiative cooling and energy injection by supernovae.

Models of this type, which use a combination of numerical and analytic methods to calculate the evolution of the galaxy population from a set of initial conditions have come to be known as "semi-analytic" models. Subsequently, more sophisticated semi-analytic models, were developed which included additional physical processes. For example, the models of Kauffmann et al. (1993) and Cole et al. (1994) predicted galaxy luminosities using stellar population synthesis techniques and included estimates of the rate of galaxy-galaxy mergers, and the models of Kauffmann (1996) and Cole et al. (2000) included more detailed treatments of metal enrichment.

While early models considered only the formation of galactic disks, the models of Kauffmann et al. (1993) and Baugh et al. (1996) were able to produce a mix of galaxy morphologies by assuming that major mergers disrupted disks and resulted in the formation of an elliptical galaxy. The accretion of additional gas could later lead to the formation of a new disk around the bulge component.

Other developments have included allowing for the effects of mergers between satellite galaxies (Somerville & Primack 1999) and modelling of the effects of dust extinction on galaxy colours and luminosities (Kauffmann et al. 1999a, Cole et al. 2000). Kauffmann & Haehnelt (2000) used semi-analytic techniques to model quasar activity due to the growth of black holes at the centres of galaxies. Semi-analytic models have also been used to investigate variations in clustering properties with luminosity, morphology and redshift (Kauffmann et al. 1997, Kauffmann et al. 1999b, Baugh et al. 1999), the properties of Lyman break galaxies (Baugh et al. 1998, Governato et al. 1998) and the evolution of cluster galaxies (e.g. Kauffmann & Charlot 1998).

Attempts have also been made to model galaxy formation using hydrodynamical simulations. The most popular technique is known as Smooth Particle Hydrodynamics, or SPH, which was first described by Lucy (1977) and Gingold & Monaghan (1977). With the addition of radiative cooling, these simulations have been able to generate populations of objects with approximately galactic masses and reasonable abundances (e.g. Katz et al. 1992, Navarro & White 1993, Evrard et al. 1994, Steinmetz & Muller 1995, Katz et al. 1996, Frenk et al. 1996, Steinmetz & Navarro 1999, Pearce et al. 1999, Pearce et al. 2001).

The most recent simulations have been able to resolve the detailed structure of galaxies forming in a cosmological context, while including additional physics such as star formation, feedback and chemical enrichment (e.g. Abadi et al. 2003, Governato et al. 2002, preprint (astro-ph/0207044), Sommer-Larsen et al. 2002). These simulations have been able to produce galaxies which strongly resemble those observed, but are so computationally intensive that it is difficult to simulate a sufficient number of galaxies to derive statistical properties (such as the luminosity function), or to explore the effect of varying star formation and feedback prescriptions.

1.3 The GALFORM Semi-Analytic Model

In this work we make extensive use of the GALFORM semi-analytic galaxy formation model developed and described in detail by Cole et al. (2000). This model uses analytic solutions and physically motivated prescriptions to treat the processes thought to be important in the formation of galaxies. Here, we briefly summarise the physics included in the model, concentrating on those processes which are particularly relevant to the work carried out in this thesis.

1.3.1 Formation of Dark Matter Halos

The starting point for the GALFORM model is a set of present day dark matter halos with known merger histories. The Press-Schechter mass function (Press & Schechter 1974) is used to determine the number of halos to be simulated as a function of mass. Halo merger trees are then generated using a Monte-Carlo algorithm based on extensions to the Press-Schechter theory proposed by Bond et al. (1991) and Bower (1991).

Most of the models employed in this thesis use halo merger histories determined from N-body simulations. However, we do make some use of the Monte-Carlo algorithm of Cole et al. (2000). In Chapter 2 it is used to investigate the effect of limited mass resolution on the semi-analytic model, and in Chapter 5 it is used to estimate the luminosity function which might be obtained if high resolution SPH simulations of large volumes could be carried out. We therefore describe the algorithm here.

Lacey & Cole (1993) derive an expression for the fraction of mass, $f_{12}(M_1, M_2)dM_1$, in halos of mass M_2 at time t_2 which, at the earlier time t_1 was contained in halos in the mass range between M_1 and $M_1 + dM_1$:

$$f_{12}(M_1, M_2)dM_1 = \frac{1}{\sqrt{2\pi}} \frac{(\delta_{c1} - \delta_{c2})}{(\sigma_1^2 - \sigma_2^2)^{3/2}}$$

$$\times \, \exp\left(-\frac{(\delta_{c1} - \delta_{c2})^2}{2(\sigma_1^2 - \sigma_2^2)}\right) \frac{d\sigma_1^2}{dM_1} dM_1. \tag{1.1}$$

where σ_1 and σ_2 are the rms density fluctuations in spheres of mass M_1 and M_2 and δ_{c1} and δ_{c2} are the critical linear theory overdensity for collapse at times t_1 and t_2. Taking the limit $t_1 \rightarrow t_2$, the following equation is obtained:

$$\frac{df_{12}}{dt_1}\bigg|_{t_1=t_2} dM_1 dt_1 = \frac{1}{\sqrt{2\pi}} \frac{1}{(\sigma_1^2 - \sigma_2^2)^{3/2}} \frac{d\delta_{c1}}{dt_1} \frac{d\sigma_1^2}{dM_1} dM_1 dt_1. \tag{1.2}$$

This gives the average mass fraction of a halo of mass M_2 at time t_2 which was in halos of mass M_1 at the time t_1. This can be used to find the mean number of progenitors of mass M_1 of the halo one time step, dt_1, earlier:

$$\frac{dN}{dM_1} = \frac{df_{12}}{dt_1} \frac{M_2}{M_1} dt_1 \qquad (M_1 < M_2). \tag{1.3}$$

Binary merger trees are built by taking the final halo and dividing its merger history into a series of time steps sufficiently small that each halo in the merger tree is unlikely to have more than two progenitors. Eqn. 1.3 is used to determine the mean number of progenitors of each halo of mass M_2:

$$P = \int_{M_{res}}^{M_2/2} \frac{dN}{dM_1} dM_1, \tag{1.4}$$

where M_{res} is the mass resolution of the merger tree. If the timesteps are sufficiently small, so that $P \ll 1$, P may be regarded as the probability that the halo has two progenitors. A random number is then drawn to determine whether the halo has one or two progenitors. If this is the case, the masses of the progenitors are chosen at random from a distribution consistent with Eqn. 1.3. The total mass available to form the progenitors is equal to the mass of the later halo minus the fraction of material accreted in the form of unresolved halos, given by:

$$F = \int_0^{M_{res}} \frac{dN}{dM_1} \frac{M_1}{M_2} dM_1, \tag{1.5}$$

The merger tree is built up by carrying out this procedure for each time step, starting with the final halo and working back in time. The required inputs for this algorithm are the density fluctuation power spectrum, which determines $\sigma(M)$, and the cosmological parameters which are used to calculate $\delta_c(t)$. Additionally, the minimum halo mass to be considered, M_{res}, must be chosen.

The binary merger tree created in this way has very high time resolution, and is used to produce a new, equivalent merger tree (with reduced temporal resolution) on a predefined grid of time steps. The new merger tree is no longer binary — several mergers may occur during one time step so that a halo may have more than two progenitors.

Before the semi-analytic galaxy formation rules are applied to the merger tree, it is split up into "branches" or halo lifetimes. The lifetime of a halo is said to end when it becomes part of a halo with f_{form} times the mass it had when it formed. The new, more massive halo is then considered to be newly formed and it is said to exist until it, in turn, becomes part of a halo with more than f_{form} times its original mass. Halo formation times are assigned by first determining the lifetimes of halos with no progenitors and working forwards in time towards the final halo. During the lifetime of a halo, properties such as its mass, mean density and angular momentum are taken to be constant. The parameter f_{form} is set to 2, but results from the GALFORM model are not very sensitive to the exact choice of f_{form}, since halo lifetimes generally end when the halo merges onto a much more massive object.

References to halo formation and the age of a halo later in this Chapter refer to this partitioning of the merger tree.

1.3.2   Halo Properties

Each halo in the merger tree is assumed to be spherically symmetric, with a density profile given by:

$$\rho(r) = \frac{\Delta_{vir}\rho_c}{f(a_{NFW})} \frac{1}{r/r_{vir}\,(r/r_{vir} + a_{NFW})^2} \quad (r \le r_{vir}), \tag{1.6}$$

where $f(a_{NFW}) = \ln(1 + 1/a_{NFW}) - 1/(1 + a_{NFW})$, and the density profile is truncated at the virial radius, r_{vir}. The virial radius is taken to be the radius within which the mean density is Δ_{vir} times the critical density, $\rho_c = 3H^2/(8\pi G)$. Δ_{vir} is calculated using the expressions given by Lacey & Cole (1993) and Eke et al. (1996), for open and flat universes respectively. The parameter a_{NFW} is set using the analytic model for the relation between a_{NFW} and halo mass presented by Navarro et al. (1997).

Each halo is also assigned an angular momentum, expressed in terms of the spin parameter

$$\lambda_h = \frac{J_h |E_h|^{1/2}}{G M_h^{5/2}}, \tag{1.7}$$

where M_h, J_h and E_h are the total mass, angular momentum and energy of the halo respectively. The spin parameter is assigned at random from a distribution consistent with the N-body simulation results of Cole & Lacey (1996). See also Barnes & Efstathiou (1987) and Warren et al. (1992).

The spin parameter is used to calculate the mean rotational velocity of the halo, under the assumptions that it is constant with radius and always aligned in the same direction.

Again, these assumptions are chosen to be consistent with N-body simulations. The rotational velocity is required to calculate the angular momentum of cooling halo gas.

1.3.3 Gas Cooling and Disk Formation

Cooling gas in a dark matter halo is assumed to form a disk at the centre of the halo, supported by angular momentum acquired through tidal torques during the halo's formation. The GALFORM model differentiates between "cold" gas, which is gas which has been incorporated into galaxies, and "hot" gas which is diffuse gas spread throughout the dark matter halo. All of the hot gas is assumed to have been shock heated during the formation process and to be distributed with a spherically symmetric density profile with a core of radius $r_{\rm core}$:

$$\rho_{\rm gas}(r) \propto 1/(r^2 + r_{\rm core}^2) \tag{1.8}$$

The gas is taken to be isothermal with a temperature equal to the virial temperature of the halo,

$$T_{\rm vir} = \frac{1}{2} \frac{\mu m_{\rm H}}{k_{\rm B}} V_{\rm H}^2 \tag{1.9}$$

where $k_{\rm B}$ is the Boltzmann constant, $\mu m_{\rm H}$ is the mean molecular mass of the gas and $V_{\rm H} \equiv (GM_{\rm h}/r_{\rm vir})^{1/2}$ is the circular velocity of the halo. These assumptions are motivated by hydrodynamical simulations including those of Navarro et al. (1995), Eke et al. (1998) and Frenk et al. (1999).

There are a number of possible choices for the core radius in the gas density profile, $r_{\rm core}$. The reference model of Cole et al. (2000) has an initial core radius for each halo which is equal to $r_{\rm core}^0 = r_{\rm NFW}/3$, where $r_{\rm NFW} = a_{\rm NFW} r_{\rm vir}$. When a merger results in the formation of a new halo, the gas core radius is allowed to increase to obtain the density at the virial radius which would have been present if no gas had cooled. The justification for this is that the densest gas, with the lowest entropy, is the most able to cool. Cooling therefore increases the minimum entropy of the gas. Analytic work (Evrard & Henry 1991, Kay & Bower 1999, Wu et al. 2000) suggests that this has the effect of increasing the core radius of the halo gas. It also seems reasonable to assume that the pressure at the virial radius remains unaffected, since it is maintained by shocks caused by infalling material.

In Chapter 3, we vary the treatment of cooling in the semi-analytic model slightly in order to find a prescription which provides the best possible match to results obtained from SPH simulations. To do this, we vary the initial core radius and also investigate

models in which the core radius is fixed so that $r_{core} = r_{core}^0$ at all times.

The cooling time of the halo gas is given by:

$$\tau_{cool}(r) = \frac{3}{2} \frac{1}{\mu m_H} \frac{k_B T_{gas}}{\rho_{gas}(r) \Lambda(T_{gas}, Z_{gas})} \qquad (1.10)$$

where T_{gas} is the temperature of the gas and $\Lambda(T_{gas}, Z_{gas})$ is the cooling function, which depends on the temperature and metallicity, Z_{gas}. The rate at which gas cools in a halo is determined by calculating the cooling radius, the radius at which the cooling time of the gas is equal to the age of the halo. However, for gas to be accreted onto the disk, it must have sufficient time to fall to the centre of the halo.

The mass of gas accreted during a time step is therefore found by calculating $r_{min} = \min[r_{cool}, r_{ff}]$ at the beginning and end of the time step, where r_{ff} is the free-fall radius. The free fall radius is defined such that the time taken for an initially stationary particle to fall to the centre of the halo from this radius is equal to the age of the halo. Any gas in the spherical shell between the radii r_{cool} and r_{ff} is added to the disk. Disk sizes are calculated by assuming that the gas retains its angular momentum as it collapses.

1.3.4   Galaxy Mergers and Spheroid Formation

In the GALFORM model, elliptical galaxies, and the bulges of spiral galaxies, are created in galaxy mergers. When dark matter halos merge, any galaxies they contain do not immediately merge. Instead, the most massive galaxy becomes the central galaxy in the new halo and the others become satellites. These satellites may eventually lose energy and angular momentum through dynamical friction and merge onto the central galaxy.

Merger timescales for the satellite galaxies are determined using the estimate obtained by Lacey & Cole (1993):

$$\tau_{mrg} = f_{df} \, \Theta_{orbit} \, t_{dyn} \frac{0.3722}{\ln(\Lambda_{Coulomb})} \frac{M_h}{M_{sat}}. \qquad (1.11)$$

where M_h is the mass of the halo, M_{sat} is the mass of the satellite galaxy, $\tau_{dyn} \equiv \pi r_{vir}/V_H$ is the dynamical time of the halo and f_{df} is an adjustable parameter which allows for uncertainties due to the approximations made in this model. The Coulomb logarithm, $\ln(\Lambda_{Coulomb})$ is taken to be equal to $\ln(M_h/M_{sat})$. Cole et al. (2000) choose to set $f_{df} = 1$, but note that a slightly higher value may be appropriate if the halo of the satellite galaxy is quickly strippped away. The factor Θ_{orbit} contains the dependence of the timescale on the orbit of the satellite galaxy:

$$\Theta_{orbit} = [J/J_c(E)]^{0.78}[r_c(E)/r_{vir}]^2, \qquad (1.12)$$

E and J are the initial energy and angular momentum of the orbit, and r_c and J_c are the radius and angular momentum of a circular orbit with the same energy. For each satellite, Θ_{orbit} is drawn from a distribution based on the simulations of Tormen (1997). Satellites then merge when the age of the halo exceeds their merger timescale. If a satellite does not merge during the lifetime of the halo its merger timescale is recalculated when the new halo forms.

A galaxy merger in the GALFORM model has several possible outcomes, depending on the ratio of the mass of the satellite galaxy, M_{sat}, to the mass of the central galaxy, M_{cen}. If the ratio $M_{\text{sat}}/M_{\text{cen}} \geq f_{\text{ellip}}$, a major merger occurs. All of the gas and stars involved in the merger are incorporated into a single bulge component. A burst of star formation converts any gas present into stars. Minor mergers, with $M_{\text{sat}}/M_{\text{cen}} < f_{\text{ellip}}$, result in the stars from the satellite galaxy being added to the bulge of the central galaxy. Any gas in the disk of the satellite galaxy is added to the disk of the central galaxy.

1.3.5 Star Formation

Star formation is assumed to take place in galactic disks at a rate proportional to the mass of cold gas, M_{cold}, present. The star formation rate is therefore given by:

$$\psi = M_{\text{cold}}/\tau_\star \tag{1.13}$$

where $\tau_\star$ is the star formation timescale. Feedback is included in the model by assuming that energy released by young stars and supernovae reheats cold gas and ejects it from the disk at a rate $\dot{M}_{\text{eject}}$, which is determined by a feedback efficiency parameter, β:

$$\dot{M}_{\text{eject}} = \beta\psi \tag{1.14}$$

The star formation timescale and feedback efficiency are functions of the properties of the galactic disk. The star formation timescale is related to the circular velocity of the disk, V_{disk}, by:

$$\tau_\star = \epsilon_\star^{-1}\,\tau_{\text{disk}}\,(V_{\text{disk}}/200\,\text{kms}^{-1})^{\alpha_\star} \tag{1.15}$$

where τ_{disk} is the dynamical time of the disk, defined as its half mass radius divided by the circular velocity at the half mass radius. The feedback efficiency is:

$$\beta = (V_{\text{disk}}/V_{\text{hot}})^{-\alpha_{\text{hot}}} \tag{1.16}$$

where $\epsilon_\star$, $\alpha_\star$, V_{hot} and α_{hot} are dimensionless parameters. In the reference model of Cole et al. (2000), these parameters have the values $\epsilon_\star$=0.005, $\alpha_\star = -1.5$, $V_{\text{hot}} = 200.0$ and

$\alpha_{hot} = 2.0$. These values were obtained by requiring that the model galaxy population must reproduce observed properties of the local galaxy population, such as the faint end of the luminosity function, the Tully-Fisher relation, gas fractions, and the sizes of low luminosity spirals.

1.3.6 Chemical Enrichment

Chemical enrichment in the GALFORM model occurs when stars return metals to the cold gas of the interstellar medium. The metal enriched gas may then be reheated by feedback processes, resulting in enrichment of the hot halo gas. For each galaxy, the model traces the mean metallicity of the stars and the cold gas separately. The metallicity of the hot halo gas is also calculated, since this affects the cooling rate and the metallicity of the gas added to galactic disks.

When stars form, it is assumed that a fraction, R, of the mass is instantaneously recycled into the interstellar medium. A fraction, p, of the mass is converted into metals. The GALFORM model allows for the direct enrichment of the hot halo gas by assuming that a fraction, e, of the metals are ejected from the disk into the hot gas phase. If the Initial Mass Function (IMF) of the stars is known, the recycled fraction, R, may be found through stellar evolution calculations. It is also necessary to know the yield, p, which is defined as the fraction of the mass incorporated into stars which is converted into metals and returned to the interstellar medium. Theoretical predictions for the yield are somewhat uncertain, so p is determined by requiring that the model reproduces the observed metallicities of local elliptical galaxies. Cole et al. (2000) set $p = 0.02$, $R = 0.31$ and assume that no metals are ejected from the disk by setting $e = 0$.

1.3.7 Stellar Population Synthesis and Dust Extinction

The model described so far generates a population of galaxies for which a large number of physical properties are known, including sizes and masses of the disk and bulge components, metallicity of the gas and stars, and the star formation history. However, if the model galaxies are to be compared with observational data, luminosities must be assigned to them. This is done using stellar population synthesis techniques.

The updated models of Bruzual A. & Charlot (1993) give the spectral energy distribution (SED), $l_\lambda(t, Z)$, of a population of stars which all have the same age, t, and metallicity, Z. By convolving this with the star formation history of a model galaxy, its

SED, $L_\lambda(t)$, may be obtained:

$$L_\lambda(t) = \int_0^t l_\lambda(t - t', Z(t')) \, \psi(t') \, dt', \tag{1.17}$$

Here, $Z(t')$ is the metallicity of the stars which formed at time t' and $\psi(t')$ is the corresponding star formation rate. When galaxies merge, their contributions to the SED of the new galaxy are summed.

These calculations require that the IMF of the stars is known. In the model of Cole et al. (2000), the IMF is assumed to be the same for all stars in all galaxies at all times. Cole et al. consider models using the IMFs proposed by Kennicutt (1983) and Salpeter (1955). It is also assumed that some of the mass converted into stars becomes a population of brown dwarfs, which do not contribute any light to the SED of the galaxy. The number of brown dwarfs present is expressed in terms of the parameter Υ, defined as:

$$\Upsilon = \frac{(\text{mass in visible stars} + \text{brown dwarfs})}{(\text{mass in visible stars})} \tag{1.18}$$

The masses here refer to the masses present before any recycling of material into the interstellar medium occurs. This has the effect of reducing all luminosities by a factor $1/\Upsilon$. Cole et al. (2000) choose Υ to obtain the best possible match to the local galaxy luminosity function.

The effect of dust extinction on the galaxy luminosities is treated using the models of Ferrara et al. (1999), which include absorption and scattering of light by dust grains in a realistic, three dimensional distribution of stars and dust.

1.4   Motivation for this Work

Numerical models of galaxy formation have developed along two very different paths. Hydrodynamical simulations have the advantage of following the evolution of the baryonic and dark matter content of the Universe in complete generality, but have limited spatial and mass resolution. The algorithms used to carry out these simulations may also lead to unphysical results in certain circumstances. For example, Okamoto et al. (2003) show that SPH simulations have difficulty in correctly treating situations involving strong shear flows. In simulations of galaxy formation, this can lead to the artificial transfer of angular momentum from the galactic disk to the surrounding diffuse, halo gas. The problem is particularly serious if the disk is poorly resolved.

Semi-analytic models are much less computationally intensive, and this allows a more thorough investigation of the effect of varying model parameters. It also means that mass

resolution is generally not a problem. However, these models usually involve a number of rather uncertain assumptions, such as spherical symmetry.

It is clearly important to know whether differences between these models and observations are real (perhaps due to the neglect of certain physical processes in the models, for example) or are due to poor approximations, invalid assumptions, or numerical problems. A detailed comparison between these two numerical treatments of the same physical processes could reveal failings of either or both of them and indicate possible areas for improvement. If the models are found to be consistent, this would suggest that their predictions may be robust, since they are unlikely to both suffer from the same problems.

In Chapter 2 we develop a semi-analytic model, referred to here as the N-body GALFORM model, which uses semi-analytic techniques to populate dark matter halos in an N-body simulation volume with galaxies. We identify reasons for the differences between the galaxy populations predicted by the standard and N-body GALFORM models.

In Chapter 3, we compare SPH and N-body GALFORM predictions for the galaxy population in a $50h^{-3}\mathrm{Mpc}^3$ simulation volume in the absence of star formation. This allows us to compare the mass of gas which cools in each model on a halo by halo basis. We also investigate the effect of varying the semi-analytic galaxy merger rate on the galaxy masses and two point correlation function.

An improved version of the N-body GALFORM model, which determines galaxy mergers using halo substructure information from the N-body simulation, is developed in Chapter 4. This is used to carry out a comparison with a high resolution SPH simulation of the formation of a halo containing a single galaxy. Star formation is included in these models, and feedback is approximated by the suppression of cooling at redshifts $z > 1$.

Finally, in Chapter 5, we carry out a comparison between the N-body GALFORM model and a set of SPH simulations of galaxy formation in which both models are intended to be as realistic as possible. Our intention here is to investigate the differences between state of the art SPH and semi-analytic models of galaxy formation, including those due to the inclusion of different physics, assumptions and prescriptions. Chapter 6 presents a brief summary of the main conclusions of this thesis. It also identifies some possible areas for future research.

Chapter 2

Galaxy Formation using N-body Halo Merger Histories

2.1 Introduction

Hierarchical models of galaxy formation must describe both the growth and collapse of density perturbations to form dark matter halos and the baryonic processes which lead to the formation of stars. Despite uncertainty as to the exact nature of the dark matter itself, the formation and evolution of dark matter halos appears to be reasonably well understood. The two main approaches to this problem are direct numerical simulations and analytic techniques such as the Press-Schechter theory (Press & Schechter 1974). Encouragingly, the mass functions of dark matter halos predicted using these very different approaches are found to agree to within 50% (Gross et al. 1998, Governato et al. 1999, Jenkins et al. 2001). The analytic model described by Sheth et al. (2001) based on the assumption that objects collapse ellipsoidally rather than spherically achieves even better agreement with N-body simulations. Mo & White (2002) present halo abundances from this and several other models.

This understanding of the hierarchical build up of structure provides the starting point for semi-analytic models of galaxy formation, which attempt to follow the development of galaxies from primordial density fluctuations. In semi-analytic models, merger histories for dark matter halos may be taken directly from dark matter simulations (e.g. Kauffmann et al. 1999a, van Kampen et al. 1999). Alternatively, extensions to the Press-Schechter theory which predict the conditional halo mass function (Bond et al. 1991, Bower 1991) and halo survival times, formation times and merger rates (Lacey & Cole 1993) may be used to construct realisations of merger histories for individual halos. Simple analytic modelling is then used to follow the evolution of the baryonic component, including pre-

scriptions for processes such as star formation and its possible effects on the remaining gas. Semi-analytic models (e.g. Cole 1991, Lacey & Silk 1991, White & Frenk 1991, Cole et al. 1994, Somerville & Primack 1999, Cole et al. 2000) have successfully reproduced many observable properties of galaxies, such as the local field galaxy luminosity function and distributions of colour and morphology. When combined with N-body simulations, semi-analytic models have also successfully reproduced galaxy clustering properties (e.g. Governato et al. 1998, Kauffmann et al. 1999a, Benson et al. 2000, Wechsler et al. 2001).

Semi-analytic models utilising merger trees generated using algorithms based on the extended Press-Schechter (EPS) formalism have two closely related advantages over models which take merger histories from N-body simulations. Creating Monte-Carlo realisations of merger trees for a set of halos generally requires fewer computing resorces than carrying out an N-body simulation of a similar number of halos. In both cases, improving the mass resolution increases the computational load, but since the load is much less in the Monte-Carlo case, significantly better mass resolution may be achieved. Methods based on the Press-Schechter theory, however are only applicable to initially Gaussian fluctation fields. N-body simulations, on the other hand, have the advantage that the non-linear evolution of density fluctuations is followed in complete generality, without the need for any of the assumptions involved in creating EPS merger trees.

There are advantages to both of these methods, and which is more appropriate depends on the problem being addressed. In this Chapter we investigate the effects of the choice of merger trees on the predictions of one particular semi-analytic model. We describe a new method of extracting merger trees from an N-body simulation and incorporate these merger trees into a semi-analytic galaxy formation model based on that of Cole et al. (2000). We compare the predictions of this model to those of a similar model utilising Monte-Carlo realisations of halo merging histories. In order to identify the reasons for the discrepancies that we find, we determine the changes that must be made to the Monte-Carlo model to reproduce the N-body results.

The use of N-body merger trees in semi-analytic models allows a halo-by-halo comparison between the semi-analytic treatment of baryonic processes, such as gas cooling, and direct numerical simulations of galaxy formation. In the next Chapter we will carry out such a comparison between a "stripped down" version of the semi-analytic model described here and a smoothed particle hydrodynamics simulation of a cosmological volume.

This Chapter is laid out as follows. In Section 2.2 we explain how we obtain merger trees from an N-body simulation. In Section 2.3 we investigate the effect on our semi-

analytic model of utilising merger trees derived from N-body simulations rather than Monte-Carlo realisations. In Section 2.4 we present our conclusions.

2.2 Extracting Merger Trees

We now present the method we used to calculate the merger histories of dark matter halos identified in an N-body simulation. The simulation, which will be referred to as the GIF simulation, was carried out by the Virgo Consortium using a parallel adaptive particle-particle/particle-mesh (AP^3M) code known as Hydra (Couchman et al. 1995, Pearce & Couchman 1997) as part of the GIF project. The simulation assumes the ΛCDM cosmology with mean mass density parameter $\Omega_0 = 0.3$, cosmological constant $\Lambda_0 = 0.7$ in units of $3H_0^2/c^2$, power spectrum shape parameter $\Gamma = 0.21$, present day rms linear fluctuation amplitude in $8h^{-1}$Mpc spheres $\sigma_8 = 0.90$, and Hubble constant $h = 0.7$ in units of $100 \text{kms}^{-1}\text{Mpc}^{-1}$. It contains 256^3 dark matter particles each of mass $1.4 \times 10^{10} h^{-1} M_\odot$ in a box of side $141.3 h^{-1}$Mpc. The gravitational softening length in the simulation is $30 h^{-1}$kpc at $z = 0$. This simulation is described in more detail by Jenkins et al. (1998), where it is referred to as ΛCDM2, and by Kauffmann et al. (1999a). While halo catalogues and merger trees based on this simulation are publically available, here we make use of only the simulation outputs themselves and construct merger trees using a somewhat different algorithm to that of Kauffmann et al. We use 44 output times from the simulation which are spaced equally in $\log_{10}(1 + z)$ between $z = 0$ and $z \sim 20$.

2.2.1 Identifying Halos

In order to construct merger histories for dark matter halos in an N-body simulation, a catalogue of halos must be produced for each simulation output using a group finding algorithm. The algorithm used here is the "friends of friends" (FOF) method of Davis et al. (1985), which simply links together any particles with separations less than the linking length b, usually expressed in terms of the mean interparticle separation. Given sufficiently large numbers of particles in each object, the FOF algorithm finds regions bounded by a surface of constant density. The density threshold is proportional to $1/b^3$.

The FOF approach has the advantage that it imposes no constraints on the geometry of the halos identified, but it may occasionally artificially join two nearby halos if a transient "bridge" of a few particles forms between them. It will be seen in Section 2.2.2 that this can cause problems when attempting to generate merger trees using FOF group

catalogues, and a method of identifying and splitting artificially joined halos is described in Section 2.2.2.

The usual choice for the linking length in cosmologies with $\Omega = 1$ is $b = 0.2$ (e.g. Lacey & Cole 1994), which identifies halos with a mean density similar to that predicted by the top hat spherical collapse model (Cole & Lacey 1996). However, in cosmologies with $\Omega < 1$ there is no rigorous justification for any particular choice. Here, we choose to set $b = 0.2$ at all redshifts as in the $\Omega = 1$ case. See Eke et al. (1996) and Jenkins et al. (2001) for further discussion.

The other parameter needed by the FOF algorithm is the minimum number of particles, N_{min}, required to constitute a group. It is important that N_{min} be as small as possible, since detailed merger trees can only be obtained for halos much larger than the smallest resolvable group. Kauffmann et al. (1999a) found that in their simulations groups as small as 10 particles are dynamically stable systems and that for 95% of these groups, 80% of the particles remain in the same group at subsequent times.

We therefore identify halos using a linking length $b = 0.2$ at all redshifts, with a minimum group size of ten particles. The resulting catalogues may still contain some groups which consist of unbound particles which happen to be close together at this particular timestep. To remove these, we follow Benson, Frenk, Baugh, Cole & Lacey (2001) and calculate the total energy of each group. Unbound groups are not immediately discarded, because they may only be unbound due to the presence of a small number of fast moving particles. The binding energy of each particle is calculated, and the least bound particle is removed from the group. This is repeated until the group becomes bound. If half of the particles are removed or the group is reduced to less than N_{min} particles we discard it. Up to 5% of all groups are discarded, with a similar number of groups being reduced in mass by this procedure. The affected groups generally consist of around 10-20 particles.

We use the procedure described above to generate halo catalogues for 44 simulation outputs between redshifts $z = 20$ and $z = 0$, spaced approximately evenly in $\log_{10}(1 + z)$.

2.2.2 Constructing N-body Merger Trees

In an idealised picture of the process of hierarchical structure formation (e.g. Press-Schechter theory), dark matter halos may increase in mass by mergers, but cannot lose mass. Consequently, any halo identified in a simulation prior to the final output time should still exist at subsequent output times, although it may have become subsumed

within a larger halo through a merger. In any case, the constituent particles of the original halo should still all be members of a single group. It should therefore be possible to identify each halo in the simulation as a progenitor of a single halo at the next output time.

In practice there are several ways in which a halo can lose particles. Halos may be disrupted by tidal forces caused by other nearby halos. The masses of simulated halos can also fluctuate because the FOF algorithm imposes a somewhat arbitrary boundary on the halo and outlying particles which are considered group members at one timestep may lie just beyond the boundary at the next timestep.

The technique we use to determine merger histories is intended to take into account this uncertainty in the definition of a halo and a possible loss of particles. First, we consider two adjacent output times from the simulation, t_1 and t_2, where $t_1 < t_2$. Each halo at time t_1 is labelled as a progenitor of whichever halo at time t_2 contains the largest fraction of its particles. This process is repeated for all pairs of adjacent output times. It is then straightforward to trace the merger history of each halo which exists at the final output time. Fig. 2.1 shows an example of a merger tree created in this way for a halo with a final mass of about $9 \times 10^{12} h^{-1} M_\odot$, or around 700 particles.

In the semi-analytic model used here, galaxies are assumed to form at the centres of dark matter halos, so the centre of each halo in the merger tree must be defined. We choose to follow Kauffmann et al. (1999a), who identified the most bound dark matter particle as the position of any galaxy which forms in the halo. We define the binding energy of a particle as the sum of its kinetic energy and the gravitational potential energy due to the other particles in the halo. This approach differs from that of Benson, Pearce, Frenk, Baugh & Jenkins (2001), who associated the central galaxy in a halo with the centre of mass. Once a galaxy forms it is assumed to follow this particle until the parent halo merges with another halo and dynamical friction, calculated as described in Cole et al. (2000), causes the galaxy to merge with the central galaxy of the new halo. We therefore check that the most bound particle of a halo remains a member of the same halo as the majority of the halo's constituent particles at the next output time. If this is not so, we choose the most bound particle from those which *are* in the correct halo at the later output time. This problem generally only occurs in smaller halos which may be easily disrupted.

During the construction of the merger trees, we also attempt to deal with the problem mentioned in Section 2.2.1 — the possibility that nearby halos may be artificially linked

by the FOF algorithm. The problem occurs if two halos become temporarily linked by a transient "bridge" of particles which causes the FOF group finder to consider them as a single, large group. When the bridge is later broken, the group splits, leaving the two original halos. Our tree building method would identify the large, joined group as a progenitor of the larger of the two final groups.

These situations are identified by looking for groups at the earlier time t_1 whose particles are shared between two or more groups at the subsequent output time t_2. This indicates that between times t_1 and t_2 the group has split into smaller groups which we refer to here as "fragments".

We split such spuriously joined groups into one new group for each fragment which contains more than N_{min} of its constituent particles. Particles belonging to one of these fragments at time t_2 are assigned to the corresponding new group at the earlier time t_1. Particles belonging to no fragment, or to a fragment with fewer than N_{min} particles from the joined group, are assigned to the new group corresponding to the fragment "closest" to their position at time t_1. The separations used are weighted by a factor $M^{-1/3}$ to account for the spatial extent of the groups, where M is the mass of the fragment.

The splitting procedure is first carried out for halos at the penultimate timestep and then repeated for each earlier output time in order of increasing redshift. For each timestep a modified group catalogue is produced, which is then used to determine whether any halos at the previous timestep need to be split. This ensures that if any bridge between a pair of halos persists for more than one timestep the halos are split at each timestep where the bridge exists.

2.2.3 Mass Conservation

In the GALFORM semi-analytic model of Cole et al. (2000), halos may gain mass through mergers with other halos. The mass of a halo always increases with time, and the difference between the mass of a halo and the sum of the masses of its progenitors is due to the accretion of small, unresolved dark matter halos.

The N-body merger trees may contain halos which decrease in mass from one timestep to the next for the reasons described in Section 2.2.2 — the nature of the definition of a halo imposed by the FOF group finder and the possibility of disruption by tidal forces. Consequently, a halo in a N-body merger tree may be somewhat *less* massive than its progenitors. In the GALFORM model this corresponds to the unphysical situation where a negative amount of mass is accreted in the form of sub-resolution halos.
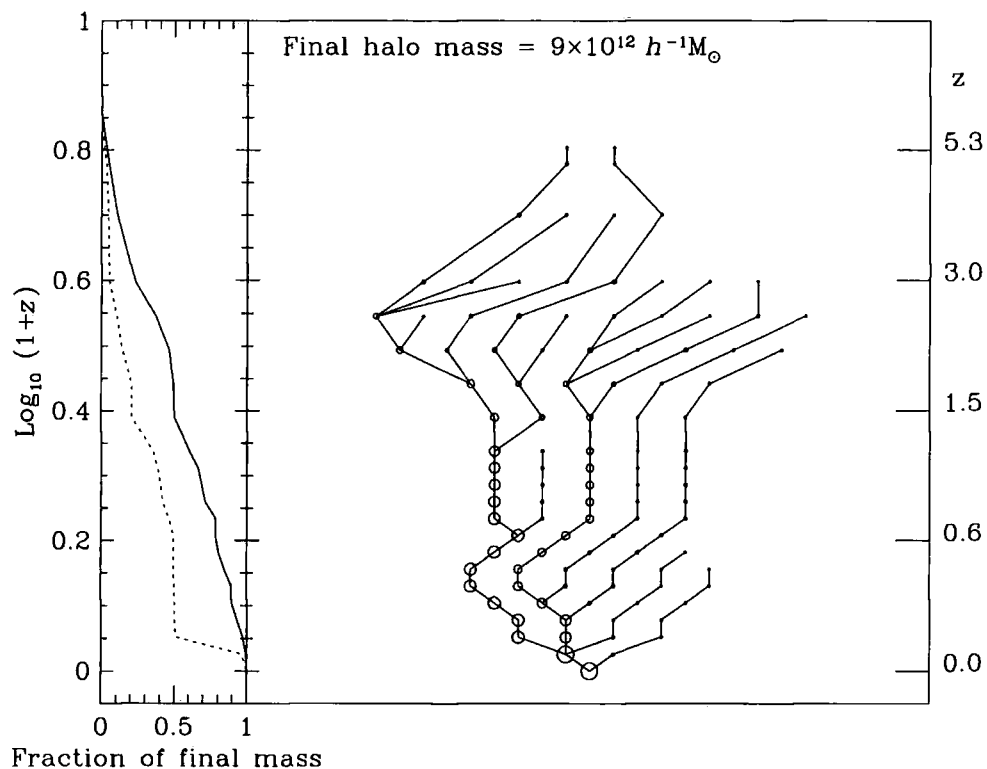
Figure 2.1: An example of a merger tree obtained from the GIF simulation for a halo of mass $9 \times 10^{12} h^{-1} M_\odot$ at redshift $z = 0$. Each circle represents a dark matter halo identified in the simulation, the area of the circle being proportional to the halo mass. The vertical position of each halo on the plot is determined by $\log_{10}(1+z)$ at the redshift at which it exists, the horizontal positioning is arbitrary. The solid lines connect halos to their progenitors. The solid line in the panel on the left-hand side shows the fraction of the final mass contained in resolved progenitors as a function of redshift. The dotted line shows the fraction of the final mass contained in the largest progenitor as a function of redshift.

The solid lines in Fig. 2.2 show the distribution of the ratio $\Sigma M_{prog}/M_{halo}$, where M_{halo} is the mass of a halo and ΣM_{prog} is the total mass of the immediate progenitors of the halo, which exist at the previous timestep. Halos at all timesteps (other than the first) are included. If these merger trees had been created using the technique of Cole et al. (2000), then this ratio would always be less than one. It can be seen from Fig. 2.2 that for halos less massive than about $10^{12}h^{-1}M_{\odot}$ the total mass in the progenitors can occasionally exceed the mass of the halo they form at the next timestep by up to 50%. More massive halos are less affected, but there are still rare instances where the largest halos have progenitors with masses 5-10% greater than the mass of the halo.

Mass conservation can be forced on the N-body merger trees by simply adjusting the masses of some of the halos. Two opposite approaches to the problem are possible. Mass can be added to those halos which are less massive than their progenitors, or mass can be removed from the progenitors themselves. In order to show that the changes made to the halo masses have little effect on the semi-analytic model, we create merger trees using both methods.

Enforcing the conservation of mass in merger trees by adding mass is relatively straightforward. If a halo is less massive than its progenitors, its mass is increased to match that of the progenitors. The halo may, in turn, be a progenitor of a later halo which may now become less massive than its own progenitors. This later halo's mass will then also be increased. Changes made to halo masses at early times may therefore propagate to later times.

Similarly, if mass is removed from a halo to force conservation of mass, it may become less massive than its progenitors and reductions in mass could then propagate to earlier times. We attempt to remove mass in such a way as to minimize the effects on earlier halos. Each halo has a certain amount of "excess" mass beyond that of its progenitors, which was accreted over the last timestep in the form of sub-resolution objects. This mass, if it exists, may be removed without the change propagating to earlier halos. When a halo which is less massive than its progenitors is found, mass is first removed from the excess mass of the largest progenitor. If still more mass must be removed, it is taken from the excess mass of the other progenitors in decreasing order of mass. If all of the excess mass of the progenitors is removed and yet more mass needs to be taken away, the masses of all of the progenitor halos are simply scaled down by a constant factor.

The dotted lines in Fig. 2.2 show the sizes of the changes we are forced to make when we enforce mass conservation by adding mass to halos. These lines show the distribution
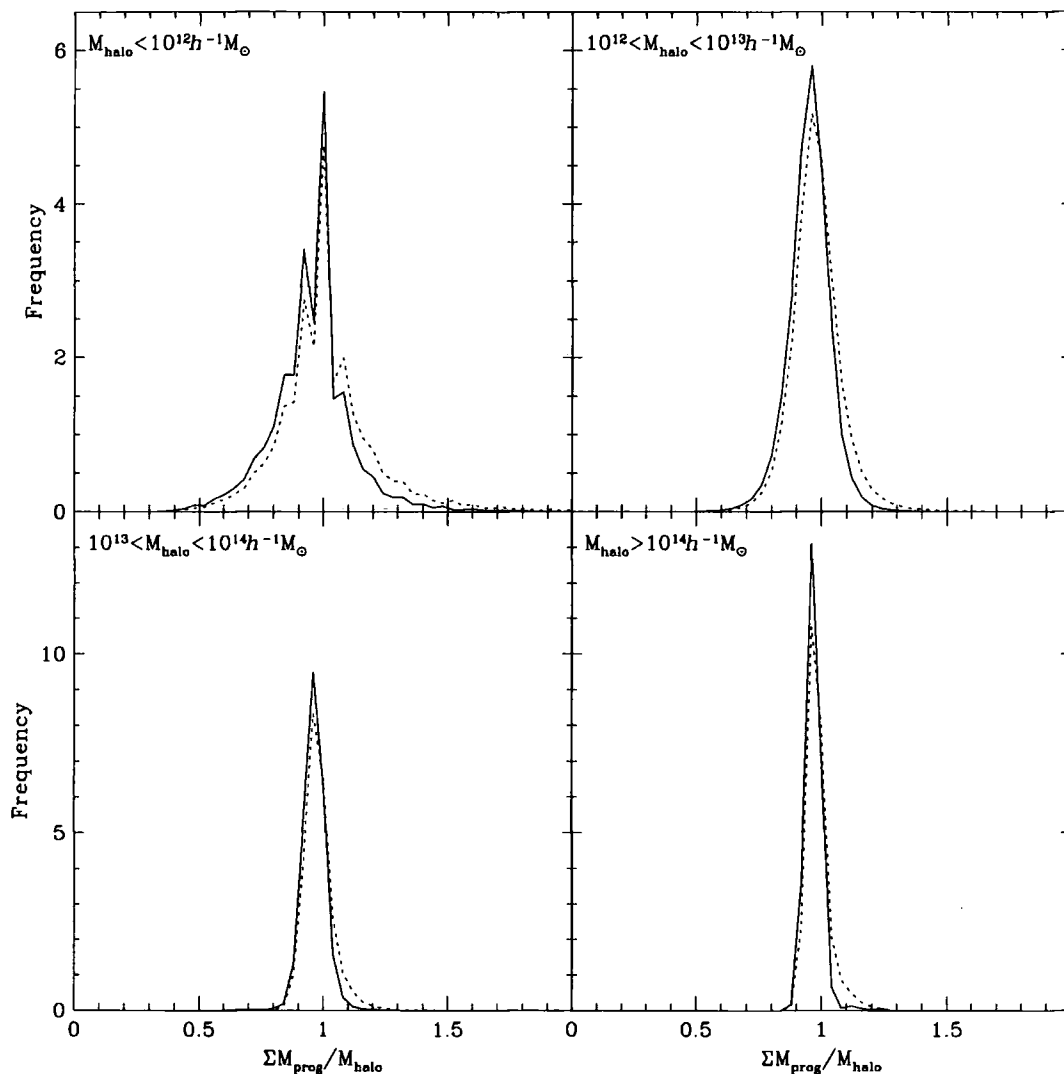
Figure 2.2: The solid lines show the distribution of the ratio of the total mass of the immediate progenitors of a halo, ΣM_{prog}, to the mass of the halo at the next timestep, M_{halo}. Each panel shows the distribution of $\Sigma M_{prog}/M_{halo}$ for halos in the mass range shown at the top of the panel. The dotted lines show the distribution of $\Sigma M_{prog}/M_{halo}$ if ΣM_{prog} is evaluated after the progenitors have been increased in mass to at least the total mass of *their* progenitors. Where this ratio is greater than 1, it is the factor by which M_{halo} must be changed to ensure mass conservation if we choose to add mass.

of the ratio $\Sigma M_{prog}/M_{halo}$ if ΣM_{prog} is evaluated after the progenitors of the halo at all previous timesteps have been made at least as massive as their own progenitors. M_{halo} is still the original halo mass. Where this ratio exceeds 1, it is the factor by which M_{halo} must be scaled to ensure that the halo is at least as massive as its progenitors. It can be seen that the required changes to individual halos are generally small, and adjustments are required much less frequently in well resolved halos. However, the masses of a minority of halos are affected quite significantly and it is necessary to show that these changes do not affect the galaxy population predicted by the semi-analytic model. The algorithms described above are two opposite ways of dealing with the problem of mass conservation in the merger trees. While artificially altering the halo masses is clearly not ideal, if, as is the case, both methods produce very similar results when the merger trees are fed into the semi-analytic model we can then conclude that the changes we have made are insignificant. This comparison is carried out in Section 2.3.3.

2.3   Comparison between GALFORM and N-body GAL-FORM

In this section we describe our semi-analytic model, indicating how it differs from the model of Cole et al. (2000) on which it is based. We also explain how merger trees obtained from a simulation may be incorporated into the model.

2.3.1   The N-body GALFORM model

We use the GALFORM semi-analytic model to treat the process of galaxy formation within the dark matter halos in the GIF simulation. The model is described in detail by Cole et al. (2000) so here we present only a brief description of features that are important to this work. The original model of Cole et al. will be referred to as "standard GALFORM", and the version using merger trees taken from a simulation will be referred to as "N-body GALFORM".

The starting point for the standard GALFORM model is a set of merger trees created using a Monte-Carlo technique. The history of each halo is divided into a number of discrete timesteps. Extended Press-Schechter theory is used to estimate the probability that a halo "fragments" into two progenitors when a step back in time of size δt is taken. The masses of the fragments are chosen at random from a distribution consistent with extended Press-Schechter theory. Halos are repeatedly split in this way to create merger

trees. A mass resolution limit is imposed on the merger trees, below which progenitors are considered to be material acquired through continuous accretion. The mass resolution is normally set sufficiently high that the results of interest are not sensitive to its value. In the N-body GALFORM model, we replace these merger trees with those calculated directly from the GIF simulation as described in Section 2.2.2. The mass resolution limit is then determined by the mass of the smallest halo which can be resolved in the simulation.

The dark matter halos in the merger tree are assumed to be spherically symmetric with the radial density profile of Navarro et al. (1996):

$$\rho(r) \propto \frac{1}{r/r_{\rm NFW}(r/r_{\rm NFW} + 1)^2},$$
(2.1)

where $r_{\rm NFW}$ is the scale radius of the halo and is related to the concentration parameter, c, defined by Navarro et al. (1997) through $r_{\rm NFW} = r_{200}/c$, where r_{200} is the radius within which the mean density of the enclosed material is 200 times the critical density required for a closed universe. Note that we choose to define the virial radius of a halo, $r_{\rm virial}$, to be the radius within which the mean density is $\Delta_{\rm virial}$ times the critical density, where $\Delta_{\rm virial}$ is the virial overdensity obtained from the spherical collapse model. The concentration parameter is set using the method described in the appendix of Navarro et al. (1997), but adapted to our definition of the virial radius. We do not allow for any scatter in the concentration parameter as a function of halo mass.

Our treatment of the cooling of gas within halos is identical to that of Cole et al. (2000). Initially, the amount of gas in each halo is taken to be equal to the mass of the halo times the universal baryon fraction. The gas is assumed to be shock-heated to the virial temperature of the halo when it forms. We assume that the radial density profile of the gas is given by

$$\rho_{\rm gas}(r) \propto 1/(r^2 + r_{\rm core}^2),$$
(2.2)

where the core radius is given by $r_{\rm core}/r_{\rm NFW} \approx 1/3$ in accordance with the simulations of Navarro et al. (1995). This core radius is allowed to grow with time from an initial value, $r_{\rm core}^0$, as gas is removed by cooling in order to maintain the same gas density at the virial radius. This ensures that the pressure at the virial radius, which would be maintained by shocks from infalling material, remains unchanged.

To determine the rate at which gas can cool and form a disk at the centre of the halo, the cooling time of the gas is calculated as a function of radius using the cooling function of Sutherland & Dopita (1993). Gas which has had time to cool and fall to the centre of the halo is added to the disk where it is available to form stars.

When halos merge, the most massive galaxy becomes the central galaxy in the new halo. The resolution of the simulations used here is insufficient to follow the evolution of substructure within the dark matter halos. Instead, the dynamical friction time scale, as defined by Lacey & Cole (1993), is used to determine when each satellite will merge on to the central galaxy. It should be noted at this point that the orbital parameters used to determine the dynamical friction time for each galaxy are assigned at random from a distribution consistent with the numerical results of Tormen (1997), even when using merger trees obtained from the simulation.

2.3.2   Parameters in the N-body GALFORM model

The GALFORM semi-analytic model requires a number of parameters to be specified, which can be divided into three categories. There are numerical parameters, parameters describing the background cosmology and parameters which describe the physical model of galaxy formation.

The numerical parameters are the mass resolution, M_{res}, the number of timesteps in the merger tree and the starting redshift. In the N-body GALFORM model these are all constrained by the properties of the simulation used to obtain the merger trees. The mass resolution is the mass of the smallest halo which our group finding algorithm can resolve, there is one timestep for each simulation output and the starting redshift is the redshift of the first output. The cosmological parameters Ω_0, Λ_0, h, σ_8, Γ and, in the case of a simulation with a baryonic component, Ω_b, are also fixed by the simulation.

The remaining parameters allow us to vary the treatment of the processes involved in galaxy formation. The parameters we are interested in are:

- r^0_{core}: the initial size of the core in the radial gas density profile, specified in terms of r_{NFW} (see eqn. 2.2).

- The evolution of r_{core} with time. The radius r_{core} may be a fixed fraction of r_{NFW} or it may be allowed to increase with time as described in Section 2.3.1

- f_{df}: A factor by which the dynamical friction time scale for a satellite galaxy, which is used to determine when the galaxy merges with the central galaxy of the halo, may be scaled. Increasing f_{df} reduces the rate at which galaxy mergers occur within halos.

The other parameters in the model are the same as those in the reference model of Cole et al. (2000), with the following minor changes: $v_{hot} = 250 \mathrm{kms}^{-1}$ and $f_{ellip} = 0.5$.

The parameter v_{hot} determines the efficiency with which energy injection from supernovae and young stars reheats and ejects cold gas from galactic disks. The parameter f_{ellip} is used to decide the outcome of mergers between central and satellite galaxies. If the ratio of the mass of the satellite to the mass of the central galaxy is greater than f_{ellip}, any gas in the disks of the two galaxies is converted into stars and an elliptical galaxy is produced. If the ratio is smaller than f_{ellip}, any stars present in the satellite are added to the bulge of the central galaxy and any gas is added to the disk. These changes to the Cole et al. model are required to obtain a realistic luminosity function at $z = 0$ with the higher baryon density, $\Omega_b = 0.038$, which we use here.

Our prescription for star formation differs slightly from that of Cole et al. In our model, the time scale for star formation is given by

$$\tau_* = \tau_*^0 (V_{disk}/200\mathrm{km\,s^{-1}})^{\alpha_*}, \tag{2.3}$$

where V_{disk} is the circular velocity of the galaxy disk and the time scale, τ_*^0, is set to 3Gyr. We set $\alpha_* = -2.5$. The way τ_* scales with redshift in this model results in reduced star formation and more gas rich mergers at high redshift and has been shown (Lacey et al. 2002) to better reproduce the properties of SCUBA and Lyman break galaxies. Kauffmann & Haehnelt (2000) also find that a star formation scheme with an increased star formation timescale at high redshift is required to reproduce observations of damped Lyα absorption systems and the increase in number density of bright quasars from $z = 0$ to $z = 2$. It should also be noted that, for the purposes of this comparison, the details of our star formation prescription are not critical, since the same scheme is used in both the standard and N-body GALFORM models.

2.3.3 Effects of mass conservation

The upper panels of Fig. 2.3 show the galaxy luminosity functions in the b_J and K bands predicted by the N-body GALFORM model with the parameters of Section 2.3.2, using the two different methods described in Section 2.2.3 to enforce mass conservation in the merger trees. Over most of the luminosity range plotted, the two curves are essentially identical but there appear to be more galaxies at very faint b_J magnitudes when mass is removed from the merger trees. The majority of these galaxies formed in halos near the 10 particle ($\simeq 1.4 \times 10^{11} h^{-1} M_\odot$) mass resolution limit imposed by the FOF group finder and their halos subsequently merged with other, larger dark matter halos. When mass conservation is enforced by removing mass from the merger trees (the dotted lines in

Fig. 2.3) it is possible to end up with some halos with mass less than the resolution limit which can harbour galaxies with b_J band magnitudes around -14 or fainter. If, instead, mass is added to halos less massive than their progenitors, then the merger trees contain no halos with masses below the FOF resolution threshold and hence fewer faint galaxies.

These sub-resolution halos often exist in the merger trees of larger halos and could affect the evolution of larger, brighter galaxies. However, the agreement of the luminosity functions suggests that any effect is insignificant. The global star formation history and Tully-Fisher relation shown in the lower panels of Fig. 2.3 are similarly unaffected.

Overall, the choice of mass conservation method appears to make very little difference to the quantities plotted in Fig. 2.3, which suggests that the small amounts of mass being added to or removed from the merger trees do not significantly affect the properties of the resulting galaxies. The only region of the luminosity function which is affected is largely populated by galaxies which formed in halos with little or no resolved merger history, where the model cannot be expected to give reliable results. For the remainder of this Chapter we choose to enforce mass conservation by adding mass to the merger trees since this does not introduce halos with masses below the resolution limit.

2.3.4 Comparison with standard GALFORM

The mass resolution of the merger trees taken from the GIF simulation is equal to 10 particle masses or $1.4 \times 10^{11} h^{-1} M_\odot$, i.e. $N_{min} = 10$. This is much larger than the mass resolution, $M_{res} = 5.0 \times 10^9 h^{-1} M_\odot$, used by Cole et al. (2000). This will clearly affect the properties of the galaxies predicted by the N-body GALFORM model, since gas will be unable to cool and start forming stars until lower redshifts when halos with masses greater than M_{res} have formed. In order to investigate the effect of limited mass resolution on the N-body GALFORM model, we identify the properties of the merger trees which differ between standard and N-body GALFORM and use this knowledge to produce a modified version of the standard GALFORM model which reproduces the behaviour of the N-body GALFORM model. We can then increase the mass resolution of the merger trees in the modified model and observe the effects on the predicted galaxy properties.

There are four main reasons why the merger trees in the two models may differ. Firstly, there is the difference in mass resolution described above. Therefore, we initially degrade the mass resolution of the standard GALFORM model to match that of the GIF simulation by setting the minimum halo mass, M_{res}, equal to the mass of $(N_{min} - 1)$ dark matter particles — any halo of this mass or less in the N-body simulation would not be
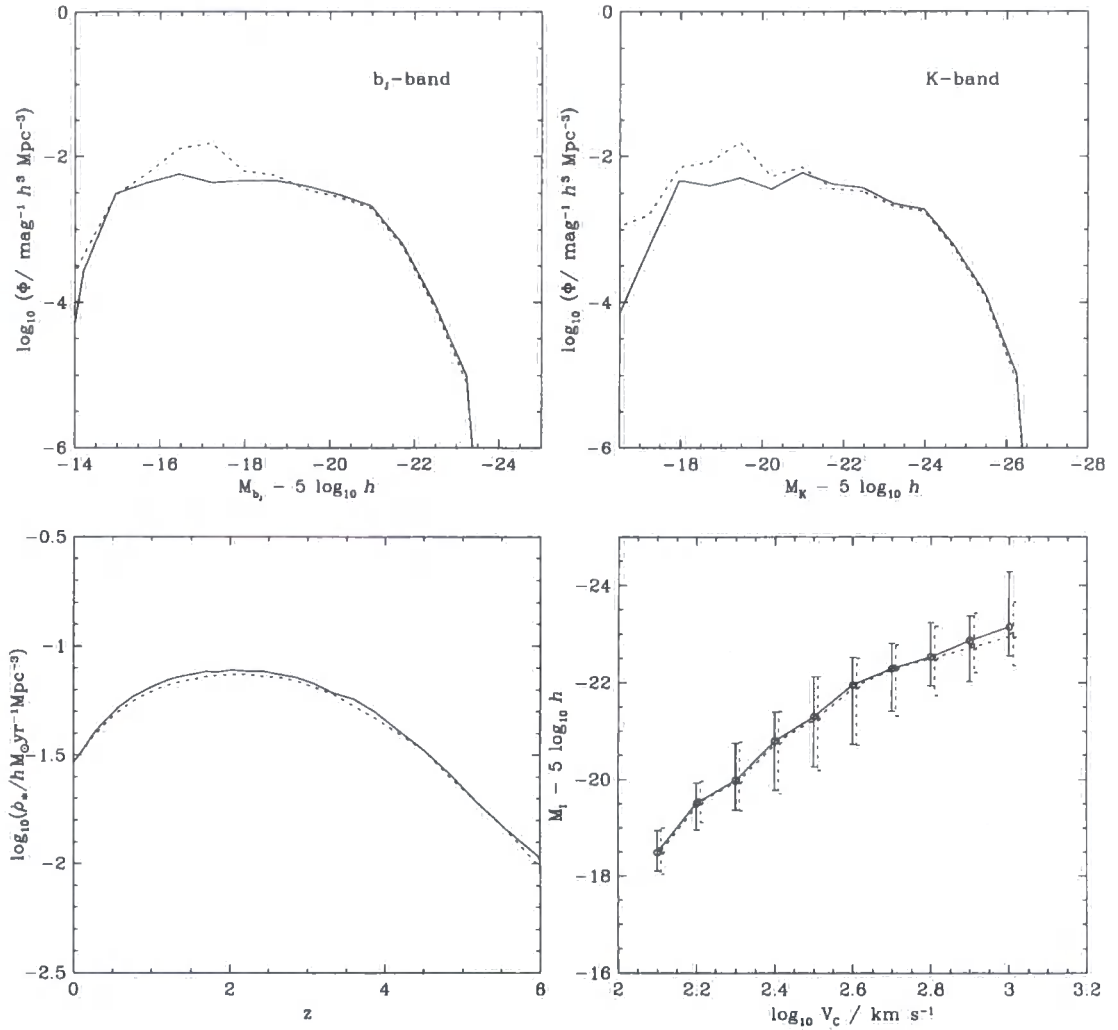
Figure 2.3: Luminosity functions, star formation histories and Tully-Fisher relations for galaxies predicted by the N-body GALFORM model using merger trees obtained from the GIF simulation with two different methods of enforcing mass conservation. The solid lines show results obtained when mass conservation in the merger trees is enforced by increasing the masses of halos less massive than their progenitors. The dotted lines show the results obtained if, instead, the masses of the progenitors of such halos are reduced.

identified by the FOF group finder and would not be included in the N-body merger trees.

Secondly, Jenkins et al. (2001) have shown that the Press & Schechter (1974) halo mass function (used in the standard GALFORM model) differs somewhat from the mass function determined from N-body simulations. We replace the Press-Schechter mass function in the standard GALFORM model with the mass function determined by Jenkins et al. This ensures that the distribution of halo masses at $z = 0$ in the standard GALFORM model matches the distribution in the simulation.

The number of timesteps also differs between the two models. In the standard GAL-FORM model we use 150 timesteps evenly spaced in $\log_{10}(1 + z)$, whereas in the N-body case we have only 44 simulation outputs. However, we find that if we degrade the time resolution of the standard GALFORM model to match that of the N-body model the properties of the galaxy populations predicted change very little.

Finally, the distribution of progenitor masses for halos of a given mass predicted by the standard GALFORM model does not reproduce the distribution found in N-body simulations with complete accuracy. Benson, Pearce, Frenk, Baugh & Jenkins (2001) show that an empirical correction can be used to bring the progenitor mass distributions in the semi-analytic and N-body merger trees into closer agreement. The threshold linear overdensity for collapse from the spherical collapse model, δ_c, is replaced with an effective threshold $\delta_c^{\text{eff}} = f_{\delta_c}\delta_c$. In the ΛCDM cosmology employed in the GIF simulation, the following form for f_{δ_c} was found by Benson et al. to give reasonable agreement between the progenitor mass functions between redshifts 0 and 3:

$$f_{\delta_c} = 1 + 0.14[\log_{10}(M_{\text{halo}}/h^{-1}M_\odot) - 15.64], \tag{2.4}$$

where M_{halo} is the mass of the final halo at redshift $z = 0$. This form of modification was suggested by Tormen (1998).

These modifications are intended to produce semi-analytic merger trees with statistical properties closely matched to those of the N-body merger trees. Fig. 2.4 shows the galaxy luminosity functions in the b_J and K bands, Tully-Fisher relations and global star formation histories for both the modified GALFORM model described above (dotted lines) and the N-body GALFORM model (dashed lines). It can be seen from the figure that these two models predict populations of galaxies with very similar statistical properties. The luminosity functions are in reasonable agreement for K brighter than about -18 and b_J brighter than about -15. The Tully-Fisher relations and star formation histories are also in close agreement.

As pointed out previously, the fainter galaxies in these models occupy halos with very poorly resolved merger histories and their properties may be largely determined by the effects of limited mass resolution. The solid lines in Fig. 2.4 show the properties of the galaxies in the modified GALFORM model when the minimum halo mass M_{res} is reduced to $5.0 \times 10^9 h^{-1} M_\odot$. This is much less massive than the smallest halo Benson et al. were able to resolve in their simulations and consequently, in this regime, eqn. (2.4) has not been tested and cannot be relied upon to produce a realistic distribution of progenitor masses. We do not expect this model to reproduce the results of Cole et al. but we show it only to provide some indication of the magnitude of the effect of introducing low mass halos into the merger trees.

This "improvement" in mass resolution increases the number of faint galaxies, which form in small, previously unresolved halos. With a higher minimum halo mass the gas in these small halos is unable to cool until it becomes incorporated into objects more massive than M_{res}. This is reflected in the luminosity functions which show that there are slightly more bright galaxies and far fewer faint galaxies at $z = 0$ in the model with poor mass resolution. The star formation history is consistent with this, showing that poor mass resolution results in reduced star formation at $z > 1$ and increased star formation at $z \approx 0$. However, calculating the global star formation rate involves a sum over all halos. At high redshifts this includes a large number of halos of low mass whose abundances may be unrealistic due to our extrapolation of eqn. (2.4). Reducing M_{res} appears to have little or no effect on the Tully-Fisher plot.

Overall, the predictions of the N-body GALFORM model closely match those of the standard GALFORM model when we take into account the differences in the halo mass function, the progenitor mass distribution and the mass resolution. The differences between the modified GALFORM models with high and low mass resolution indicate that, at low luminosities, the properties of the galaxies in the N-body model are seriously affected by the resolution of the simulation. In order to attempt accurately to reproduce the properties of observed galaxy populations with b_J band magnitudes fainter than about -17, an N-body simulation with significantly improved mass resolution would be required.

2.4 Conclusions

In this Chapter we have examined how the statistical properties of the galaxies predicted by a semi-analytic model depend on the way in which the dark matter halo merger
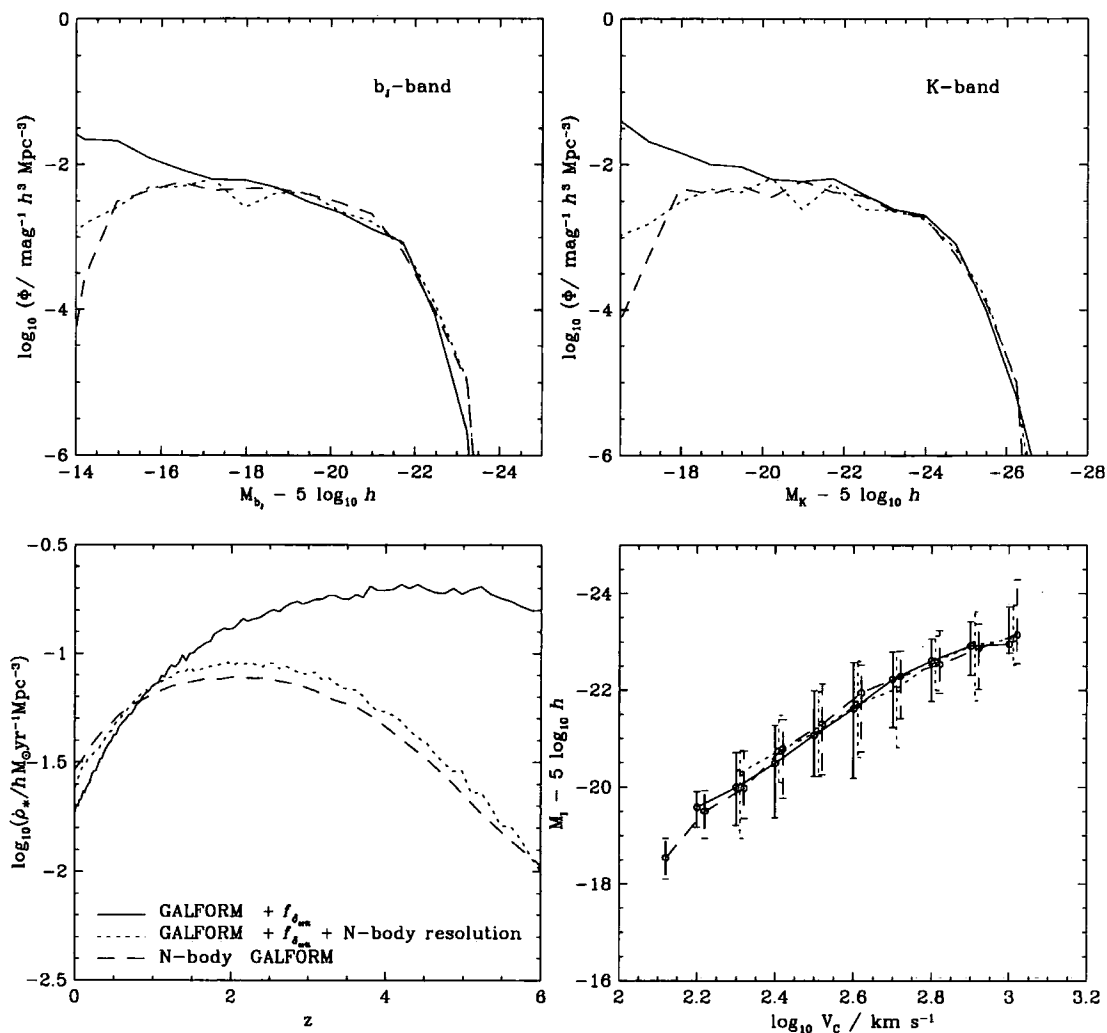
Figure 2.4: Luminosity functions, star formation histories and Tully-Fisher relations for three different models. The solid lines correspond to the GALFORM model using Monte Carlo generated merger trees, with the modifications explained in the text and a mass resolution of $5 \times 10^9 h^{-1} M_\odot$. The dotted lines show results from the same model with a mass resolution of $1.4 \times 10^{11} h^{-1} M_\odot$, equivalent to that of the GIF simulation. The dashed lines show results obtained from the N-body GALFORM model which uses merger trees derived from the simulation.

histories are created. We have developed a method for calculating merger histories from N-body simulations and used the resulting merger trees in a semi-analytic model of galaxy formation based on that of Cole et al. (2000). We refer to this model as N-body GALFORM and compare it to an otherwise identical "standard GALFORM " model, which uses halo merger histories generated using the Monte-Carlo algorithm of Cole et al. This algorithm is based on the extended Press-Schechter (EPS) theory.

We find that in a significant number of cases, halos in the N-body merger trees are less massive than their progenitors at the previous timestep. When this happens we are forced artificially to adjust the masses of the halo or its progenitors, since in our semi-analytic galaxy formation model halos may not lose mass. However, the luminosity function, Tully-Fisher relation and global star formation history of the galaxies predicted by the semi-analytic model remain almost exactly the same whether we add mass to the halo or remove mass from the progenitors when we encounter this problem. We conclude that the changes we are forced to make to the halo masses have very little effect on the semi-analytic model.

If the mass resolution in the standard GALFORM model is degraded to that of the N-body simulation and the empirical fit of Benson, Pearce, Frenk, Baugh & Jenkins (2001) is used to correct the distribution of halo progenitor masses, we obtain luminosity functions and Tully-Fisher relations in very good agreement with the N-body GALFORM model. This shows that, apart from the issue of mass resolution, the only significant statistical differences between the N-body merger trees and those of Cole et al. are due to the known discrepancy between EPS theory and the results of N-body simulations.

By improving the mass resolution in the standard GALFORM model to that used by Cole et al. we were able to obtain an indication of the effects of limited mass resolution on the N-body model. The mass resolution in the N-body merger trees is imposed by the particle mass in the GIF simulation, since halos with fewer than 10 particles $(1.4 \times 10^{11} h^{-1} M_\odot)$ are not resolved. This limitation has a noticeable effect on the galaxy luminosity function and we find slightly more very bright galaxies, since gas may only cool in resolved halos. If only massive halos are resolved, cooling is delayed resulting in brighter galaxies at $z = 0$. However, the most obvious effect of poor mass resolution is a drastic reduction in the number of galaxies with b_J magnitudes fainter than about -17. This demonstrates that the mass resolution of the GIF simulation is insufficient to make reliable predictions at these magnitudes. At brighter magnitudes the luminosity functions remain in good agreement.

In conclusion, when used as the starting point for semi-analytic modelling of galaxy formation, merger trees taken from an N-body simulation using the technique described here result in similar galaxy populations to those obtained using the (slightly modified) Monte-Carlo algorithm of Cole et al. This supports the reliability of our method and provides a means to populate large cosmological N-body simulations with semi-analytic galaxies at a fraction of the computational cost of a hydrodynamic simulation of the same volume. When applied to the dark matter component of an Smooth Particle Hydrodynamics (SPH) simulation, our model will also allow us to compare SPH and semi-analytic treatments of galaxy formation, and in particular the cooling of gas within halos, on a halo-by-halo basis. This comparison is reported in the next Chapter.

Chapter 3

Gas Dynamics in SPH and Semi-analytic Models of Galaxy Formation

3.1 Introduction

A range of physical processes are responsible for the formation and evolution of the galaxies we see in the universe today. The starting point for current hierarchical cold dark matter models of galaxy formation is the gravitational amplification and eventual collapse of primordial density fluctuations to form the dark matter halos in which stars and galaxies may form. This process is now quite well understood, and predictions of halo mass functions from analytic techniques such as Press-Schechter theory (Press & Schechter 1974) and its extensions (Bond et al. 1991, Bower 1991, Lacey & Cole 1993, Sheth et al. 2001) are in good agreement with numerical simulations (e.g. Gross et al. 1998, Governato et al. 1999, Jenkins et al. 2001).

Unfortunately, the behaviour of the baryonic component of the universe is more complex and less well understood. While the dynamics of the dark matter are determined by gravitational forces alone, gas is subject to hydrodynamical forces and radiative effects. The situation is further complicated by the absence of a complete theory of star formation and the fact that star formation involves length and mass scales many orders of magnitude smaller than the galaxies themselves forces those modelling galaxy formation to resort to recipes and prescriptions to obtain star formation rates. Nevertheless, semi-analytic models have met with considerable success, for example in reproducing the local field galaxy luminosity function and distributions of colour and morphology (e.g. Cole 1991, Cole et al. 1994, Cole et al. 2000, White & Frenk 1991, Lacey & Silk 1991, Somerville &

Primack 1999) and galaxy clustering properties (e.g. Kauffmann et al. 1999a, Benson et al. 2000, Wechsler et al. 2001). In this Chapter, we compare two possible ways of modelling the process which provides the raw material for star formation – the cooling of gas within dark matter halos. Such a model is a necessary part of almost any treatment of the hierarchical formation of galaxies, yet there is still some uncertainty as to which of the approaches currently in use are reliable and whether they are in good agreement.

While Eulerian numerical techniques may be employed in the modelling of galaxy formation in cosmological volumes (e.g. Cen & Ostriker 2000), here we concentrate on the Lagrangian method known as smoothed particle hydrodynamics (SPH), first described by Lucy (1977) and Gingold & Monaghan (1977). SPH simulations have been able to predict the formation of objects of approximately galactic mass with appropriate abundances in a cosmological context (e.g. Katz et al. 1992, Navarro & White 1993, Evrard et al. 1994, Steinmetz & Muller 1995, Katz et al. 1996, Frenk et al. 1996, Steinmetz & Navarro 1999, Pearce et al. 1999, Pearce et al. 2001) and allow the investigation of the dynamics of galaxies within clusters and the spatial distribution of galaxies.

Semi-analytic and SPH galaxy formation models rely on very different sets of assumptions and approximations. For example, semi-analytic models assume that dark matter halos are spherically symmetric and that infalling gas is shock-heated to the virial temperature of the halo, whereas SPH simulations impose no restrictions on halo geometry but assume that continuous distributions of gas and dark matter may be well represented by a limited number of discrete particles. Consequently, SPH and semi-analytic models have complementary strengths and weaknesses. Semi-analytic models are computationally much cheaper than simulations, which allows extremely high mass resolution in halo merger trees and more thorough investigation of the effects of varying parameters or the treatment of particular processes. SPH simulations contain fewer simplifying assumptions but have limited dynamic range and without sufficiently large numbers of particles may suffer from numerical effects.

The aim of this Chapter is to compare SPH and semi-analytic treatments of the gas dynamics involved in galaxy formation in order to gauge the effects of the uncertainties present in the two techniques. A previous comparison carried out by Benson, Pearce, Frenk, Baugh & Jenkins (2001) found that SPH and semi-analytic models give similar results for the thermodynamic evolution of cooling gas in cosmological volumes. In particular, the global fractions of hot gas, cold dense gas and uncollapsed gas agreed to within 25% and the mass of gas in galaxies in the most massive halos differed by no

more than 50%. However, their analysis was restricted to a statistical comparison because their semi-analytic model employed merger histories created using a Monte-Carlo algorithm, that of Cole et al. (2000). We improve on the work of Benson et al. by calculating the merger trees directly from the simulations so that the merger histories of the halos in the semi-analytic and SPH treatments are the same. This removes a source of uncertainty from the comparison, since any differences between the models must be due entirely to differences in the treatment of the *baryonic* component. Our method also allows a comparison between halos on an individual basis and lets us investigate whether the dependence of the cold gas mass on the halo's merger history is the same in the SPH and semi-analytic cases.

Our approach is that of "modelling a model", using a semi-analytic model to reproduce the behaviour of the simulation including the effects of limited mass resolution. Since we are interested primarily in the rate at which cooling occurs in the two models, we use a simulation which allows radiative cooling but which does not include any prescription for star formation or feedback. We attempt to model this simulation using a "stripped down" semi-analytic model which also neglects these phenomena. Hierarchical models of galaxy formation without feedback predict that most of the gas in the universe cools in low mass objects at high redshift (e.g. White & Rees 1978, Cole 1991, White & Frenk 1991). Consequently, we cannot expect either our SPH simulation or our stripped down semi-analytic model to cool realistic quantities of gas, and where differences between the two approaches are found it may not be possible to conclude that one is more "correct" than the other. However, the changes which must be made to the semi-analytic model to match the SPH simulation may provide insight into the level of agreement between the two techniques and the reasons for any discrepancies.

The layout of this Chapter is as follows. In Section 3.2 we describe our semi-analytic model and give details of the SPH simulation we use. In Section 3.3 we compare properties of the two models, including galaxy masses, cold gas mass in halos as a function of redshift and the spatial distribution of the galaxies. In Section 3.4 we present our conclusions.

3.2   The Models

3.2.1   The SPH Simulation

SPH is a Lagrangian numerical method which follows the motion of a set of gas elements represented by discrete particles. The thermal energy and velocity of each particle are

known at any given time and each particle has a fixed mass. Properties of the gas at the position of a particle can be estimated by smoothing these quantities over the N_{SPH} nearest neighbouring particles. The gas properties are then used to calculate the forces acting on each particle in order to update the positions and velocities. In cosmological simulations both dark matter and gas particles are included and the particles are initially distributed in a manner consistent with a cosmological power spectrum. If the process of galaxy formation is to be simulated then radiative cooling of the gas must also be included.

The SPH simulation used here was performed using the Hydra code. This particular implementation includes a modification, described by Pearce et al. (2001), to prevent the rate of cooling of hot gas being artificially increased by nearby clumps of cold, dense gas, or "galaxies". Any gas hotter than 10^5K is assumed not to interact with gas at temperatures below 12 000K. Thus, for cooling purposes the density estimate for a hot particle near a galaxy is based only on the neighbouring hot particles and the cooling rate is unaffected by the presence of the galaxy.

The simulation has 80^3 gas and 80^3 dark matter particles with individual masses of $2.57 \times 10^9 h^{-1} M_{\odot}$ and $2.37 \times 10^{10} h^{-1} M_{\odot}$ respectively, contained in a cube of side $50 h^{-1}$Mpc. The power spectrum is that appropriate to a cold dark matter universe with the following parameter values: mean mass density parameter $\Omega_0 = 0.35$, cosmological constant $\Lambda_0 = 0.65$, baryon density parameter $\Omega_b = 0.0377$, Hubble constant $h = 0.71$, power spectrum shape parameter $\Gamma = 0.21$ and rms linear fluctuation amplitude $\sigma_8 = 0.90$. The gravitational softening length is $25 h^{-1}$kpc, fixed in physical coordinates.

The metallicity of the gas in the simulation, measured in terms of the mass fraction of metals, Z, is uniform and varies linearly with time according to:

$$Z = 0.3 Z_{\odot} \, t(z)/t_0, \tag{3.1}$$

where $Z_{\odot}$ denotes the solar metallicity, $t(z)$ is the age of the universe at redshift z and t_0 is the age of the universe at $z = 0$.

This simulation makes no attempt to treat star formation and does not include any heating or feedback processes.

3.2.2   The Semi-analytic Model

The semi-analytic model used here is the N-body GALFORM model described in the previous Chapter. The model uses the output from an N-body simulation to calculate halo

merger histories and semi-analytic techniques to model baryonic processes. Briefly, halo merger trees are constructed by identifying halos at each simulation output time using the friends-of-friends (FOF) algorithm of Davis et al. (1985). Each halo at each output time is identified as a progenitor of whichever halo contains the largest fraction of its mass at the next output time. The merger history of each halo at the final time can then be traced back. Semi-analytic techniques are used to treat the shock heating of gas during the formation of a halo, the cooling of gas within halos and, in the general case, the formation of stars and the merging of galaxies within halos. The full model predicts a wide range of galaxy properties including luminosity, stellar masses of the bulge and disk components and cold gas mass. Galaxy positions can be obtained since each galaxy is associated with a particle in the N-body simulation. Initially, this will be taken to be the most bound particle of the halo in which the galaxy formed, but if the galaxy subsequently merges with the central galaxy of another halo it will be associated with the most bound particle of that halo.

In order to allow a direct comparison between the predictions of this model and those of the SPH simulation, the merger trees must be calculated from the dark matter component of the SPH simulation. Consequently, the time and mass resolution in the halo merger trees are determined by the properties of the SPH simulation and differ from the time and mass resolution of the simulation employed by Helly et al. We have a total of 61 outputs from the SPH simulation, the first 26 of which are logarithmically spaced in expansion factor between redshifts $z \sim 10$ and $z \sim 1.5$. The remaining outputs are equally spaced in time between $z \sim 1.5$ and $z = 0$. This is something of an improvement in time resolution over the GIF simulation used in the previous Chapter. However, the predictions of the GALFORM model were not significantly affected when the number of timesteps was increased, so we do not expect this difference to be important.

There are two parameters which we vary in order to model the SPH simulation. The N-body GALFORM model assumes that the distribution of mass in dark matter halos is described by the radial density profile found by Navarro et al. (1996). This profile contains a single free parameter, which can be expressed as the concentration parameter, c, defined by Navarro, Frenk & White or a halo scale radius, $r_{NFW} = r_{200}/c$, where r_{200} is the radius within which the mean density is 200 times the critical density for a closed universe. Like Cole et al. (2000), we set r_{NFW} using the method described in the appendix of Navarro et al. (1997). No scatter is included in the scale radius as a function of halo mass. The radial density profile we assume for the hot gas within halos is given by Eqn. 2.2. This

profile also contains one parameter, the core radius r_{core}, which we specify as a fraction of r_{NFW} and may be held at a fixed value or allowed to increase with time from an initial value r_{core}^0.

We also allow ourselves the freedom to vary the rate at which mergers occur between galaxies in the same dark matter halo. This is specified in terms of a merger timescale parameter, f_{df}, which is a prefactor in the standard dynamical friction timescale. Reducing f_{df} increases the rate at which mergers occur. See Cole et al. (2000) for details of the merger scheme we use.

3.3 Comparison between SPH and N-body GALFORM

In this section we compare the results of the SPH simulation with the N-body GALFORM model, which uses merger trees derived from the dark matter component of the SPH simulation. Fig. 3.1 shows the positions and masses of the galaxies which form in a $5h^{-1}$Mpc thick region in both the SPH simulation and N-body GALFORM . The SPH "galaxies" (i.e. clumps of cold gas) shown here were identified using a FOF group finder on gas particles with temperatures between 8 000 and 12 000K (see Section 3.3.1).

3.3.1 Modelling SPH with N-body GALFORM

In order to produce a semi-analytic model of the SPH gas simulation using N-body GAL-FORM we must first remove the treatment of star formation, feedback and chemical enrichment from GALFORM. We set the metallicity of the gas to be the same as that in the simulation, using eqn. (3.1).

The cooling rate of the gas in our simulation depends on its density, which is estimated by searching for the N_{SPH} nearest neighbours. The density of gas in halos with less than $N_{SPH} = 32$ gas particles, or a total gas mass less than $8.2 \times 10^{10}h^{-1}M_\odot$, will in general be severely underestimated with an associated suppression of the cooling rate. Consequently, the mass of gas which cools is dependent on the particle mass.

In order to model this effect in the semi-analytic treatment, we first investigate the variation of the mean estimated density of gas in halos in the SPH simulation with halo mass. A characteristic volume for each gas particle can be obtained by dividing its mass by its SPH density estimate. The total volume of the gas in a halo is calculated by summing the volumes of its constituent gas particles. The total volume is then divided by the mass of gas in the halo to obtain an estimate of the mean gas density. Fig. 3.2 shows

SPH

Galform
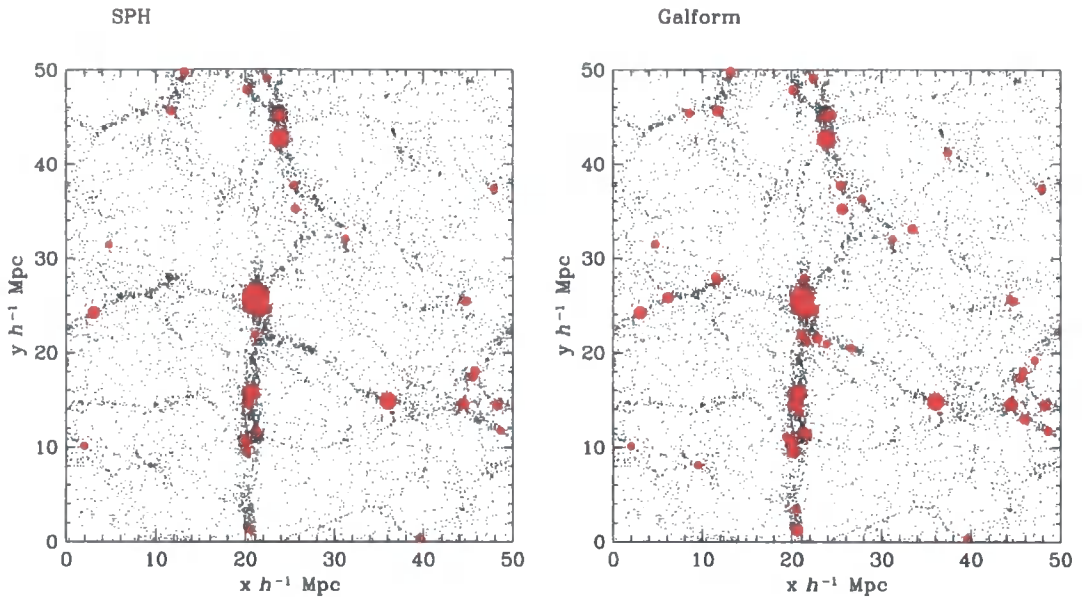
Figure 3.1: Positions and masses of galaxies in a $5h^{-1}$Mpc thick slice through the simulation volume. The panel on the left shows galaxies found in the SPH simulation using a friends of friends algorithm to identify clumps of cold gas particles. The panel on the right shows the galaxies predicted by the N-body GALFORM model. Each circle represents a galaxy, and the area is proportional to the mass of the galaxy. Dark matter particles are shown as dots. Only galaxies with masses greater than 32 gas particle masses, or $8.2 \times 10^{10} h^{-1} M_{\odot}$, are shown.

this density estimate plotted against halo mass, at redshift $z = 0$. In halos identified using the FOF group finder with $b = 0.2$ we expect the mean gas density to be several hundred times the universal mean gas density. The dotted line shows the median of the mean densities of halos of a given mass. Halos with more than 32 particles have approximately constant mean density, although the density does increase somewhat with halo mass.

The estimated density rapidly drops once the halo mass falls below 32 dark matter particle masses. Since the cooling time of the gas is inversely proportional to its density this could significantly affect the amount of gas which cools in the smaller halos in the simulation. We incorporate this effect into the semi-analytic model by increasing the cooling time for gas in halos of fewer than 32 particles. A least squares fit to Fig. 3.2 gives:

$$\log_{10} \frac{\bar{\rho}_{\text{SPH}}}{\rho_{\text{crit}} \Omega_b} = 1.23 \log_{10} M_{\text{halo}} - 11.79, \tag{3.2}$$

where $\bar{\rho}_{\text{SPH}}$ is the mean gas density estimated from the SPH simulation and M_{halo} is the

mass of the halo. The cooling time in our model is inversely proportional to the mean density of the gas in the halo. In halos of fewer than 32 particles we replace the cooling time, $\tau_{\rm cool}$, with a longer cooling time, $\tau_{\rm cool}^{\rm SPH}$, given by

$$\tau_{\rm cool}^{\rm SPH} = k\,\tau_{\rm cool}\frac{\Omega_b\,\rho_{\rm crit}}{\bar{\rho}_{\rm SPH}}, \tag{3.3}$$

where $\rho_{\rm crit}$ is the critical density. We set the constant of proportionality, k, in this relation by requiring that the cooling time for halos of 32 particles be unchanged.

Halo by halo comparison

The masses of individual galaxies in the N-body GALFORM model depend on the rate at which galaxy mergers occur within dark matter halos. Since the merger rate in the SPH simulation may not be the same as that in the semi-analytic model, we first compare the total amount of gas which cools in halos of a given mass. This quantity should be independent of the merger rate, at least in the semi-analytic case, and can be used to compare the treatment of cooling in the two models. In the SPH simulation a large galaxy forming at the centre of a halo through mergers may gravitationally affect the density, and hence the cooling rate, of nearby gas, but we do not expect this to be a large effect and the mass of gas which cools should be only weakly dependent on the merger rate.

We adopt two different models for the evolution of the gas density profile in the semi-analytic treatment. The first is that used by Cole et al. (2000) in which the core radius in the gas profile increases with time in order to maintain the gas density at the virial radius. We may vary the initial core radius, $r_{\rm core}^0$, in order to adjust the amount of gas which cools (the standard choice adopted by Cole et al. was $r_{\rm core}^0 = 0.33 r_{\rm NFW}$. The second is a simpler model in which the core radius remains a constant fraction of the halo scale radius, $r_{\rm NFW}$. Again, the size of this fixed core may be varied in order to adjust the rate at which cooling occurs.

In order to quantify the mass of cold gas present in halos in the SPH simulation, we first associate gas particles with dark matter halos. A gas particle is considered to belong to a halo if it lies within a linking length $b = 0.2$ of a dark matter particle which belongs to that halo. In the unlikely event that dark matter particles from more than one halo are found within the linking length, the gas particle is assigned to the halo containing the nearest dark matter particle. The linking length used in this procedure is the same as that used to identify dark matter halos with the FOF group finder. This ensures that the condition for a gas particle to be associated with a halo is consistent with the definition
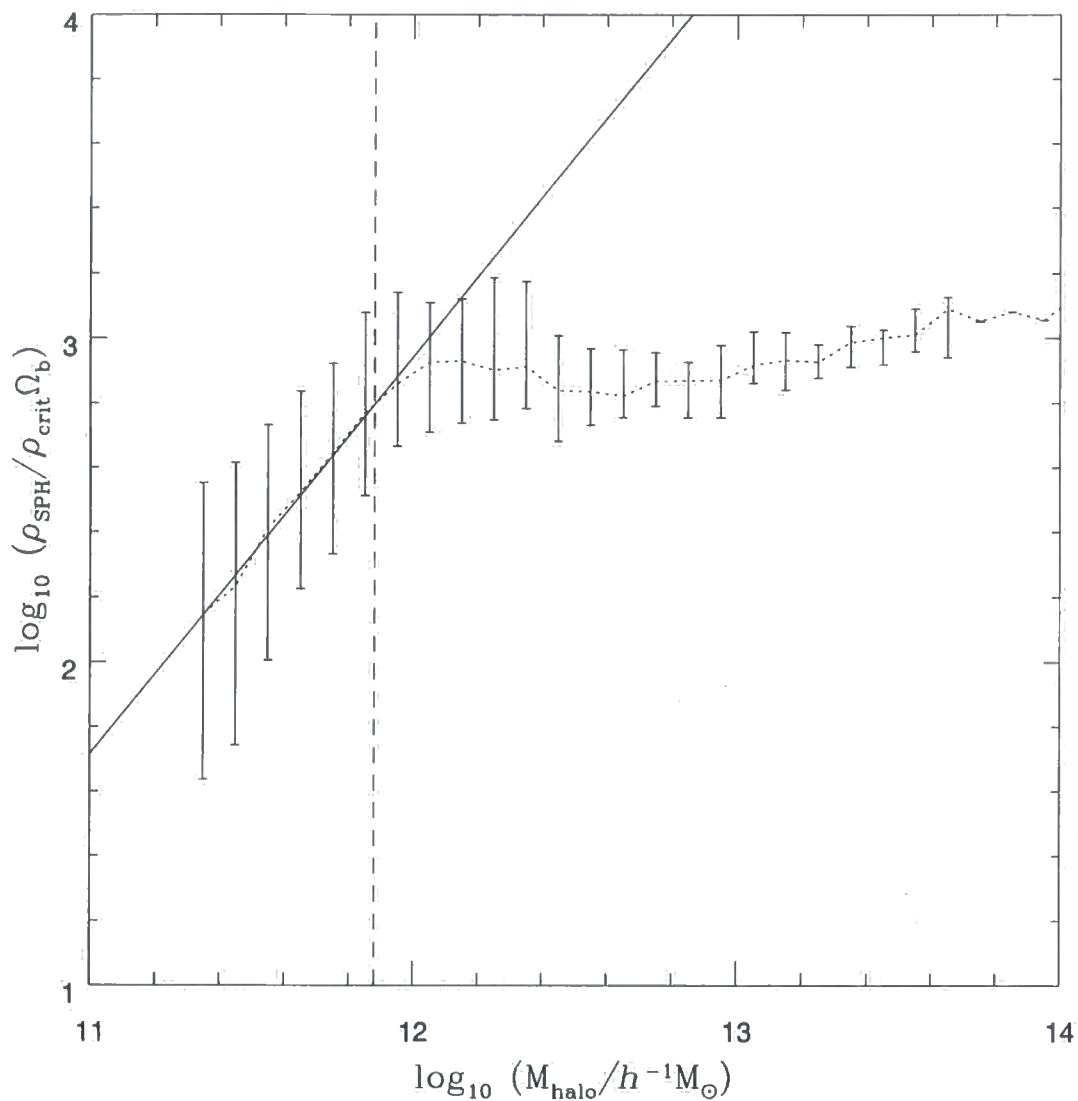
Figure 3.2: Mean halo gas density ρ_{SPH} plotted against halo mass M_{halo} at redshift $z = 0$. The density is expressed in terms of the universal baryon density. The mean density is calculated from density estimates for individual particles in the SPH simulation. The dotted line shows the median of the mean halo gas densities as a function of halo mass. The error bars show 10 and 90 percentile limits. The vertical dashed line is at a halo mass corresponding to 32 dark matter particles. The solid line is a power law fit to the median density for halos of fewer than 32 particles.

of halo membership used for the dark matter particles.

The cooling function in our simulation permits gas to cool only to a temperature of 10^4K. This allows us to distinguish between gas which has been heated and has subsequently cooled to 10^4K and the diffuse cold gas in voids which has never been heated and is at much lower temperatures. The mass of gas which has cooled in each halo is obtained by summing the masses of all gas particles associated with the halo and having temperatures between 8 000K and 12 000K. In the N-body GALFORM model, the amount of cold gas in each halo is simply the mass of gas which has cooled from the hot phase, since the model includes no star formation.

Fig. 3.3 shows the mean fraction of gas which has cooled as a function of halo mass, in both N-body GALFORM and the SPH simulation. Here we consider four different N-body GALFORM models. We vary the initial core radius in the gas profile between $r^0_{\mathrm{core}} = 1.0 r_{\mathrm{NFW}}$ and $0.15 r_{\mathrm{NFW}}$ and either fix the core radius as a fraction of the NFW scale radius or allow it to increase with time as described earlier. In the case of a fixed core, $r_{\mathrm{core}} = r^0_{\mathrm{core}}$ at all times.

The dotted lines in Fig. 3.3 show N-body GALFORM models which include the modification to the cooling time in low mass halos described by eqn. (3.3). All four models reproduce the quantities of cold gas observed at redshift $z = 0$ in the SPH simulation remarkably well, for halos of mass greater than about $10^{12} h^{-1} M_\odot$ or around 40 dark matter particles — in all but the worst case the difference is less than 50%. We find that if the core radius in the gas density profile is allowed to increase as gas cools, the fraction of cold gas is not particularly sensitive to the choice of intitial core radius, although a small initial value, $r^0_{\mathrm{core}} = 0.15 r_{\mathrm{NFW}}$, gives a slightly better match than if the core is initially larger. If the core radius is fixed as a fraction of the NFW scale radius a much larger value, $r^0_{\mathrm{core}} = 1.0 r_{\mathrm{NFW}}$, is necessary.

The dashed lines in the figure show the fraction of gas which cools if cooling is allowed to occur at the normal rate in halos of all masses down to the mass of the smallest halo we can resolve in the simulation. Surprisingly, this appears to have little effect on halos with fewer than 32 dark matter particles for which the cooling rate has been altered. The fraction of gas which has cooled in larger halos also increases by a similar amount. The extra cold gas in these halos must have cooled in progenitors of fewer than 32 particles before being incorporated into larger halos. Overall, the change is not large, with some halos having around 10-20% more cold gas on average. This suggests that our results are not particularly sensitive to the way in which we model the loss of cooling efficiency in

low mass halos, although in both cases the agreement between the SPH simulation and the semi-analytic model is poor in such halos.

Fig. 3.4 shows a direct comparison between the masses of cold gas in individual halos in the SPH simulation and the four N-body GALFORM models of Fig. 3.3, again using the modified cooling time for low mass halos. The mass of cold gas predicted by N-body GALFORM is plotted against the mass of cold gas in the simulation for each halo, with the initial core radius set to r_{NFW} in the upper panels and $0.15r_{\mathrm{NFW}}$ in the lower panels. In the models shown on the left-hand side the core radius remains fixed at its initial value at all times. The long-dashed lines show where the points would lie if the simulation and the semi-analytic models were in perfect agreement.

Again, in all four cases the mass of cold gas in the SPH simulation is well correlated with the mass of cold gas in the N-body GALFORM model. The small scatter, at least at high masses, shows that the dependence of cold gas mass on merger history must be similar in the SPH simulation and the semi-analytic model. N-body GALFORM with a gas density profile with a fixed core radius appears to cool on average more gas in halos of all masses than the SPH simulation. This can be alleviated to some extent by increasing the size of the core in the gas profile but it appears that a rather large core in the gas distribution would be required to obtain good agreement. Allowing the core radius to increase as gas cools reduces the rate of cooling and results in closer agreement with the simulation; the best agreement is obtained for a small initial core radius of around $0.15r_{\mathrm{NFW}}$, although the mass of cold gas in each halo is clearly not particularly sensitive to the initial core radius in this GALFORM model.

Fig. 3.5 shows the mass of cold gas in progenitors of four of the larger halos in the simulation as a function of redshift. The mass of cold gas in the simulation (solid lines) at a given redshift is obtained by summing the masses of all cold gas particles associated with the progenitors of the final halo at that redshift. Particles are associated with halos using the method described earlier in this section and, as before, "cold" particles are those with temperatures in the range 8 000–12 000K. Similarly, the mass of cold gas in the N-body GALFORM model is obtained by summing the masses of the galaxies in the progenitor halos. Here we show results for two models, one with r_{core} fixed at $r_{\mathrm{core}}^{0} = 1.0r_{\mathrm{NFW}}$ (dotted lines) and the other with a growing core which has an initial core radius $r_{\mathrm{core}}^{0} = 0.15r_{\mathrm{NFW}}$ (dashed lines). The model of Cole et al. used a gas profile with a larger initial core radius, $r_{\mathrm{core}}^{0} = 0.33r_{\mathrm{NFW}}$.

The long dashed lines show the mass of cold gas in progenitors in the simulation if
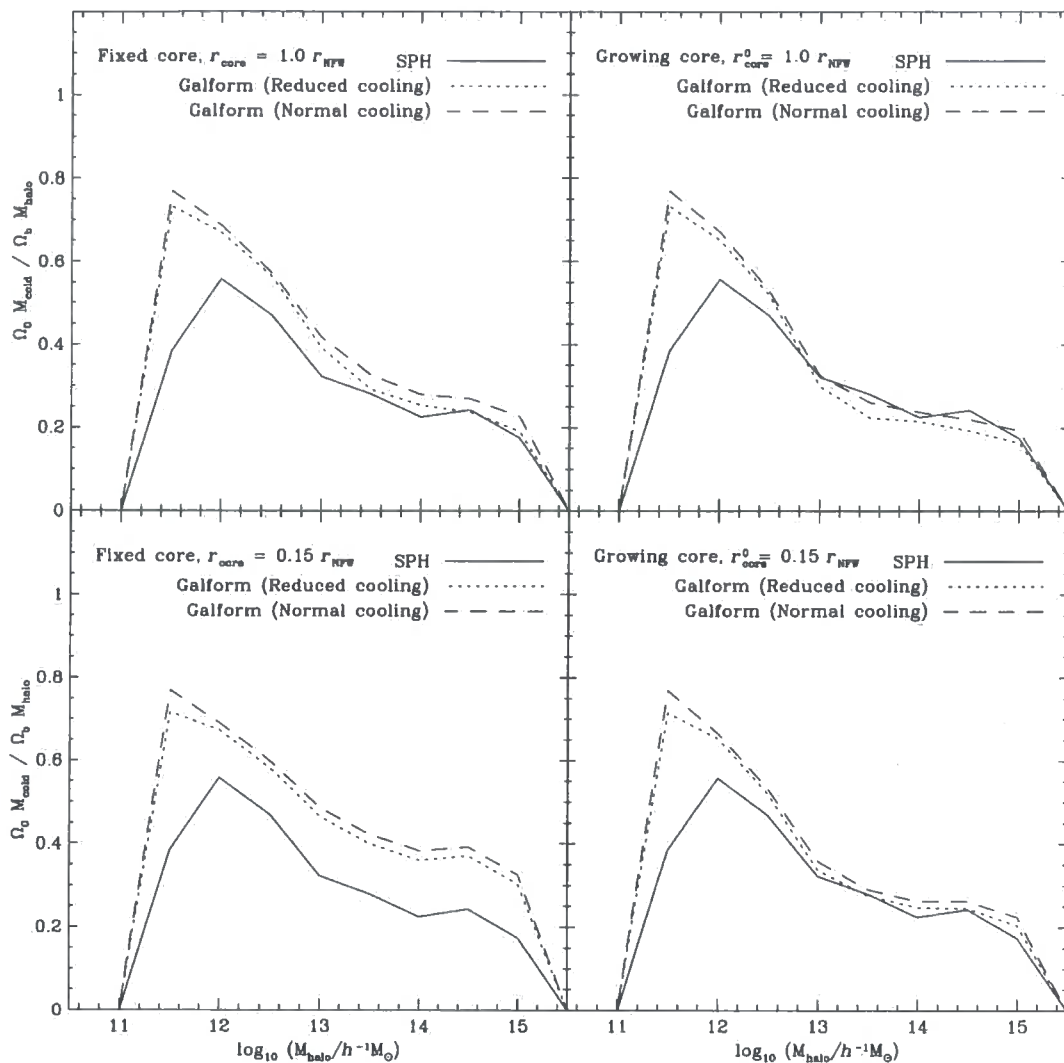
Figure 3.3: Mean fraction of halo gas which has cooled at redshift $z = 0$ as a function of halo mass. The solid lines show the mean cooled gas fraction in halos in the SPH simulation and are the same in all four panels. The dotted lines show the cold gas fraction in N-body GALFORM models where the cooling time in low mass halos is increased according to eqn (3.3). The dashed lines show N-body GALFORM models without this adjustment. In the upper panels the initial core radius is set equal to the NFW scale radius of the halo. In the lower panels the core radius is set to 0.15 times the scale radius. In the panels on the left hand side the core radius remains fixed at its initial value for all redshifts, in the panels on the right it is allowed to increase to maintain the density of gas at the virial radius.
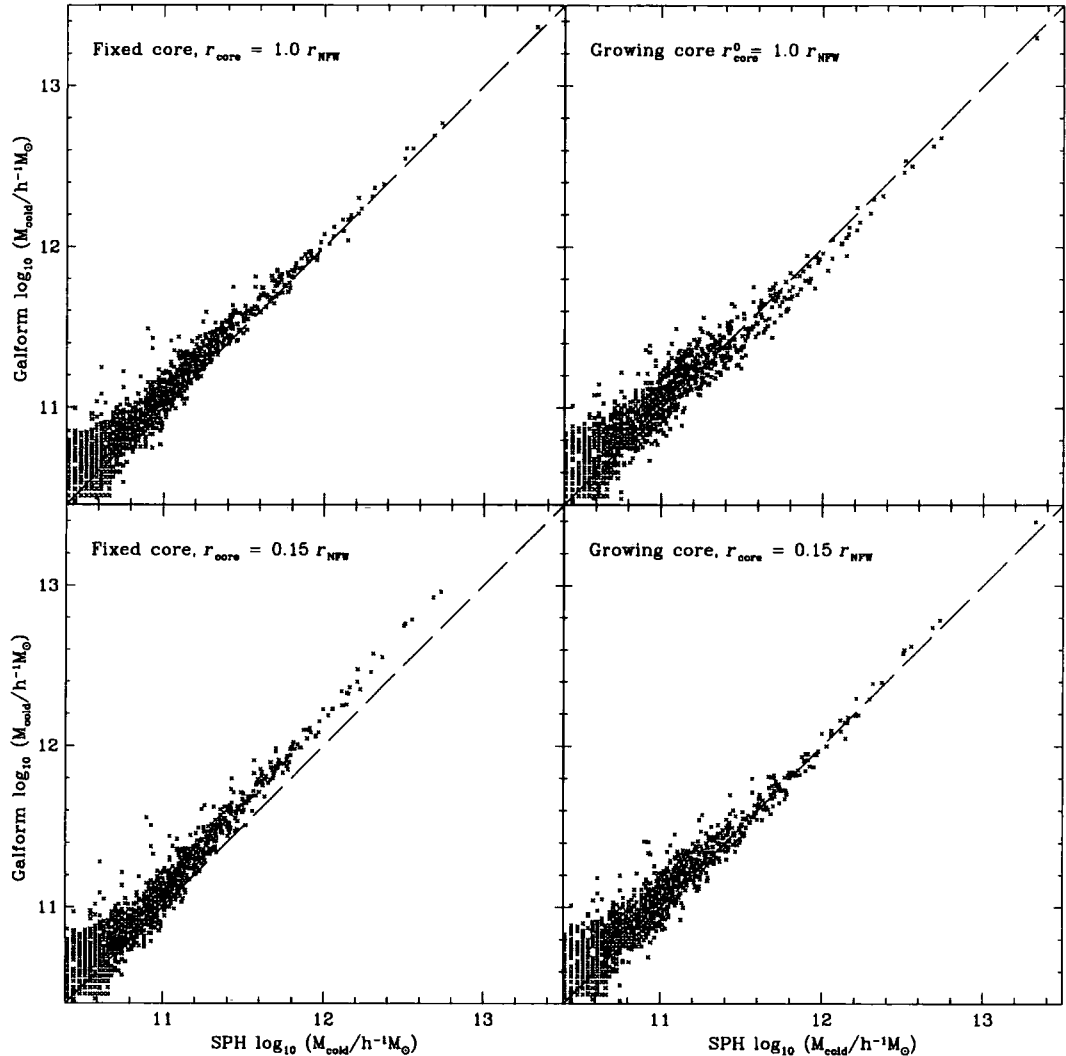
Figure 3.4: Halo cold gas mass, $M_{\rm cold}$, in four different N-body GALFORM models plotted against halo cold gas mass in the SPH simulation at redshift $z = 0$. Each point corresponds to a single dark matter halo. The upper panels show N-body GALFORM models with $r^0_{\rm core} = 1.0r_{\rm NFW}$. The lower panels have $r^0_{\rm core} = 0.15r_{\rm NFW}$. In the panels on the left, the core radius in the gas density profile is a fixed fraction of the NFW scale radius. In the panels on the right the core radius is allowed to grow in order to maintain the gas density at the virial radius.

instead of associating gas particles with halos directly, we use the FOF group finder to first identify clumps of cold gas and then associate clumps with dark matter halos. A clump is assigned to a halo if a dark matter particle from that halo is found within a dark matter linking length of the clump's centre of mass. If particles belonging to several halos are found in this region, the nearest to the centre of mass is used. A linking length $b = 0.02$ is used to identify the clumps and a minimum group size of 10 particles is imposed on the clumps. These lines are shown in Fig. 3.5 only to illustrate that there is some dependence on the way in which we define "cold halo gas" in the simulation. This second method will certainly underestimate the mass of cold gas because the group finder imposes a minimum mass on the clumps, missing smaller groups of cold particles. Also, at high redshift the gravitational softening length exceeds the linking length used to identify the clumps, so particles which ought to be considered part of a clump may not have collapsed to sufficiently high densities to be picked up by the group finder. We find that most of the discrepancy between these two SPH results is due to cold particles in small groups of fewer than five particles, at least with $b = 0.02$.

It is also possible that the first method of counting individual gas particles associated with halos overestimates the mass of cold gas in smaller halos, where the linking length becomes a significant fraction of the radius of the halo. Any particle within a linking length of the outer dark matter particles of the halo may be associated with that halo. Despite this uncertainty, it appears that more of the cold gas found in the simulation cooled at high redshift than in either of the N-body GALFORM cases considered. At redshift 2 the discrepancy is approximately a factor of 2. Allowing the core radius to increase from a small initial value helps somewhat by encouraging more cooling initially and slightly suppressing it later, but the improvement is small compared to the size of the discrepancy with the SPH simulation for redshifts greater than around 2. Reducing the initial core radius in this model further has little effect on these results.

We have tried to model the effect of limited resolution on cooling in SPH blobs of fewer than 32 dark matter particles, but in the N-body GALFORM model no cooling is possible in halos of fewer than 10 dark matter particles. It appears that in our SPH simulation some cooling *does* occur in these halos. However, it may not be useful to model the rate of cooling in this regime, since it is entirely artificial and likely to be dependent on the details of the particular SPH implementation. In any case, when halos in the SPH simulation first grow to 10 dark matter particles they may have already cooled some gas. These halos will eventually be incorporated into larger halos, where the cold gas mass
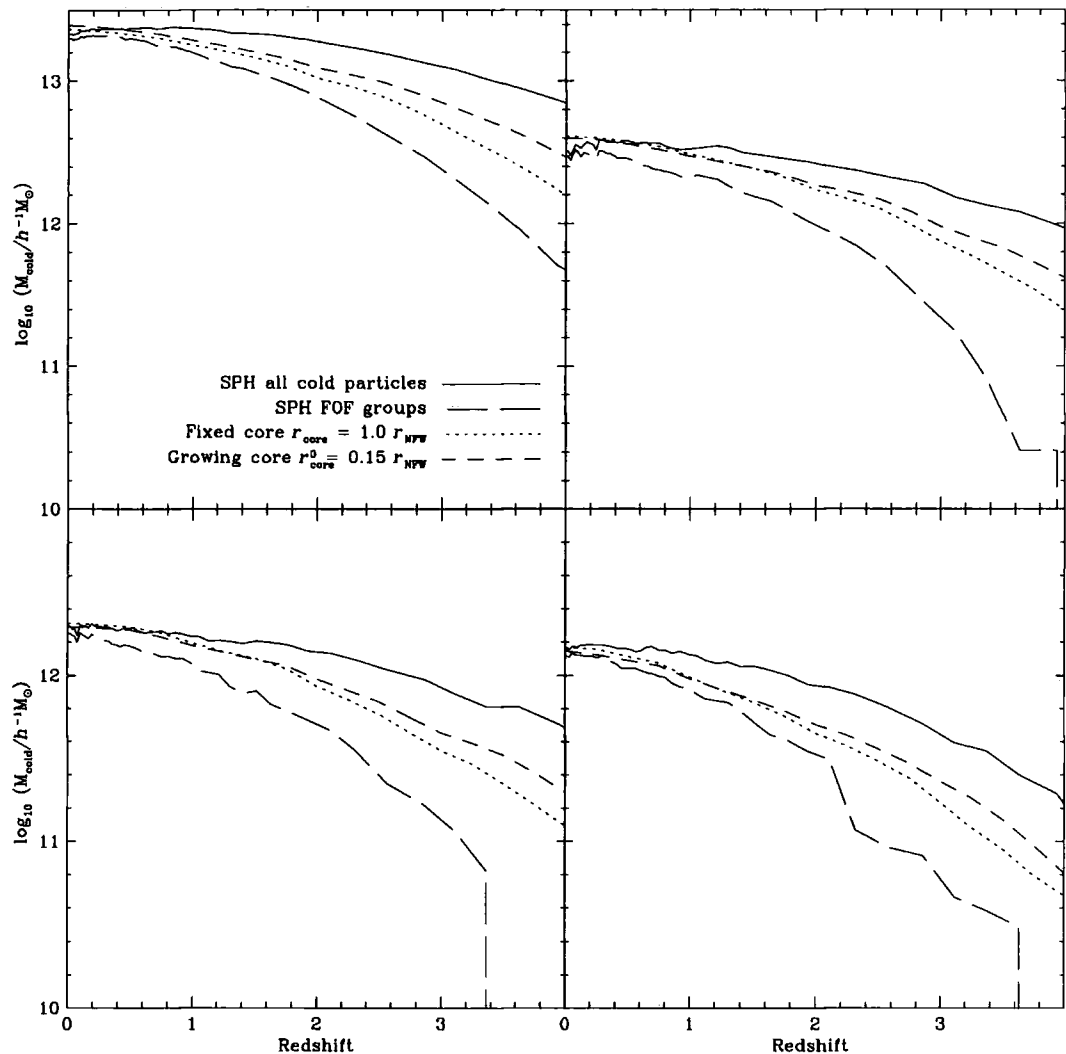
Figure 3.5: Mass of cold gas in the progenitors of four halos as a function of redshift. Each panel corresponds to a single halo at $z = 0$. The solid line shows the mass of cold gas in the SPH simulation obtained by summing the masses of all cold gas particles in the progenitors. The long dashed line shows the mass of cold gas obtained by summing the masses of all FOF groups of cold particles in the progenitors. The dotted lines correspond to an N-body GALFORM model with a fixed core radius in the gas density profile with $r_{core} = r_{NFW}$. The short dashed lines correspond to a model with a growing core radius of initial value $r^0_{core} = 0.15 r_{NFW}$.

becomes dominated by material which cooled in well resolved halos so that at late times the SPH and GALFORM calculations converge.

Galaxy by galaxy comparison

Fig. 3.6 shows the number density of galaxies as a function of mass in the SPH simulation and in the N-body GALFORM model at redshift $z = 0$. Here, SPH "galaxies" are groups of particles identified by the FOF group finder applied to all particles with temperatures in the range 8 000–12 000K. We use a linking length $b = 0.02$ and impose a minimum group size of 10 particles. The results are insensitive to the specific choice of b within reasonable bounds. Two N-body GALFORM cases are shown, one with a core of fixed size $r_{core} = r_{NFW}$ in the gas density profile, the other with a growing core of initial size $r_{core}^0 = 0.15 r_{NFW}$. In both cases N-body GALFORM predicts about 50% more galaxies with masses around $3 \times 10^{11} h^{-1} M_\odot$ or less and fewer galaxies with masses greater than this for the latter choice of r_{core}^0. The deficit in the number of massive galaxies is more apparent in the model with a large, fixed gas core radius. Since we know that the total amount of gas cooled in the semi-analytic models in each halo is similar to the amount that cooled in the simulation (see Fig. 3.4), this suggests that there is more merging occurring in the simulation. This does not necessarily indicate a failure of the semi-analytic model, however, since it is possible that numerical effects in the simulation contribute significantly to the merger rate.

To test this hypothesis, we varied the merger timescale parameter, f_{df} in the semi-analytic models. Fig. 3.7 shows galaxy number density as a function of mass for three N-body GALFORM models with $f_{df} = 0.5, 1.0$ and 2.0. All three have gas profiles with growing cores of initial radius $r_{core}^0 = 0.15 r_{NFW}$. Doubling the merger timescale ($f_{df} = 2.0$) drastically reduces the number of more massive galaxies and prevents the formation of any galaxies more massive than $10^{12} h^{-1} M_\odot$. Halving the merger timescale ($f_{df} = 0.5$) improves agreement with the simulation by increasing the masses of the largest galaxies and reducing the number of small galaxies. However, the improvement is relatively small and, in any case, the treatment of mergers in the N-body GALFORM model reproduces the distribution of masses observed in the simulation reasonably well with our default $f_{df} = 1.0$.

The N-body GALFORM model described in Section 3.3 does not allow semi-analytic galaxies to be compared with their SPH counterparts on a one to one basis because mergers between galaxies in N-body GALFORM are treated in a statistical manner. While
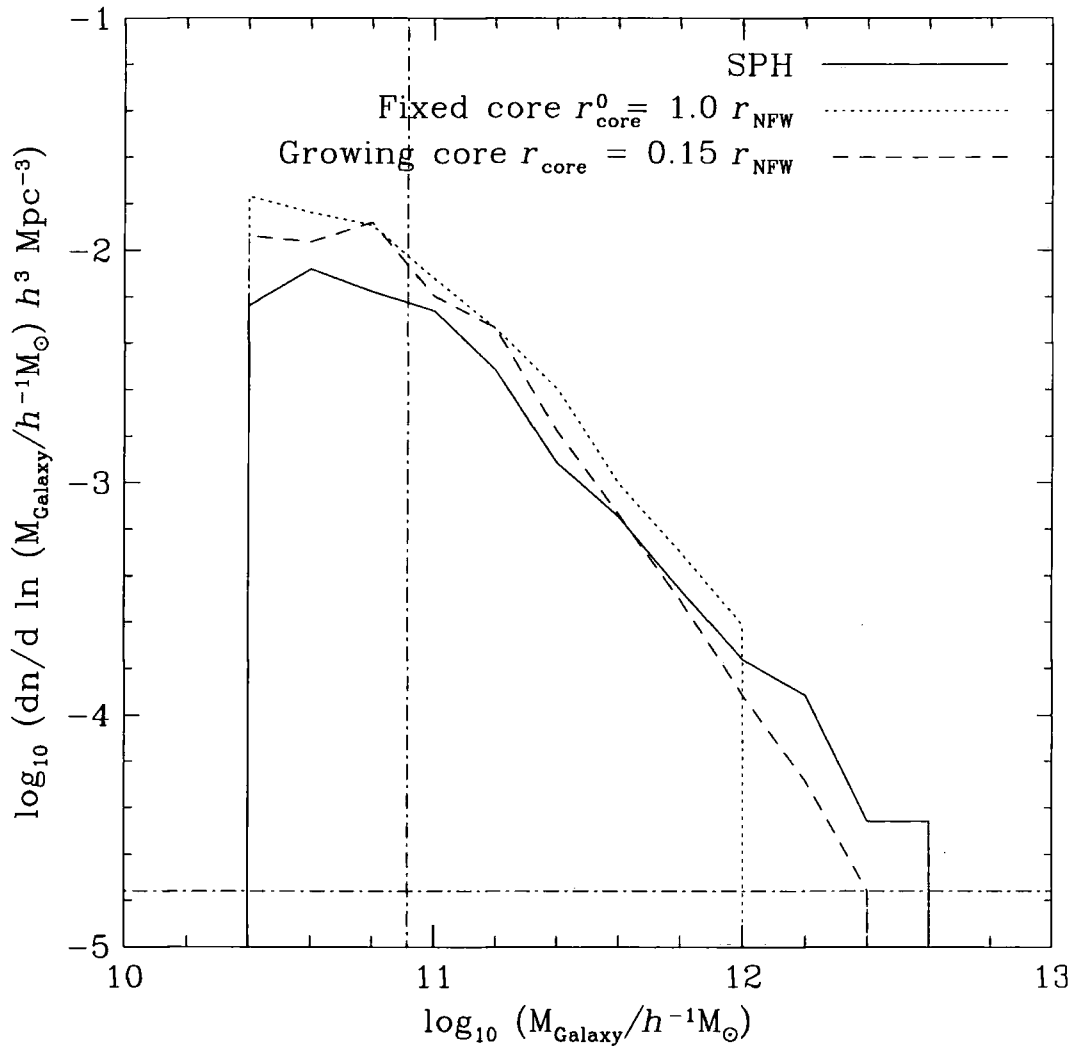
Figure 3.6: Galaxy number density as a function of cold gas mass at redshift $z = 0$. The solid line shows galaxy number density in the SPH simulation. The other lines correspond to N-body GALFORM models with 1) a fixed core radius $r_{core} = r_{NFW}$ (dotted line) and 2) a growing core which initially has $r^0_{core} = 0.15 r_{NFW}$ (dashed line). The horizontal dot-dashed line shows the number density equal to one object per simulation volume. The vertical dot-dashed line is at a mass equal to 32 gas particle masses.
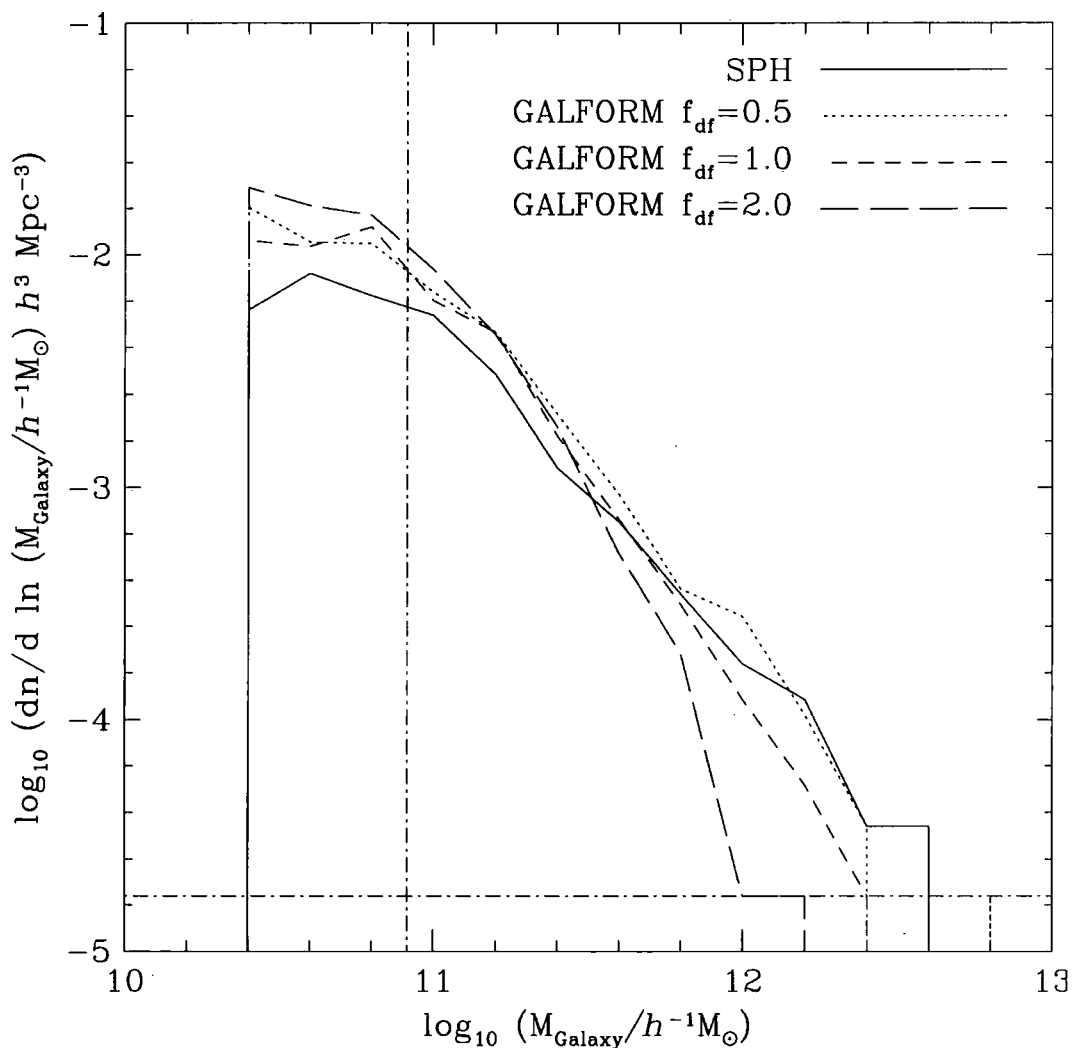
Figure 3.7: Galaxy number density as a function of cold gas mass at redshift $z = 0$ for N-body GALFORM models with three different merger rates. All three models have gas profiles with a growing core radius which is initially set to $r^0_{core} = 0.15r_{NFW}$. The merger timescale parameter f_{df} is varied between 0.5 (dotted line), 1.0 (short dashed line) and 2.0 (long dashed line). The short dashed line is identical to the short dashed line in Fig. 3.6. The solid line shows the galaxy number density in the SPH simulation and is identical to the solid line in Fig. 3.6. The horizontal dot-dashed line shows the number density corresponding to one object per simulation volume. The vertical dot-dashed line is at a mass equal to 32 gas particle masses. The curves are truncated at 10 gas particle masses.

the agreement between the galaxy mass distributions suggests that the overall merger rate in the N-body GALFORM model is similar to that seen in the simulation, we cannot expect mergers to occur between the same galaxies in the two cases, and hence it is not possible to identify clumps of cold gas particles with individual semi-analytic galaxies.

This problem could be avoided by following the substructure within dark matter halos to determine when mergers between galaxies occur, using a method similar to that of Springel, White, Tormen & Kauffmann (2001). Unfortunately the halos in our simulation typically contain too few particles for this to be practical. Any dark matter substructure is rapidly destroyed by numerical effects.

In order to compare the masses of individual galaxies directly, we need an alternative way to ensure that the same galaxies merge in each model. We do this by using information from the baryonic component of the SPH simulation to merge N-body GAL-FORM galaxies. We first populate the simulation volume with galaxies calculated using the N-body GALFORM model, with merging of galaxies completely suppressed. We find the halo in which each semi-analytic galaxy first formed, and identify the gas particles associated with that halo as those with indices corresponding to the indices of the dark matter particles in the halo — this is possible because in our SPH simulation gas and dark matter particles with the same indicies are initially at the same locations and tend to remain in the same halos at later times. By redshift $z = 0$ some of these particles will be contained within SPH galaxies. Each semi-analytic galaxy is assigned to the SPH galaxy which contains the largest number of gas particles from the halo in which it formed. This procedure often results in several semi-analytic galaxies being assigned to the same blob of cold gas at redshift $z = 0$. These galaxies are assumed to have merged and their masses are added together. It is possible to think of rare situations where our method might incorrectly merge galaxies, but this is the best that can be done within the limitations of the SPH simulation.

We are only able to detect SPH galaxies with 10 particles or more, so it is inevitable that sometimes a semi-analytic galaxy will not be assigned to any SPH galaxy. This would occur if the semi-analytic galaxy formed in a halo which, in the simulation, failed to cool enough particles to constitute a group by redshift $z = 0$. Such galaxies are generally found in small, recently formed halos and typically have masses of around 10 gas particle masses or less. These galaxies account for about 20% of the total semi-analytic galactic mass in the simulation volume. We also find that a small number (about 2%) of the SPH galaxies have no corresponding semi-analytic galaxy. Almost all of these are poorly

resolved objects close to the 10 particle threshold.

Since the unmatched semi-analytic galaxies largely correspond to SPH galaxies which have yet to gain enough cold particles to be identified by the group finder, we simply omit them from the comparison shown in Fig. 3.8. Here, we compare the masses of the merged semi-analytic galaxies with the corresponding galaxies in the SPH simulation. Each point on the plot represents a single SPH galaxy which has been associated with one or more semi-analytic galaxies. We have split the galaxies into two categories – central galaxies (left panel) and satellite galaxies (right panel). This allows us to test the assumption made in the GALFORM model that no gas cools onto satellite galaxies. If this is not true, galaxies which are considered to be satellites in the N-body GALFORM model will have systematically lower masses than their SPH counterparts. It therefore makes sense, for this purpose, to use information from the semi-analytic model (and not the SPH simulation) to determine whether each galaxy is a satellite. The semi-analytic mass of each galaxy shown in Fig. 3.8 is the sum of the masses of the GALFORM galaxy fragments which have been associated with the corresponding SPH galaxy. We identify the galaxy as a central galaxy if any one of those fragements was a central galaxy before we applied our SPH merging scheme. If all of the fragments were satellites, the galaxy is considered to be a satellite.

There is clearly a very strong correlation between the mass of each simulated galaxy and its semi-analytic counterpart, although the N-body GALFORM galaxies appear to be systematically more massive by up to 25% at low masses. The scatter in this plot is comparable to that in Fig. 3.4. There appears to be little or no systematic difference between satellite and central galaxies, which suggests that no significant amount of cooling of gas onto satellite galaxies is occurring in the simulation. There are a few outlying points where the GALFORM and SPH masses are drastically different – these are mainly satellites, but there are as many with much *higher* GALFORM masses than SPH masses as there are with lower masses. These are most likely a result of the SPH merging algorithm assigning GALFORM galaxy fragments to the wrong SPH galaxy.

Finally, we compare the clustering of galaxies in the two models. While the spatial distribution of dark matter halos in the N-body GALFORM model is identical to that in the simulation, the number of galaxies in each halo and their distribution within the halo may differ. Fig. 3.9 shows two point galaxy correlation functions for galaxies in the SPH simulation and two different N-body GALFORM models, both of which have gas profiles with growing core radii which are initially set to $r^0_{\rm core} = 0.15 r_{\rm NFW}$. In the first GALFORM
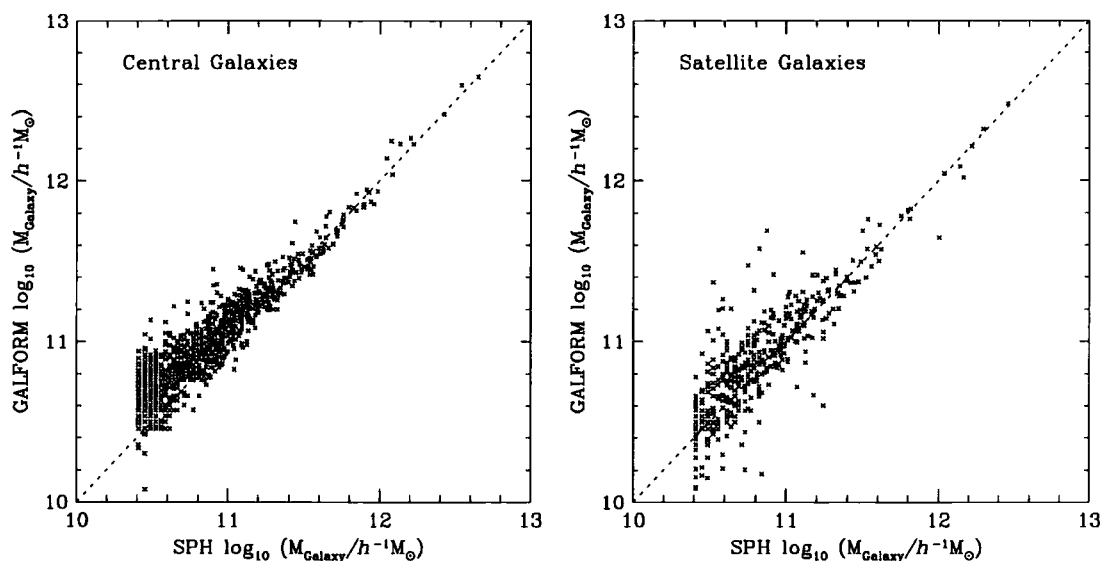
Figure 3.8: Comparison between galaxy masses in the SPH and N-body GALFORM models. The merger scheme described in Section 3.3.1 is used to identify N-body GALFORM galaxies with SPH galaxies. Galaxies lying on the dashed line have equal masses in both models. The panel on the left shows only galaxies which are considered to be central galaxies in the N-body GALFORM model. The panel on the right shows only galaxies which are satellites in the N-body GALFORM model.

model, merging between galaxies is treated using the dynamical friction approach of Cole et al. with $f_{df} = 0.5$, which gives a closer match to the distribution of galaxy masses in the simulation than our default value of 1.0 (see Fig. 3.7.) In the second GALFORM model, we use the SPH based merging scheme described earlier in this section and put each merged GALFORM galaxy at the position of its associated SPH galaxy. In each case, we include only the 700 (left panel of Fig. 3.9) or 300 (right panel) most massive galaxies in our calculation. This ensures that the overall density of galaxies in the volume is the same in each sample. Picking the 700 largest galaxies excludes all galaxies less massive than about $8 \times 10^{10} h^{-1} M_{\odot}$ or 30 gas particles. Picking the 300 largest galaxies corresponds to a minimum mass of approximately $1.5 \times 10^{11} h^{-1} M_{\odot}$ or around 60 gas particles.

The correlation function has been calculated on scales of up to $25 h^{-1} \text{Mpc}$. This is half of the size of the simulation box, so the results presented here should not be treated as predictions of the true galaxy correlation function. Instead, the plots in Fig. 3.9 are intended to compare the relative clustering of GALFORM and SPH galaxies in our *small* simulation volume. All three models show qualitatively similar behaviour. When

we consider the larger sample of galaxies (left panel in Fig. 3.9), we see an anti-bias relative to the dark matter on scales of less than a few h^{-1}Mpc, with galaxies tracing the dark matter on larger scales. This behaviour agrees with previous semi-analytic (e.g. Kauffmann et al. 1999a, Benson et al. 2000) and SPH simulation (e.g. Pearce et al. 2001) results. If we include only the 300 most massive galaxies in the simulation volume (right panel in Fig. 3.9), we see that on large scales these more massive galaxies are more strongly clustered than the dark matter in all three cases.

The N-body GALFORM model with $f_{df} = 0.5$ is in close agreement with the SPH simulation on scales larger than a few h^{-1}Mpc when we use the 700 most massive galaxies. This is to be expected since we have the same distribution of dark matter halos in each case and the merger rate in the semi-analytic model has been adjusted to reproduce roughly the distribution of galaxy masses in the simulation. On length scales smaller than this, where the correlation function is sensitive to the details of our treatment of galaxy mergers within halos, there is a difference of almost a factor of 2 between the SPH simulation and the GALFORM model with $f_{df} = 0.5$. The treatment of mergers in this model reproduces the overall distribution of galaxy masses but the merger rates and galaxy distributions in halos of a given mass may not be in close agreement. When we merge GALFORM galaxies by associating them with groups of cold gas in the SPH simulation (short dashed lines in Fig. 3.9), the correlation functions agree to within about 25% on these small scales. If we consider only the 300 most massive galaxies in each case, the correlation function for the model with $f_{df} = 0.5$ drops to almost an order of magnitude below that of the SPH simulation on scales of about $0.3h^{-1}$Mpc. Again, this is due to differences in the merger rates in halos of a given mass since the discrepancy disappears if we use our SPH-based merging algorithm.

Once we ensure that the same galaxies merge in each model, any remaining differences between the correlation functions shown must be due to differences in the galaxy masses. The most massive 700 objects in the SPH model must be a somewhat different population to the 700 most massive objects in the semi-analytic model. In fact, we find that the two samples possess only 590 objects (about 85%) in common. This is an inevitable consequence of the scatter in the relation between SPH and semi-analytic galaxy masses shown in Fig. 3.8. Unless there is zero scatter, there will always be galaxies just massive enough to be included in the correlation function for one model which will not be included in the sample for the other. This explains why the level of agreement is reduced when we consider only the most massive galaxies, where we might have expected to obtain improved
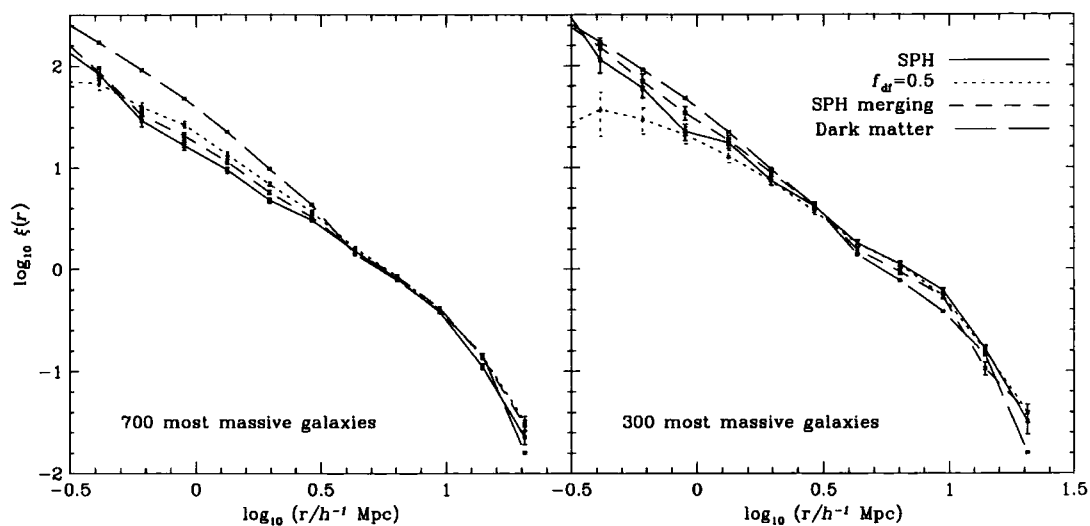
Figure 3.9: Two point galaxy correlation functions for three different models - the SPH simulation (solid lines), an N-body GALFORM model with merger rate parameter $f_{df} = 0.5$ (dotted lines) and an N-body GALFORM model using the SPH based merger scheme described in Section 3.3.1 (short dashed lines). The long dashed lines show the correlation function for the dark matter in the SPH simulation. The 700 most massive galaxies in each case are included in the calculation for the left panel and only the 300 most massive galaxies are included in the right panel. Both N-body GALFORM models have a gas density profile with a core radius which is allowed to grow from an initial value of $r^0_{core} = 0.15 r_{NFW}$.

agreement. By increasing the minimum mass required for a galaxy to be included in each sample we increase the proportion of galaxies which have masses close to the threshold and the fraction of galaxies common to both samples falls slightly to 237 out of 300, or about 80%.

3.4 Discussion and Conclusions

In this Chapter we have used the N-body GALFORM model to compare the results of a semi-analytic calculation of the radiative cooling of gas in halos with results from a cosmological SPH simulation. We have tried to reproduce the results of the simulation by adjusting the semi-analytic cooling prescription and modelling the effects of limited mass resolution on the SPH cooling rate.

We compared properties of halos in the simulation with the properties of the same halos in the N-body GALFORM model. First, we looked at a global property of the halo

population, the average fraction of cooled gas at redshift $z = 0$ as a function of halo mass. We found that a model in which the gas density profile with an initially small core radius which is able to increase with time provided the best match to the mean cold gas fractions seen in the SPH simulation among those considered. The level of agreement was excellent for halos with masses above the resolution limit of the SPH simulation.

Our method also enabled us to compare the cool gas content of individual halos. For the gas density profile described above, and also for a profile with a fixed core radius, the total mass of cold gas in each halo was found to be in remarkably good agreement at cold gas masses greater than about $10^{12}h^{-1}{\rm M}_\odot$. In poorly resolved halos with lower cold gas masses the scatter in this comparison increased substantially, to a factor of about 3. We found that much of the cold gas found in the more massive halos in the N-body GALFORM model generally cooled at later times than the gas in the same halos in the SPH simulation. By a redshift of 2 in the N-body GALFORM case, the progenitors of the halos contained only half as much cold gas as was present in the simulation. As the redshift increases, the mass of cold gas in the SPH simulation becomes dominated by material which cooled in very small halos, where the cooling rate may be strongly affected by resolution effects and depends sensitively on the SPH implementation (Springel & Hernquist 2002). These effects are difficult to model reliably and so the discrepancy between the GALFORM and SPH cold gas masses increases at higher redshifts.

We then turned our attention to the properties of individual "galaxies" (i.e. cold gas clumps) at redshift $z = 0$. Our best fit model gave a distribution of galaxy masses in good agreement with those in the SPH simulation for galaxies of more than 32 particles when we used the merger timescale of Cole et al. (2000), although the N-body GALFORM model contained a somewhat greater number of low mass galaxies and fewer very massive galaxies than the simulation. Doubling the merger rate in the GALFORM model improved the agreement at all masses, but note that the merger rates in the SPH simulation may not be reliable due to the effects of artificial viscosity (Frenk et al. 1996).

In our semi-analytic approach, galaxy mergers are treated in a probabilistic fashion based on the dynamical friction timescale. Thus, a direct identification of semi-analytic and SPH galaxies is not possible. In order to circumvent this problem, we suppressed all merging in the N-body GALFORM model and then used information from the SPH simulation to merge the semi-analytic galaxies and to associate the merged galaxies with groups of cold gas particles in the simulation. This gave us a semi-analytic mass for each galaxy in the SPH simulation. We found that these masses were generally similar (within

about 50% for larger galaxies) with a scatter close to that seen in the comparison of halo cold gas masses.

Finally, we examined the clustering properties of the more massive galaxies in the SPH simulation and two N-body GALFORM models. The first used the dynamical friction treatment of galaxy mergers, the second used our SPH merging scheme. We found that the correlation functions of galaxies in both GALFORM models agreed well with the SPH simulation on scales larger than typical group and cluster sizes, but that on scales of a few h^{-1}Mpc or less the correlation function of galaxies in the GALFORM model with merging based on the dynamical friction timescale was higher by almost a factor of 2. Using the SPH merging scheme reduced this discrepancy to about 25%.

Our comparison shows that it is possible to reproduce accurately gas cooling, and to a lesser extent galaxy merger rates, in an SPH simulation using semi-analytic methods. Benson, Pearce, Frenk, Baugh & Jenkins (2001) demonstrated that the overall rate of cooling, globally and in halos of a given mass, predicted by SPH and semi-analytic models show remarkable consistency. They found that the overall fractions of hot gas, cold, dense gas and uncollapsed gas agreed to within 25% at $z = 0$. The cold gas fractions in halos of a given mass were found to agree to within 50%, with the SPH simulation cooling more gas than the semi-analytic model. This is consistent with the results presented here, since our best semi-analytic model assumes a gas density profile with a smaller core radius than that of Benson et al. , resulting in a higher central gas density in each halo and more rapid cooling.

Here we have shown that, with only minor changes to the semi-analytic model, very close agreement can be obtained on a halo by halo basis when merger trees are taken from the SPH simulation. The agreement between SPH and semi-analytic masses for individual halos indicates that the dependence of the cooling rate on merger history is very similar in the two cases. Given the quite different limitations and assumptions inherent in the two techniques, this is a remarkable result. While we have allowed ourselves some freedom to adjust the semi-analytic model in order to maximise the level of agreement with the simulation, it should be noted that in our best fit model, the only changes we have made to the cooling model of Cole et al. (2000) are a slightly smaller core in the gas density profile and an increased cooling time in small halos. Neither of these changes have a large effect on the mean cold gas fraction at $z = 0$.

Springel & Hernquist (2002) show that when SPH is formulated in terms of the thermal energy equation, substantial overcooling may occur in halos of fewer than several

thousand particles – for example, gas may cool as it passes through shocks which have been artificially smoothed out by the SPH algorithm. They demonstrate that a new formulation ('entropy SPH') using entropy rather than thermal energy as an independent variable, which conserves both energy and entropy, can significantly reduce this problem. This conclusion would seem to suggest that the quantities of gas cooling in the majority of halos in our SPH simulation may be overestimated. This could explain why a gas profile with a smaller core radius than that used by Cole et al. is required in our semi-analytic model to reproduce the quantities of cold gas in the simulation. However, the Hydra SPH code which we use here is significantly different from the GADGET code (Springel, Yoshida & White 2001) employed by Springel & Hernquist and it is not clear to what extent our simulation suffers from the overcooling effect.

In an independent investigation carried out concurrently with this one, Yoshida et al. (2002) compared gas cooling in SPH simulations carried out using GADGET with a semi-analytic model based on that of Kauffmann et al. (1999a). This model contains a simpler cooling prescription than used in this work – the gas within each halo is assumed to trace the dark matter exactly at all times so there is no core radius. Yoshida et al. adopt a similar approach to our own, taking halo merger histories from the dark matter in their SPH simulations and neglecting star formation and feedback in both models. They show results for two of the SPH implementations investigated by Springel & Hernquist – one is the entropy SPH implementation discussed above, the other is a 'conventional' implementation based on taking the geometric means of the pairwise hydrodynamic forces between neighbouring particles. Yoshida et al. find good agreement between the masses of individual galaxies in their semi-analytic model and the entropy SPH implementation. SPH galaxy masses, however, can differ by a factor of 2 between the two SPH implementations considered, but Yoshida et al. believe the entropy SPH to be the more reliable technique and note that their 'conventional' SPH implementation actually suffers the overcooling problem more severely than other conventional implementations, including the Hydra code which we have used here.

Overall, it appears that the differences between cooling rates predicted by SPH and semi-analytic techniques are small, and quite possibly comparable to the uncertainty in the SPH results. As well as providing evidence to support the treatment of cooling in current semi-analytic galaxy formation models, these results show that semi-analytic modelling provides a convenient, alternative way to add a baryonic component to an N-body simulation, which is at least as reliable as an SPH simulation. When used to investigate

star formation and feedback prescriptions this approach allows the investigation of large regions of parameter space at little computational cost and so can provide an indication of how these phenomena may be included in full hydrodynamic simulations.

Chapter 4

Formation of a Single Galaxy at High Resolution

4.1 Introduction

In Chapter 2 we developed a method of populating an N-body simulation volume with semi-analytic galaxies by taking halo merger histories from the dark matter component of the simulation. This allowed us to carry out a direct comparison between SPH and semi-analytic predictions for a $50h^{-1}$Mpc volume of a ΛCDM universe in the absence of star formation and feedback. However, there are at least two significant drawbacks to this approach. SPH calculations are computationally intensive; large volumes may only be simulated with relatively poor mass resolution. In the simulation used in Chapter 2 a halo which might be expected to harbour a galaxy of similar mass to the Milky Way would contain only around a hundred particles. Consequently our comparison was restricted to larger halos where mass resolution was less of a problem, and there was little to be learned by investigating individual galaxies in detail.

Improved resolution may be obtained using the technique of "zooming in" on a region of interest in a simulation. Two of the earliest examples of simulations using this approach are described by Frenk et al. (1996) and Tormen et al. (1997). An initial simulation of a large volume with relatively poor mass resolution is carried out, then an object is picked out for resimulation. All of the particles in the object are traced back to their positions at the beginning of the simulation to determine the region from which the object formed. The particles in this region are replaced with a larger number of particles of lower mass. The initial conditions for the new simulation are created using the same density field as the original simulation, but with additional small scale fluctuations in the high resolution region. The simulation therefore initially consists of a volume largely filled

with the original, low resolution particles plus a region of interest populated with much higher resolution particles. If required, SPH gas particles may also be added to the high resolution region with the same distribution as the dark matter particles – for example, one gas particle may be placed on top of each high resolution dark matter particle. In this way very high resolution simulations of individual galaxies with realistic initial conditions and long range tidal forces may be carried out.

The second problem is that the semi-analytic model we employed previously included a statistical treatment of mergers between galaxies that was largely independent of the simulation. A pair of galaxies which merged in one model would not necessarily merge at the same time in the other. We were able to work around this limitation by preventing mergers in the semi-analytic model and then using information from the simulation to merge the resulting galaxy fragments, but this is clearly far from ideal. Ultimately, we wish to carry out a detailed, object by object comparison between state of the art SPH simulations of the formation of individual galaxies and a full semi-analytic treatment of the same process. Since this will involve prescriptions for star formation and feedback, our previous approach is no longer appropriate. Preventing mergers in the semi-analytic model would affect the star formation rate and hence the mass of gas reheated by feedback. In any case, for an unbiased comparison between the two models, the semi-analytic model ought to be independent of the baryonic component of the SPH simulation.

It is therefore necessary to develop a semi-analytic model in which galaxy mergers are determined using the dark matter component of the simulation. This can be achieved by associating each satellite galaxy in a dark matter halo with the surviving core of the progenitor halo in which it formed. When this core merges onto the centre of the halo, the satellite galaxy may be assumed to have merged. Given sufficient numerical resolution, this will also provide more reliable positions for the semi-analytic galaxies. Springel, White, Tormen & Kauffmann (2001) use this technique to populate a cluster mass halo with semi-analytic galaxies, which allows them to investigate the variation of galaxy morphology with distance from the cluster centre.

In this Chapter we modify the N-body GALFORM semi-analytic model to use substructure within dark matter halos to determine galaxy positions and mergers. However, we do not immediately attempt to compare this model with a realistic SPH simulation. Any differences between full SPH and semi-analytic treatments of the formation of a galaxy could arise in a number of ways – cooling and star formation rates may differ, feedback implementations may not be equivalent, limited resolution may affect the models in different

ways, or there may be differences in the initial properties and quantity of gas available in newly formed halos. There may also be evidence that SPH galaxies are able to obtain gas through mechanisms quite unlike the spherical cooling flows which supply semi-analytic galaxies. In the hydrodynamic simulations of Katz et al. (2003), galaxies appear to accrete gas which is channelled along filaments to the centre of the halo without ever being shock heated to the virial temperature. In order to understand the possible differences which may arise, we will initially consider a simplified simulation which includes radiative cooling and star formation, but no attempt at modelling feedback. Additionally, cooling in this simulation is allowed only at redshifts $z < 1$, which ought to reduce the effects of limited resolution on the galaxy population and provides an opportunity to test some of the assumptions of the semi-analytic model regarding the state of the hot halo gas before cooling begins.

The remainder of this chapter is laid out as follows. Details of the SPH simulation are presented in Section 4.2. In Section 4.3 we explain how halo catalogues and halo merger trees are obtained from the dark matter component of the simulation, and in Section 4.4 the algorithm used to determine galaxy positions and mergers using substructure is described. Section 4.5 tests some of the assumptions of the semi-analytic model regarding hot halo gas against the simulated halos at $z = 1$, and Section 4.6 compares the masses of the semi-analytic and SPH galaxies. Finally, our conclusions are presented in Section 4.7.

4.2 The Simulation

The simulation used here is an SPH simulation of the formation of a single galaxy in a cubic volume of side $35.325h^{-1}$Mpc. The total final mass of the galaxy, including its dark matter halo, is approximately $10^{12}h^{-1}$M$_\odot$. The cosmological parameters for this simulation are $\Omega_0 = 0.3, \Lambda_0 = 0.7, \Omega_b = 0.045, \sigma_8 = 0.9$ and $h = 0.7$. There are 50 output times, spaced logarithmically in terms of the expansion factor, between redshifts $z = 50$ and $z = 0$.

The region around the galaxy contains 161 009 dark matter particles of mass $1.7 \times 10^7 h^{-1}$M$_\odot$ and an equal number of SPH gas particles of mass $2.6 \times 10^6 h^{-1}$M$_\odot$. Outside this central high resolution area the gas and dark matter are represented by approximately 400,000 collisionless particles with much greater masses – these are present to provide the tidal forces which the galaxy would be subjected to during its formation.

Before the simulation was run, the high resolution region was chosen to be large enough

that the galaxy and all of its progenitors would be composed entirely of high resolution particles. It is particularly important that this be true because the low resolution particles have no SPH counterparts, and if a halo is composed partly of the high mass particles it will be missing gas particles. The behaviour of the gas within the halo will not then be treated correctly. While it is difficult to guarantee prior to running the simulation that this will not happen, it is possible to test for this problem once the simulation is complete. In this case, it turns out that there is little or no "contamination" of the simulated galaxy's progenitors by low resolution particles.

The simulation includes radiative cooling, a prescription for star formation and an extremely simple attempt at modelling feedback – cooling is just switched off until redshift $z = 1$. While this cooling cut off is not at all realistic, it conveniently reduces resolution problems in the simulation and can easily be reproduced in the semi-analytic model. Hydrodynamic simulations (e.g. Eke et al. 1998, Navarro et al. 1995) suggest that when the dark matter halos form, gas in the halo is shock heated to temperatures comparable to the virial temperature of the halo. The cooling function employed here does not allow gas to cool below temperatures of about 10^4K, so no cooling is likely to occur in halos with virial temperatures of less than this. This temperature corresponds to halo masses of between 40 and 80 dark matter particles between redshifts zero and one.

The star formation rate, $\dot{\rho}_*$, for each SPH particle is given by:

$$\dot{\rho}_* = C_* \rho_{\text{gas}}/t_{\text{ff}} \tag{4.1}$$

where

$$t_{\text{ff}} = 1/\sqrt{4\pi G \rho_{\text{gas}}} \tag{4.2}$$

and $C_* = 0.04644$. Here, ρ_{gas} is the SPH gas density and G is the gravitational constant. Stars are only allowed to form when the gas has a temperature of less than 3×10^4K and a density greater than $1.16 \times 10^{-24}h^2\text{g cm}^{-3}$. This scheme was chosen to reproduce the Kennicut law (Kennicutt 1998) in simulations which include realistic feedback. Without feedback its only effect is to convert dense clumps of cooled gas particles into collisionless star particles, thereby reducing the complexity of the SPH calculations.

4.3   Obtaining a Merger Tree for the Simulated Galaxy Halo

4.3.1   The Subfind Algorithm

As in Chapter 2, the starting point for the semi-analytic model we use here is a catalogue of dark matter halos for each output time. However, since we now wish to associate semi-analytic satellite galaxies with substructure within the halos, a more sophisticated group finding algorithm than friends of friends is needed. We use the Subfind algorithm, described by Springel, White, Tormen & Kauffmann (2001) and implemented by Volker Springel, which identifies substructure in dark matter halos by looking for self-bound groups of particles which form local density maxima. Subfind is applied to halos located using the usual friends of friends algorithm and works as follows:

For each particle in the halo, an estimate of the local dark matter density is obtained by averaging over nearby particles using a smoothing length equal to the distance to the N_{dens} nearest neighbour.

The particles within the halo are then considered in decreasing order of density. For each particle i, with density ρ_i, the N_{ngb} nearest neighbours are found, and within this set those with higher density than ρ_i are picked out. Of these, the two nearest particles to particle i are selected. If no particles are selected in this way, particle i is a local density maximum and is considered to be a new subgroup. If one particle belonging to a subgroup is selected, or two belonging to the same subgroup are selected, particle i is added to that group. Finally, if two particles belonging to different subgroups are selected the two subgroups are recorded and then joined to form a single subgroup. Particle i is added to the new subgroup.

For each halo this produces a set of subgroups corresponding to local density maxima, including one which represents the background mass distribution of the halo. The subhalos are then required to be gravitationally self bound. Particles with positive total energy (gravitational plus kinetic) are removed one at a time, with the potential energy being re-calculated between removals. If fewer than N_{ngb} particles remain the subgroup is discarded. We choose to set $N_{\mathrm{ngb}} = 10$ and $N_{\mathrm{dens}} = 10$.

The algorithm will often assign particles to more than one subgroup. Almost all of the particles in the friends of friends halo will belong to the background group, and many will also be part of genuine substructures within the halo. In principle there could be any number of levels of substructure within substructure, so to simplify the subgroup catalogue particles are assigned to the least massive subgroup they have been identified

with.

4.3.2 Building the Merger Tree

In order to obtain a merger tree for the simulated galaxy, we first need a set of halos for each simulation output time. As in Chapter 2, we wish to avoid including chance groups of particles in the halo catalogue by requiring that the groups be bound. To do this, we apply the Subfind algorithm to a set of friends of friends halos identified using a linking length $b = 0.2$ and minimum group size N_{min}=10. We then attempt to identify one or more of the subgroups in each group as the background mass distribution of a halo. There may be more than one such background subgroup if friends of friends has artificially linked two or more halos. Particles belonging to subgroups within each background subgroup are added to the background subgroup to produce what we will refer to as a "main halo".

Main halos are identified by considering all of the subgroups in a FOF halo in increasing order of mass. The most massive subgroup is always considered to be a main halo. For each of the remaining subgroups we identify all particles which belong to a more massive subgroup and are within a linking length of at least one particle belonging to the subgroup. The subgroup is added to whichever more massive subgroup the greatest number of these particles belong to. If no such particles are found, the subgroup must be joined to the rest of the FOF group by unbound particles and is considered to be a new main halo. This results in the assignment of all subgroups to a main halo. In the majority of cases, where the FOF algorithm has correctly identified a single halo, the main halo is simply the original friends of friends group minus particles not bound to any subgroup. Fig. 4.1 shows examples of the less common case, where FOF groups are split into more than one main halo.

There are also cases where a friends of friends halo contains no self bound subgroups. These groups are generally close to the 10 particle minimum mass imposed by the FOF group finder and are discarded. Fig. 4.2 shows the six most massive examples of this. These groups tend to be simply loose collections of particles without the central dense regions that would be required for significant cooling to occur. Hence it seems reasonable to omit these halos from the merger tree and therefore from the semi-analytic cooling calculations.

A catalogue of these main halos is produced for each simulation output time and used to construct a merger tree for the dark matter halo of the simulated galaxy. As in Chapter 2, each halo is considered to be a progenitor of whichever halo at the next output
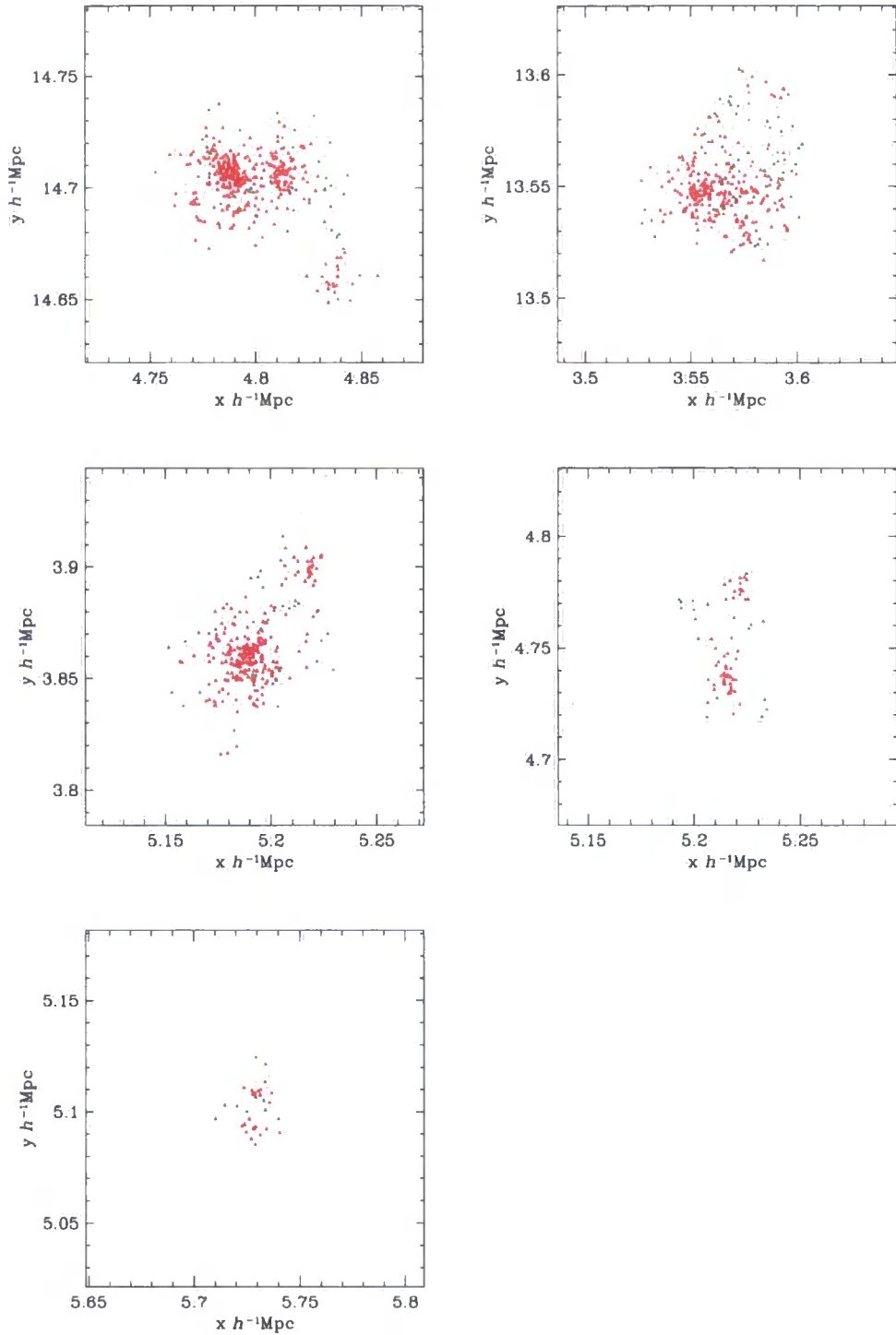
Figure 4.1: Halos which are split into more than one main halo using the algorithm described in the text. Red dots indicate particles belonging to a main halo. Green dots are particles which belong to the friends of friends group but are not bound to any subgroup. In all five cases shown the FOF group is split into two main halos.
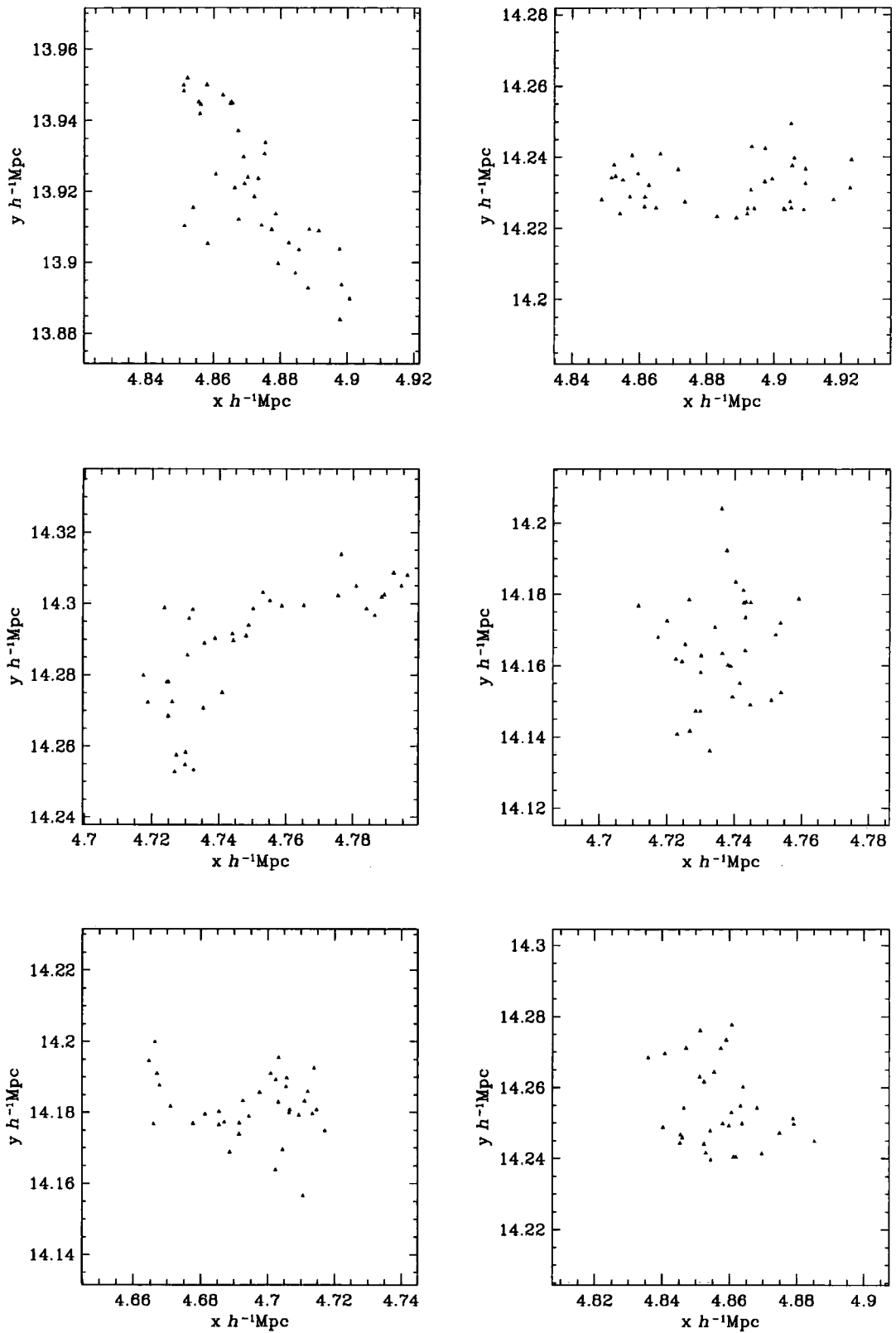
Figure 4.2: The six most massive friends of friends halos in the simulation with no bound subgroups at $z = 1$.

time contains the greatest number of its particles.

Previously, we devised an algorithm to deal with situations where two halos were joined at one timestep but not at the next – if particles from a halo were in different halos at the next time step the halo would be broken up into two or more halos at all earlier times. This had the desired effect of splitting halos joined by tenuous "bridges" of particles. However, since we now make use of substructure information in the construction of our halo catalogues, as described earlier in this section, this procedure should be redundant. In fact, we find that it can cause the semi-analytic model to behave unrealistically in certain circumstances.

If the splitting algorithm is applied to the dark matter merger tree of the simulated galaxy, we find that halos which are split from a much more massive halo (usually the most massive progenitor of the final object) often contain very few SPH gas particles. This happens when the small halo falls into the more massive one, passes through it, and emerges from the other side having been stripped of most of its hot gas. The small halo is considered to be separate from the more massive halo even while embedded within it, and in the semi-analytic model it will continue to cool gas during this time. If we discard the splitting algorithm no cooling will be allowed in such objects, which would be more physically reasonable – this is what is usually assumed to happen in semi-analytic models and appears to happen in the simulation. Therefore we do not split halos during the construction of the merger tree.

However, a new problem then arises. When one of these small halos first falls into the more massive halo, any semi-analytic galaxy it contains will become a satellite. But if the halo then emerges and becomes a separate object again it is likely that it will quickly fall back into the massive halo, at which point it may contribute *another* satellite galaxy. To avoid this, we look for situations where a subgroup within a halo (other than the background subgroup) is a progenitor of the background subgroup of a halo at the next timestep. Following Springel, White, Tormen & Kauffmann (2001), we consider a subgroup to be a progenitor of a subgroup at the next timestep if more than half of the N_{link} most bound particles are members of the later subgroup. If this occurs, we remove the halo from the merger tree at this output time. We also remove its descendent halos at later output times as long as they remain separate from the massive halo. This will prevent the possibility of forming two satellite galaxies from a single progenitor halo.

4.4   Semi-analytic Galaxy Positions and Mergers using N-body Substructure

In the model described in Chapter 2, mergers between semi-analytic galaxies were treated in a statistical fashion. The energy and angular momentum of each satellite was assigned at random using a distribution consistent with numerical simulations. A dynamical friction timescale was then calculated to determine when the galaxy should merge. Satellite galaxies were placed at the position of the most bound particle of the halo in which they formed. Note that the velocity of this particle will not generally be consistent with the orbit assumed for the dynamical friction calculation and satellites will not necessarily be placed close to the central galaxy just prior to merging on to it. Central galaxies in this model were placed on the most bound particle in their dark matter halo.

Here, we wish to obtain positions by associating the galaxies with the dark matter subgroups found by the Subfind algorithm, and to use the subgroups to determine when galaxy-galaxy mergers occur. The centre of a halo is defined as the most bound particle of the most massive subgroup. Any gas which cools in the halo accretes onto a central galaxy at this location. When the halo merges onto a more massive halo, it will survive for some time as a subgroup within the halo. Any central galaxy from the less massive halo is now a satellite and will be associated with this subgroup. If the subgroup merges onto the centre of the massive halo, the satellite galaxy is assumed to have merged onto the central galaxy.

We implement this as follows. Having obtained a catalogue of halos and subgroups, as described in Section 4.3.2, we link the subgroups between consecutive timesteps by looking at the N_{link} most bound particles, as explained in the previous Section. Note that usually one subgroup in each halo will be the background mass distribution ("background subgroup" for short) of a halo and will contain the bulk of its mass.

We then examine the progenitors of the final halo, starting at the earliest output time where progenitor halos are detected and working towards redshift $z = 0$. Whenever a halo has more than one progenitor, the background subgroups of all but the most massive of these are registered as potential satellite galaxies. The descendents of these subgroups are found at subsequent output times and for each the coordinates of the most bound particle are recorded. For each progenitor halo, other than the most massive, we then have the coordinates of the substructure it becomes at later output times as a function of time. This is where the central galaxy from the progenitor halo will be placed when it

becomes a satellite.

Sometimes no descendent can be found for a subgroup, or the descendent may be the background subgroup of the parent halo. This happens when a substructure genuinely merges onto the centre of the halo or is just stripped of mass until it is no longer detected by Subfind. We wish to distinguish between these two situations – in the first case, any galaxy assigned to the subgroup should merge onto the central galaxy. In the second case, it is possible that the subgroup may be some distance from the centre of the halo and we need to continue to track its position despite being unable to detect it.

We make this distinction by recording the indices of the particles which belonged to the subgroup at the last output time where it was detected by Subfind. At each subsequent output time, we calculate the centre of mass of these n particles and a characteristic radius, r_{sg}, given by

$$r_{sg} = \left(\frac{1}{n} \sum_{i=1}^{i=n} \frac{1}{r_i} \right)^{-1} \tag{4.3}$$

where r_i is the distance between the ith particle and the centre of mass of all n particles. This radius estimate is used because it is not strongly affected by single particles at large distances. If r_{sg} becomes greater than the distance between the centre of mass of the particles and the centre of the halo, the subgroup is considered to have merged onto the centre of the parent halo. We record the timestep at which this occurs, so that any semi-analytic galaxy associated with this subgroup can be merged onto the central galaxy at the appropriate time. Otherwise, we record the coordinates of the centre of mass of the particles as if they were still an identifiable subgroup and continue to do so until the merger condition is met.

4.5   Properties of the Simulated Halos

Before we attempt to directly compare the semi-analytic model to the SPH simulation, we first examine the properties of the simulated halos at redshift $z = 1$. At this stage no cooling has occurred, so this allows us to test the assumptions of the semi-analytic model regarding the initial state of the hot halo gas. Here, we concentrate on those relevant to the treatment of cooling:

1. The baryon fraction in each halo is equal to the universal baryon fraction.

2. When a halo forms, the gas is shock heated to the virial temperature of the halo,

given by

$$T_{\text{virial}} = \frac{0.5 \mu m_{\text{H}} V_{\text{H}}^2}{k_{\text{B}}} \qquad (4.4)$$

where μm_H is the mean atomic mass of the gas, V_{H} is the circular velocity of the halo and k_{B} is the Boltzmann constant.

3. The gas is taken to be isothermal.

We do not expect large deviations from these assumptions because simulation results were used as a guide in the construction of the semi-analytic model. For example, the density profile of the hot halo gas is inspired by hydrodynamic simulations carried out by Eke et al. (1998). These simulations, as well as those of Navarro et al. (1995), also support the assumption that the gas is approximately isothermal and at the virial temperature. However, by first testing the assumptions made regarding the hot halo gas we hope to determine whether any differences we find between the SPH and semi-analytic models are due to differences in the initial hot gas distribution or if the models only diverge once cooling begins.

4.5.1   The Baryon Fraction

The most basic assumption made in the semi-analytic model regarding the hot halo gas is that the mass of gas is initially equal to the mass of the halo multiplied by the universal baryon fraction. This determines the total mass of material available for galaxy formation. Fig. 4.3 shows the mass of baryons in each halo at $z = 1$ in the SPH simulation plotted against the total halo mass. In the upper panel, the mass of gas and dark matter is measured within the virial radius of the halo, taking the most bound particle of the most massive subgroup in the halo as the centre. The virial radius is measured from the simulation by expanding a sphere around the most bound particle until the enclosed dark matter density falls to the overdensity predicted for virialised objects by the top hat spherical collapse model at this redshift. In the lower panel, the mass of dark matter in the halo is simply the total mass of dark matter particles considered to be part of the main halo. For each gas particle we then identify any dark matter particles which are within the friends of friends linking length and belong to a halo. If any are found, the gas particle is assigned to whichever halo the closest of these belongs to.

The most massive halos appear to have around 90% of the expected mass of baryons. This small shortfall may be due to our use of the dark matter only to define the boundaries of the halos – unlike the dark matter, the gas is subject to pressure forces and tends to
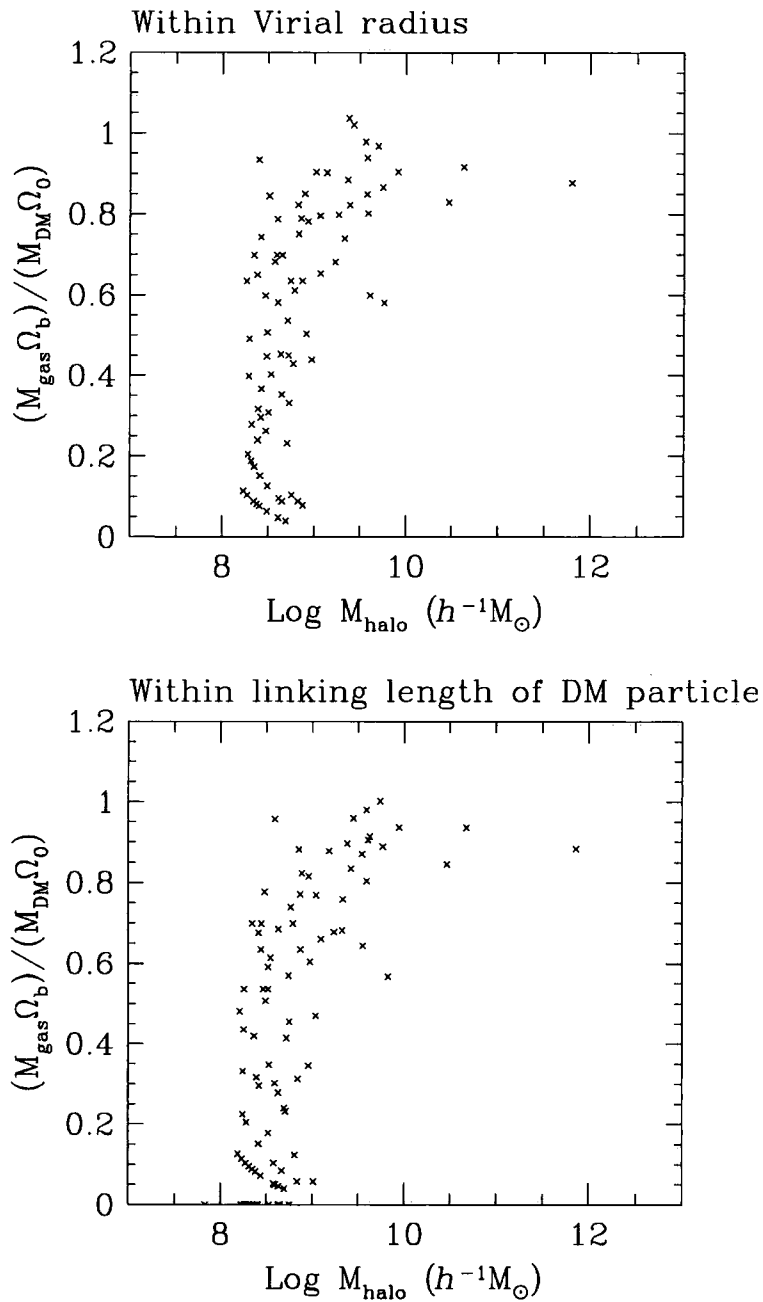
Figure 4.3: The baryon fraction in progenitor halos of the final galaxy at $z = 1$. In the upper panel, the mass of gas and dark matter is measured within the virial radius. In the lower panel, the dark matter mass is the mass of the main halo. The gas mass includes all particles within a linking length of dark matter particle belonging to the halo.

have a slightly more extended distribution. The missing gas is most likely just outside the (somewhat arbitrary) boundaries we have imposed on the halos. Halos with masses down to a few times $10^9 h^{-1} M_\odot$ still typically have around 80% of the expected mass of baryons, but at lower masses there are many halos containing very little gas. These objects are not well resolved, having fewer than 50 dark matter particles each, and may have been stripped of their baryonic mass in encounters with other, more massive halos.

These results would suggest that assumption (1), above, agrees well with the simulation for halos consisting of 50-100 particles or more, but breaks down in poorly resolved halos. Thus we can expect the semi-analytic model to allow cooling and star formation in halos which, in the simulation, have not been able to retain any significant quantity of gas.

4.5.2 The Gas Temperature

Next, we test the assumption that gas within halos is shock heated to the virial temperature of the halo. The SPH algorithm tracks the specific internal energy of each gas particle, so the mass weighted mean gas temperature for a halo is obtained by simply taking the mean of the temperatures of the particles belonging to the halo. If assumption (2) holds, this ought to be in agreement with Equation 4.4.

Fig. 4.4 shows the mean gas temperature in the SPH simulation as a function of halo mass. Here we assign gas particles to halos according to the halo membership of nearby dark matter particles, as described above. The temperature assumed in the semi-analytic model is shown in the figure as a solid line. At masses below around $10^9 h^{-1} M_\odot$ there are many halos with unexpectedly high mean SPH gas temperatures. These may be objects which have undergone close encounters with much more massive halos – this is likely to occur quite frequently because at this stage the simulation contains a single, relatively massive halo surrounded by many much smaller objects.

At higher masses, there is a strong correlation between halo mass and temperature with a slope very close to that expected. However, there is an offset between the SPH and semi-analytic gas temperatures, with the SPH temperatures typically being around 75% of what is assumed in the semi-analytic model.

In the semi-analytic model, the halo is taken to be in hydrostatic equilibrium, and under this assumption the gas temperature can be calculated from the dark matter and gas density distributions. One possible explanation for the discrepancy between the SPH and semi-analytic temperatures is that this assumption is not entirely accurate.
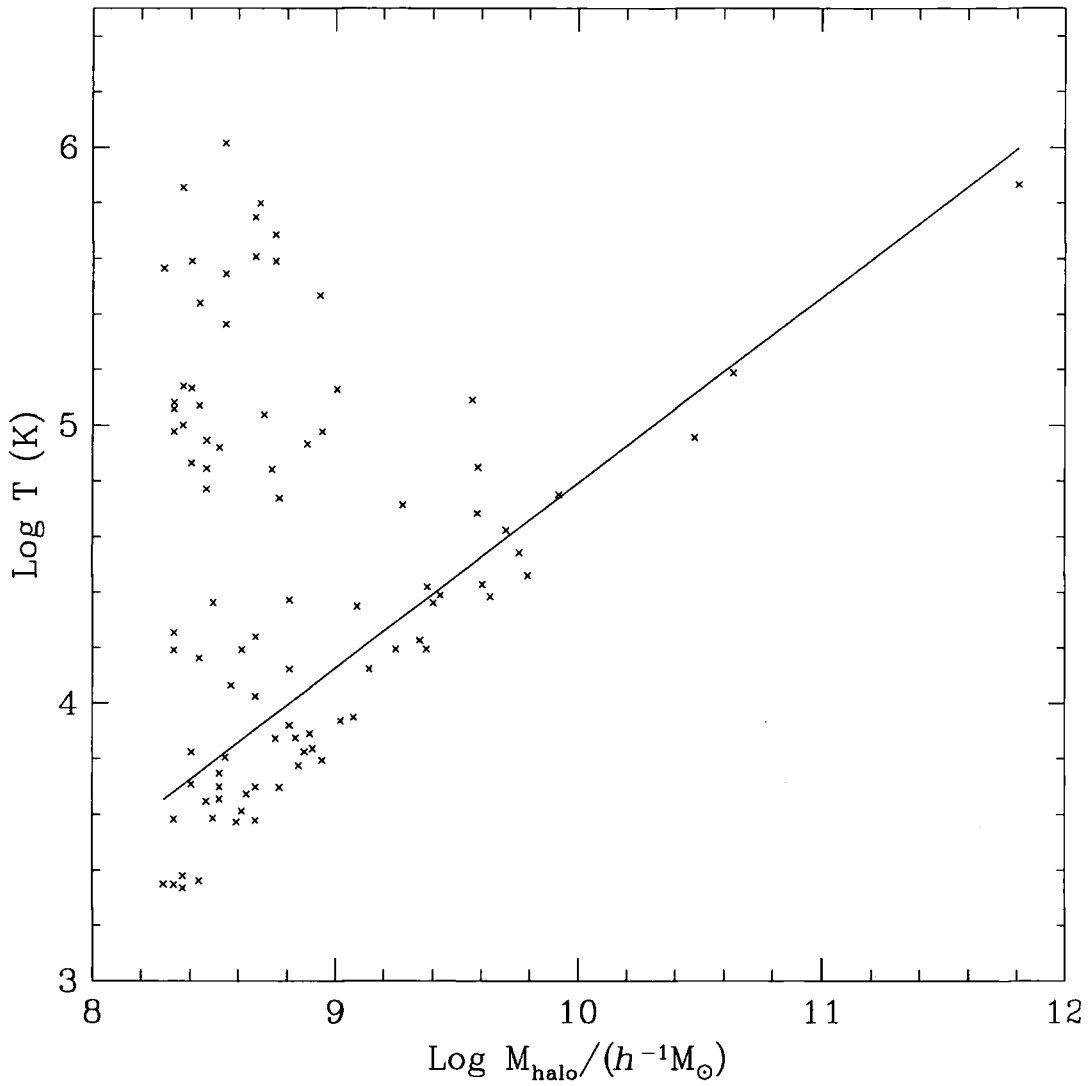
Figure 4.4: The mass weighted mean gas temperature of each halo in the SPH simulation at $z = 1$ as a function of total halo mass. The solid line shows the temperature assumed by the semi-analytic model as a function of halo mass.

Since we know the distribution of gas and dark matter in the simulation, the gas temperature required for hydrostatic support may be calculated and compared with the SPH gas temperature.

If we assume spherical symmetry, the pressure required for hydrostatic support may be obtained from:

$$dP(r) = -\frac{GM(r)\rho(r)}{r^2}dr \qquad (4.5)$$

where $P(r)$ is the gas pressure at a radius r, G is the gravitational constant, $M(r)$ is the total mass interior to the radius r, and $\rho(r)$ is the gas density as a function of radius. Our approach is to take the pressure at the virial radius to be zero, and numerically integrate this equation to obtain the pressure as a function of radius. The expected gas temperature, $T(r)$, may then be obtained from

$$P(r) = \frac{\rho(r)k_B T(r)}{\mu m_H} \qquad (4.6)$$

The integration is performed by dividing the halo into spherical shells centered on the most bound particle of the main halo. The radii of the shells are chosen so that each contains one gas particle. The density of each shell is then a single gas particle mass divided by the volume of the shell, and the interior mass is the total mass of the particles within the radius of that shell's gas particle. In this way we obtain a hydrostatic temperature estimate for each gas particle.

Fig. 4.5 shows a test of this numerical integration procedure. A spherical halo with gas and dark matter density profiles proportional to r^{-2}, truncated at an outer radius r_{max}, was created by putting down gas and dark matter particles at random in such a way that all radii less than r_{max} were equally likely. In the upper panel there are 40,000 particles of gas and dark matter in the sphere, giving the halo a similar mass to that of the main progenitor of the simulated galaxy at $z = 1$. In the lower panel the number of particles was reduced to 2000 to determine how this would affect the accuracy of the results. The temperature obtained by numerical integration of Equation 4.5 is shown by the solid lines in the left panels. The analytic solution for the temperature, assuming zero pressure at $r = r_{\mathrm{max}}$, is indicated by the dotted lines. The panels on the right show the ratio of the correct (analytic) temperature to the temperature obtained by numerical integration. It can be seen that this integration method appears to produce reasonably accurate results down to very small radii, even when the number of particles in the halo is reduced.

Isothermal sphere with 40000 dark matter particles

Isothermal sphere with 2000 dark matter particles
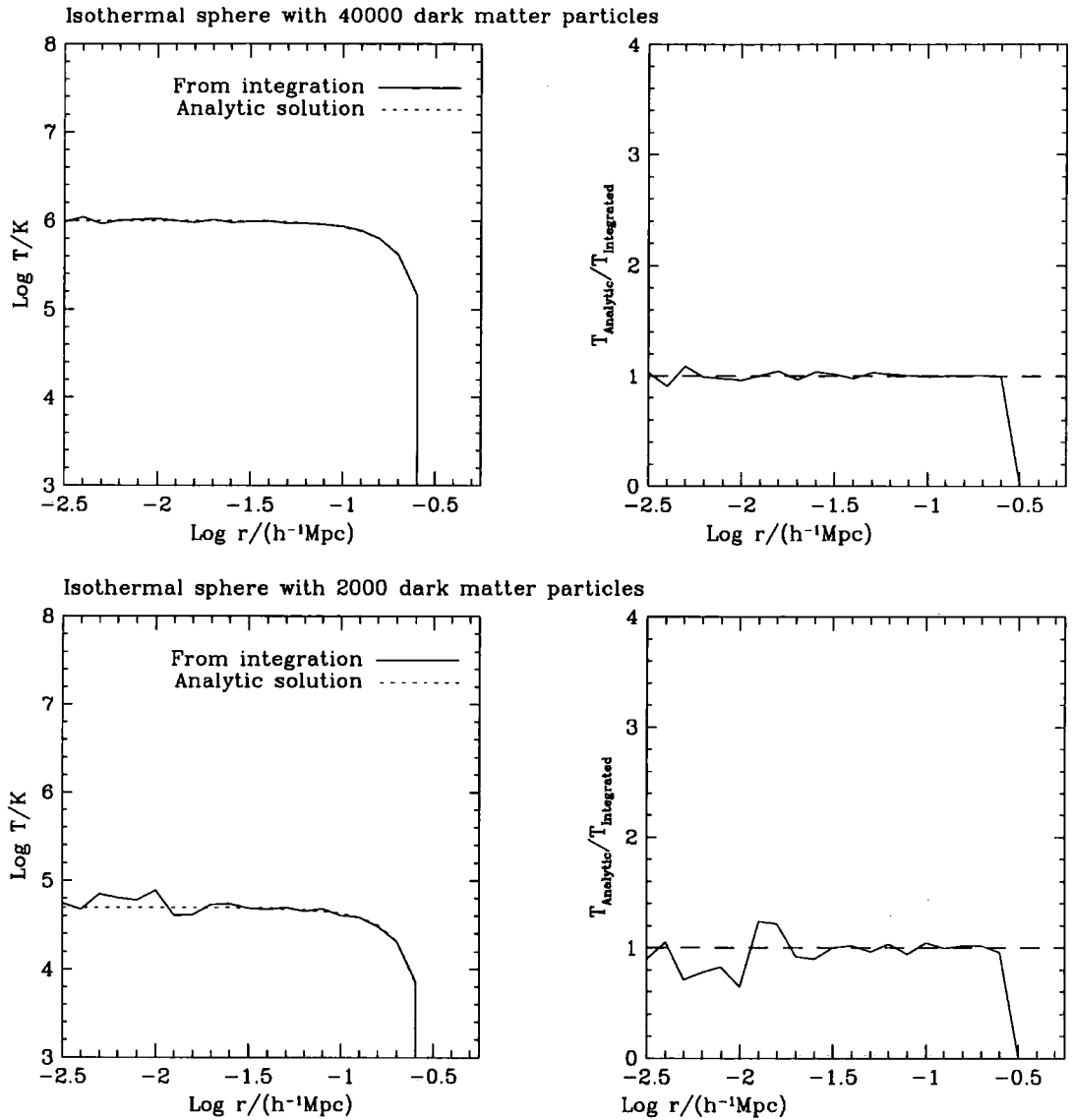
Figure 4.5: The temperature profile derived by integrating the equation of hydrostatic equilibrium for two N-body realisations of isothermal spheres containing 40 000 (upper panels) and 8 000 (lower panels) particles of gas and dark matter. Solid lines show the results of numerical integration as described in the text. The exact, analytic solution for a truncated isothermal sphere is shown by the dotted lines. Both the derived temperatures (left panels) and the ratio of the analytic to the numerical results (right panels) are shown.

Most massive halo, with 28196 dark matter particles

Second most massive halo, with 2817 dark matter particles

Third most massive halo, with 2004 dark matter particles
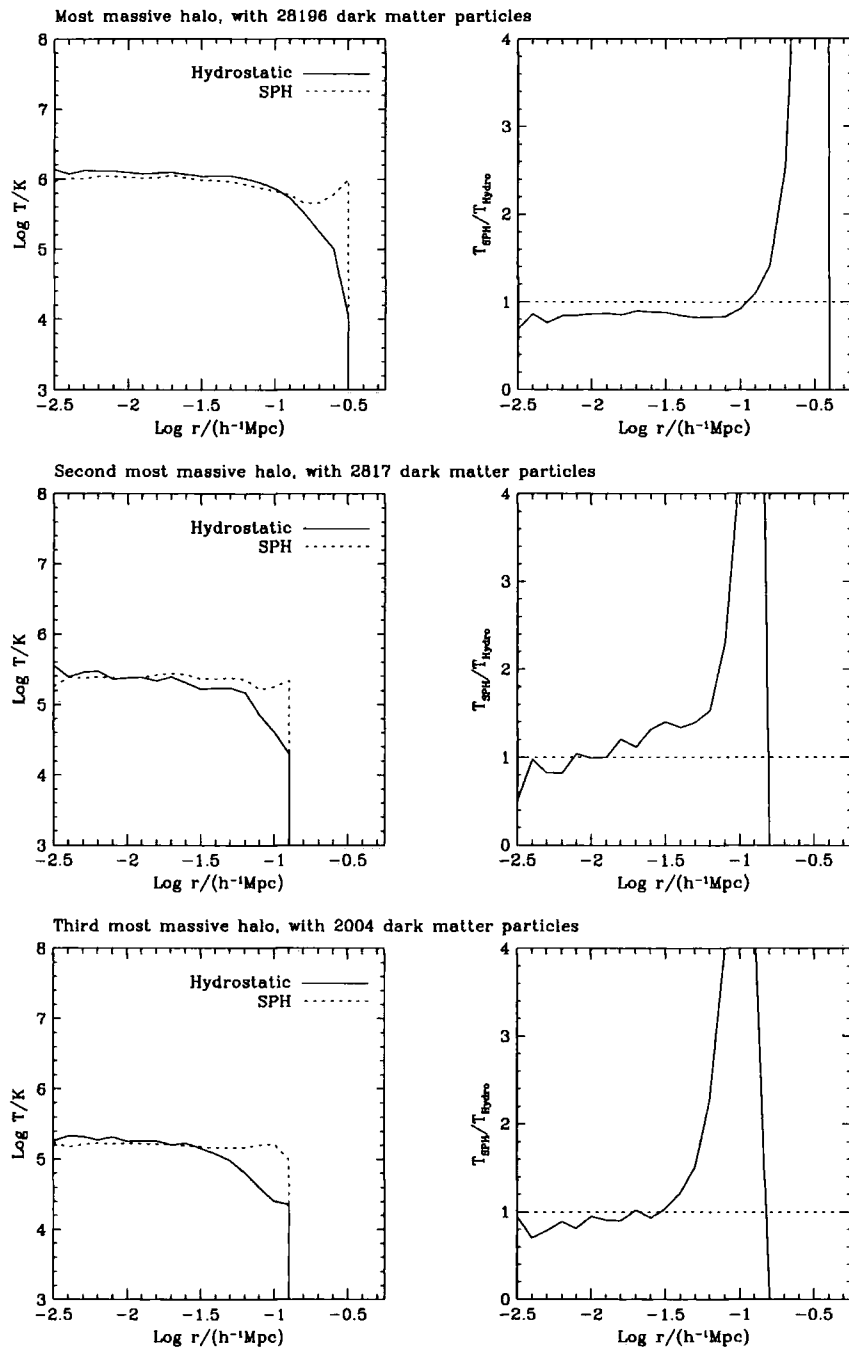
Figure 4.6: Spherically averaged temperature profiles for the three most massive halos in the simulation at $z = 1$. Solid lines indicate the temperature obtained by integration of the equation of hydrostatic equilibrium (see text for details). The dotted lines show the SPH gas temperature, obtained by calculating the mean temperature of the particles in spherical shells. The panels on the left show the actual gas temperature profiles, and the panels on the right show the ratio of the SPH gas temperature to the temperature required for hydrostatic equilibrium.

In Fig. 4.6, the same integration technique is used to calculate the temperature required for hydrostatic equilibrium in the three most massive progenitor halos in the simulation at $z = 1$. In the inner parts of all three halos, the temperature obtained is close to that calculated by the SPH algorithm. This indicates that the halos are indeed approximately in equilibrium. The discrepancy between the temperatures in the outer regions may occur because the pressure at the outer radius will not be zero – in practice the pressure in the outermost regions will be maintained by infalling material, which is certainly not in hydrostatic equilibrium.

In the most massive, and hence best resolved, halo the gas temperature appears to be systematically lower than is required for hydrostatic equilibrium by around 10-20%. This due to the presence of a small amount of non-thermal support in the halo and has been observed previously in cluster simulations (e.g. Frenk et al. 1999) However, this is clearly too small an effect to account for the offset seen in Fig 4.4.

A possible explanation for the offset is that the way in which we define halo masses in the simulation is not entirely equivalent to the definition used in the semi-analytic model. Alternatively, it may be that the gas density profile differs somewhat from that assumed in the model, in which case the temperature required for hydrostatic equilibrium would not be that given by Equation 4.4. The effect of this offset on the semi-analytic model may be investigated by varying the temperature assumed for the hot halo gas. Fig. 4.7 compares the masses of galaxies in a model where the gas temperature is taken to be $0.75T_{\mathrm{virial}}$ with the masses of the same galaxies if the gas temperature is assumed to be equal to the virial temperature. Galaxies present in one model but not the other are plotted near the axes. This change in temperature has very little effect, since without feedback the halos tend to cool all of the available gas. There are a few galaxies present in the standard model which disappear when the gas temperature is reduced. This happens because the cooling function for the halo gas is cut off at temperatures below $10^4\mathrm{K}$. The halos where these galaxies form have virial temperatures such that $0.75T_{\mathrm{virial}} < 10^4\mathrm{K}$ and are consequently unable to cool any gas in the low temperature model.

4.6 Comparison between the models

4.6.1 The Semi-analytic Model

We now compare the masses of individual galaxies between the SPH and semi-analytic models. The semi-analytic model we use here has the same treatment of cooling as de-
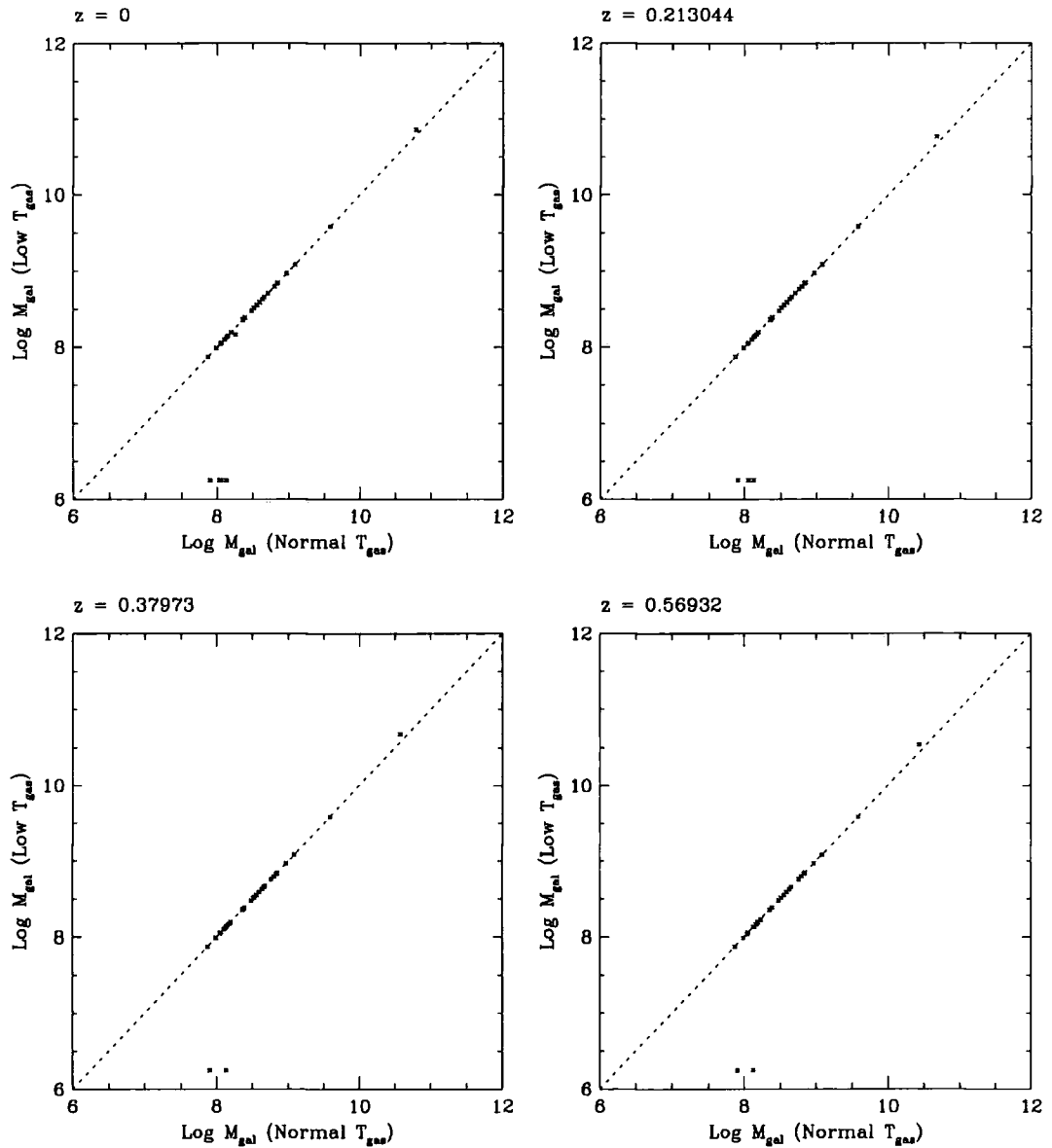
Figure 4.7: Masses of galaxies in a semi-analytic model in which the diffuse halo gas is assumed to be shock heated to 75% of the virial temperature of the halo plotted against the masses of the same galaxies if the gas is assumed to be shock heated to the virial temperature. The four plots correspond to four different redshifts, as indicated at the top of each panel.

scribed in Chapter 2, with the initial core radius, r^0_{core}, set to $0.66r_{NFW}$. This core radius is allowed to increase in such a way that the density of hot gas at the virial radius is maintained as cooling proceeds. Cooling is only allowed in halos of mass greater than $N_{SPH}(m_{dark} + m_{gas})$, where m_{dark} and m_{gas} are the masses of the dark matter and gas particles respectively. Halo masses and merger trees are obtained as described in Section 4.3.2. Galaxy positions and mergers are determined using the methods explained in Section 4.4. In accordance with the SPH simulation, no feedback prescription is included, and cooling is only allowed to occur at redshifts $z < 1$. We have made no attempt to match the star formation rate in the semi-analytic model to the simulation. Instead, we will simply consider the total mass of cold gas and stars in each galaxy. Without feedback, this is independent of the star formation rate.

4.6.2   Identifying SPH Galaxies

Masses for the SPH galaxies are obtained by running a friends of friends group finder on the cold (temperatures less than 10^5K) gas and star particles in the simulation. The exact choice of temperature cut is not critical, since only gas which has cooled is likely to reach the very high overdensities required by friends of friends with a linking length $b \simeq 0.01$. The gas and star particles in this simulation have equal masses, which allows us to use a single linking length for both species. The left hand panels in Fig. 4.8 show the effect of increasing b from 0.0075 to 0.015. The masses of the galaxies found using $b = 0.0075$ are plotted against the mass of the nearest galaxy identified using $b = 0.015$. The position of a galaxy is taken to be the position of its centre of mass. Increasing the linking length will sometimes join objects which would otherwise have been considered separate. In Fig. 4.8, such objects appear as multiple points at the same position on the y axis. The right hand panels show the effect of increasing b from 0.015 to 0.03. With a few exceptions, the galaxy masses are insensitive to the choice of b for masses greater than about $10^8 h^{-1} M_\odot$, or around 50 particles. The exceptions are cases where friends of friends with $b = 0.03$ artificially links objects which, by eye, are clearly separate. In the following sections we use a linking length $b = 0.015$ and a minimum group mass of 10 particles, although we note that groups of around 50 particles or less are likely to be very unreliable.

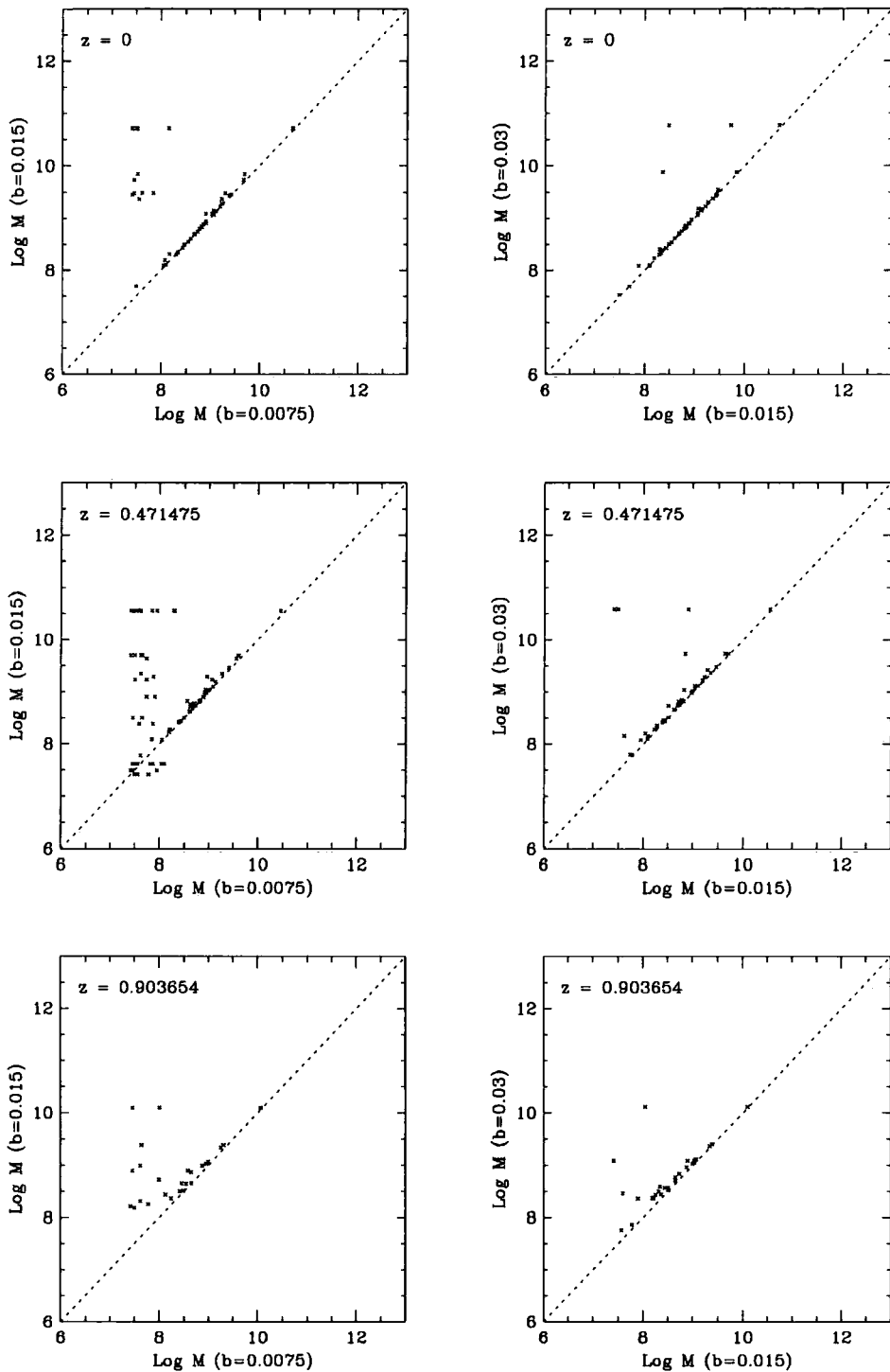Figure 4.8: Effect of varying the FOF linking length on the masses of SPH galaxies at redshifts $z = 0$ (top), $z \simeq 0.5$ (middle) and $z \simeq 0.9$ (bottom). In the panels on the left, the masses of galaxies identified using the FOF algorithm with $b = 0.015$ are plotted against the masses obtained with $b = 0.0075$. The panels on the right show the effect of increasing b to 0.03 on the galaxy masses.

4.6.3   Galaxy by Galaxy Comparison

To compare galaxy masses, we require some way of identifying galaxies in one model with "the same" galaxies in the other. The simplest approach is to consider a single timestep and look at the galaxy positions. Since mergers in the semi-analytic model now correspond to mergers between dark matter subhalos in the simulation, we may expect the positions of semi-analytic galaxies to correspond closely to the positions of the SPH galaxies – unless clumps of cold gas and stars in the simulation become separated from their associated dark matter. For each SPH galaxy, we locate the closest GALFORM galaxy. If the SPH galaxy is also the closest to the GALFORM galaxy, we consider the galaxies to be a match. Only galaxies within a friends of friends linking length, $b = 0.2$, are considered. Galaxies with masses equivalent to fewer than 50 gas particles are excluded from the matching procedure. The distribution of galaxies at three different redshifts is shown in Fig. 4.9. Galaxies are plotted as coloured circles, with the area of the circle proportional to the mass of the galaxy. Galaxies in one model which are matched to galaxies in the other are shown in green. Here, we have set $N_{\rm SPH} = 50$.

The semi-analytic model clearly produces many more low mass galaxies than the SPH simulation. This would appear to be consistent with the low baryon fraction seen in many poorly resolved halos in the simulation (see Fig.4.3), but occurs despite the suppression of cooling in halos of fewer than 50 particles. There are relatively few SPH galaxies which cannot be matched to GALFORM galaxies at $z = 0$, and only one containing a significant fraction of the total cooled mass – around 640 gas particle masses in cold gas and stars (the central galaxy contains around 20,000 gas particle masses). This particular galaxy is a consequence of the way cooling suddenly begins at redshift $z = 1$. At $z = 1$, the halo in which this galaxy formed has, according to the halo finding algorithm we use, just merged with a more massive halo and is not able to cool any gas. However, the halos are only just linked and in dotplots the smaller halo is clearly still intact so that in the SPH simulation gas is able to cool here for a short time. This results in an SPH galaxy where no GALFORM galaxy could have formed. The second most massive unmatched galaxy, containing about 115 gas particle masses, formed in similar circumstances. The problem arises because in the semi-analytic model mergers are treated as instantaneous events, so we are forced to (somewhat arbitrarily) define the moment at which the halos are considered to be merged. In reality, mergers are events with a finite duration and our definition may not be appropriate in all cases – especially when we are forced to take
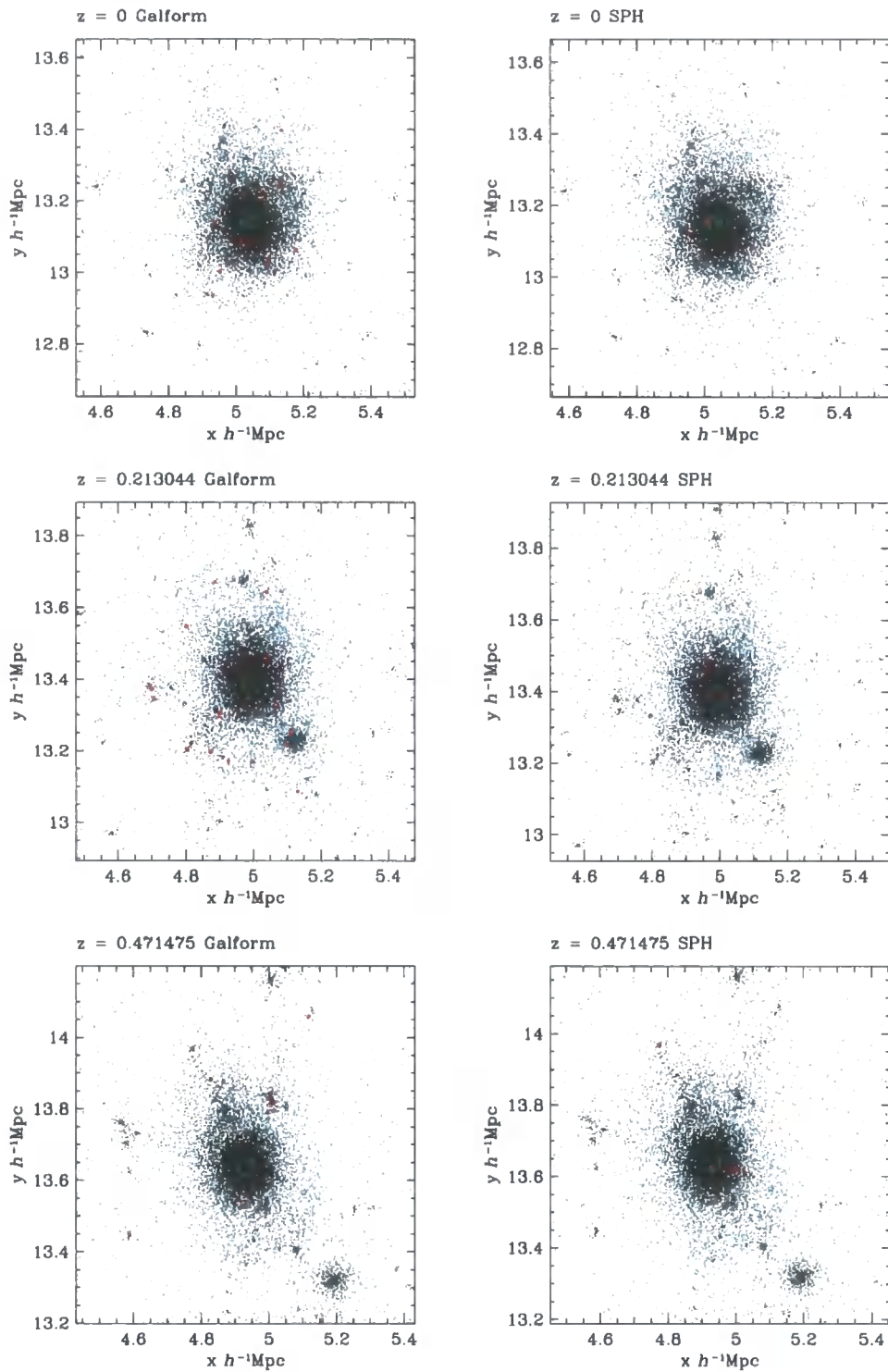
Figure 4.9: The distribution of SPH (right hand panels) and semi-analytic (left hand panels) galaxies at three different redshifts. Matched galaxies are plotted as green circles. Unmatched galaxies are shown in red. The area of each circle is proportional to the mass of the galaxy. Dark matter particles are plotted as black points if they belong to a halo, and cyan points otherwise.

one of the simulation output times as the time of the merger. Fortunately, this particular problem is rather less likely in simulations without the artificial cooling cut off at $z = 1$, where the galaxy would have accreted mass over many time steps before the merger.

Of the remaining five unmatched SPH galaxies at $z = 0$, the three most massive (with 104, 49 and 47 gas particle masses) are matched to GALFORM galaxies for several timesteps after their formation, but cease to be matched soon after entering the main halo in the simulation. This would happen if the clump of cold gas and stars comprising the SPH galaxy became offset from the core of the halo in which it formed, possibly due to hydrodynamic forces (both real and, possibly, artificial) which would not affect the trajectory of the dark matter core. The position of the galaxy would then no longer correspond to the assumed position of the semi-analytic galaxy and no match would be found. The two remaining unmatched SPH galaxies, with 31 and 19 gas particle masses, are too poorly resolved for us to draw any useful conclusions regarding their origin.

The number of unmatched GALFORM galaxies varies with the cooling threshold, N_{SPH}. Fig. 4.10 compares the masses of individual galaxies between the models for three different choices of N_{SPH} at six different redshifts. Unmatched SPH galaxies are plotted along the x axis and unmatched GALFORM galaxies are plotted along the y axis. The main effect of increasing N_{SPH} from 50 to 100 is to remove some of the low mass semi-analytic galaxies which have no SPH counterparts. The number of galaxies which are matched is almost completely unaffected. Setting N_{SPH} as high as 200 removes most of the unmatched GALFORM galaxies but also prevents the formation of some of the galaxies which *do* exist in the SPH simulation. For the remainder of this section we employ a model with $N_{\mathrm{SPH}} = 100$, which we use to investigate the reliability of our matching scheme and the nature of the remaining unmatched GALFORM galaxies.

4.6.4   Reliability of the Matching Algorithm

As noted earlier, a few of the unmatched semi-analytic galaxies at low redshift are found to be matched to SPH galaxies for a number of time steps after their formation, only ceasing to match after existing for several time steps as satellite galaxies in the most massive halo in the simulation. Since galaxies are matched using their positions only, this would occur if the centre of mass of the cooled gas and stars comprising the SPH galaxy became offset from the dark matter substructure where the semi-analytic galaxy is placed. Upon entering the dense halo environment, the galaxy may be subject to hydrodynamic forces (some artificial) which do not affect its associated dark matter. Alternatively, the
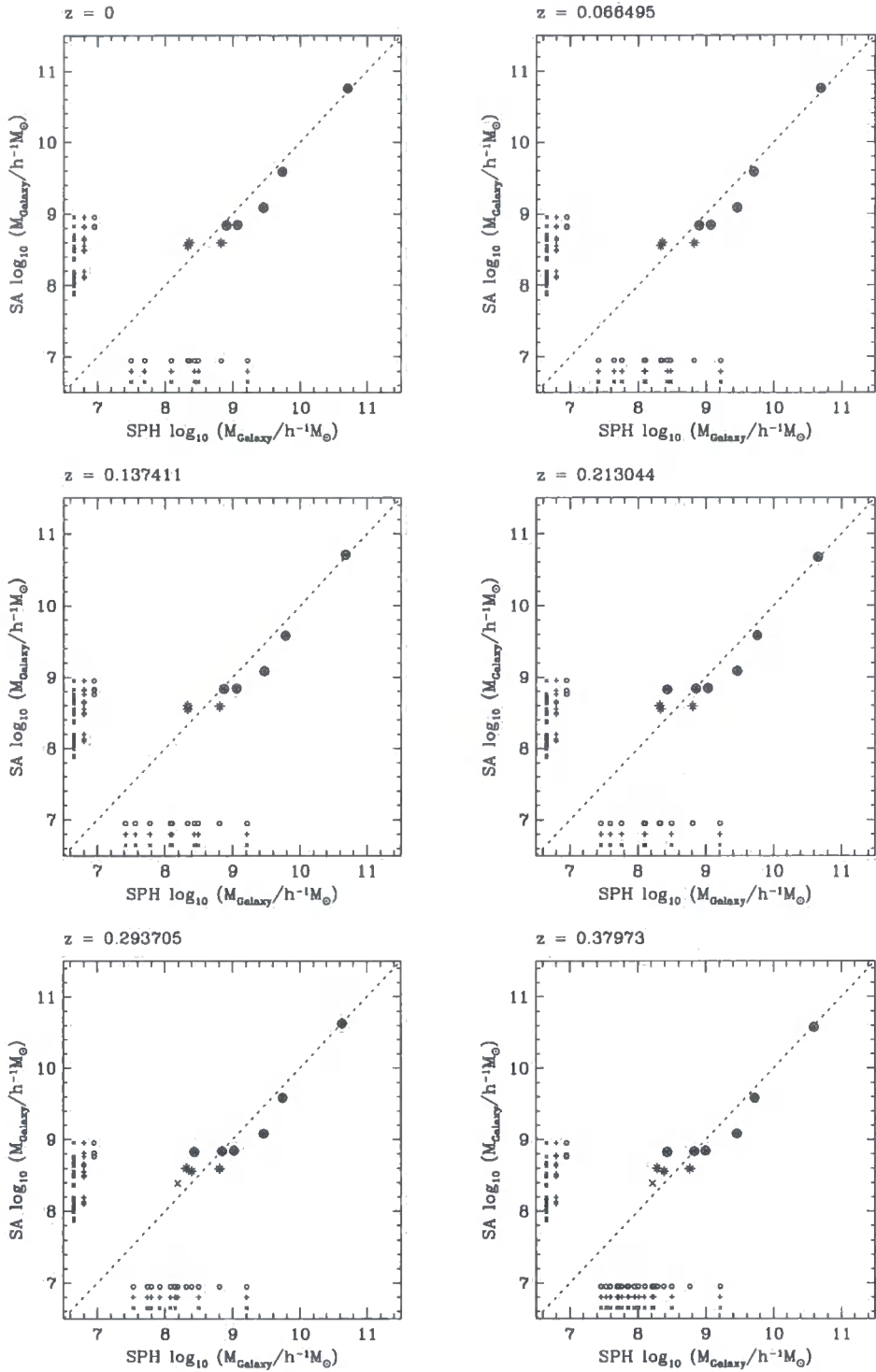
Figure 4.10: Comparison between SPH and semi-analytic galaxy masses at six different redshifts for semi-analytic models with the cooling threshold parameter, N_{SPH}, set to 50 (plotted as diagonal crosses), 100 (horizontal/vertical crosses) and 200 (circles). The masses of unmatched galaxies are plotted along the appropriate axes using smaller symbols. The unmatched points corresponding to the three different choices of N_{SPH} have been offset from each other for clarity.

position of the substructure may become unreliable once it is reduced to a small number of particles. In either case, the galaxies clearly ought to be considered matched at subsequent time steps even if their positions have diverged somewhat.

In order to achieve this, we first carry out position based matching using the same scheme as before. We then consider adjacent pairs of timesteps, t_1 and t_2 (where $t_2 > t_1$), starting with the second earliest at which galaxies are found. For each SPH galaxy at time t_2, any progenitor SPH galaxies at time t_1 are located. If one or more of these are matched to galform galaxies, the semi-analytic descendents of these galaxies are found at time t_2. If exactly one *unmatched* semi-analytic galaxy at time t_2 is found in this way, it is considered to be matched to the SPH galaxy. While this procedure could, in principle, identify more than one semi-analytic galaxy for each unmatched SPH galaxy, in practice we always find either zero or one possible matches. It is unlikely that more than one galaxy would ever be identified unless our positional matching algorithm incorrectly matched one of the progenitor SPH galaxies at the earlier timestep.

This is repeated for all subsequent pairs of time steps. Any new matches obtained at early time steps are used in the analysis of later steps. This ensures that if an SPH galaxy is found to correspond to a semi-analytic galaxy at one timestep the galaxies will be considered to be matched at all later times, even if their positions begin to diverge.

The effect of this approach on the results shown in Fig. 4.10 is to reduce the number of unmatched galaxies, but only by one to three per time step and only at redshifts $z < 0.3$. The galaxies affected have masses of around $10^8 h^{-1} M_\odot$, or approximately 50 particles. Therefore, for all but the least well resolved galaxies, the simple position based scheme continues to match all galaxies after they become satellites. Of course, it may be that some of the galaxies being matched are at similar positions by chance, and did not originate in the same progenitor halo.

It is possible to test whether this occurs if, in both the SPH and semi-analytic models, the "descendents" of each galaxy at subsequent timesteps can be found. If a pair of galaxies (one SPH and one semi-analytic) are matched at one timestep then their descendents at the next also ought to be matched to each other. With one exception, we find that in every case where the descendents of a matched pair of galaxies are both matched they are matched to each other. It follows that if a galaxy is correctly matched when it first forms (which is likely since it will generally be the only galaxy in the halo), then at later times it will almost always be correctly matched if it is matched at all. It is very unlikely that a semi-analytic galaxy could, by chance, be repeatedly matched to an SPH galaxy

which formed in a different progenitor halo.

Any failure to match galaxies which really are present in both models would result in both unmatched SPH and unmatched GALFORM galaxies. While we find a relatively large number of unmatched GALFORM galaxies, there are fewer unmatched SPH galaxies – and some or even all of these appear to be due to the sharp cutoff in cooling at redshifts $z > 1$. The unmatched GALFORM galaxies must therefore genuinely have no counterparts in the SPH simulation, and are the result of some difference between the models.

4.6.5   Improvements to the Semi-analytic Model

In the semi-analytic model, when a halo merges onto another more massive halo, any hot gas it contains is assumed to be stripped away so that no further cooling onto its central galaxy may occur. For consistency between the SPH simulation and the semi-analytic model, our halo finding algorithm should therefore consider two halos to be merged only when the merger has progressed to the point where the hot gas from the less massive halo is no longer able to cool. The massive, unmatched SPH galaxies noted above are present because this is not the case for the halo finding algorithm described in Section 4.3.2. This algorithm splits off subgroups which are only linked to the rest of the halo by particles which are not bound to any subgroup in the halo. In practice very few halos are split in this way (almost all of the particles are bound to some subgroup) and the resulting halo catalogues are extremely similar to the original friends of friends catalogues. Halos are usually considered merged as soon as member particles from each halo are within a linking length of each other. At this stage it is possible that the gas is not disturbed sufficiently to significantly affect cooling in the simulation. However, in the semi-analytic model this is exactly the point at which cooling onto the centre of the less massive halo is switched off.

In an attempt to alleviate this problem, and possibly eliminate some of the unmatched galaxies, we modify our halo finding algorithm. When two halos merge, they become subgroups within the resulting halo. The more massive of the two will become the most massive subgroup, which we consider to be the main halo. The other becomes a satellite subgroup and gradually loses mass to the main halo. We choose to regard these satellite subgroups as independent galaxies if they have retained some fraction, M_{frac}, of the mass they had at the last timestep where they were considered to be a separate halo. This means that a halo is not considered merged until some of its outer layers of dark matter are lost to the main halo, which might plausibly be around the same time at which its

hot gas begins to be stripped away to become part of the main halo. Such an approach is rather arbitrary and not rigorously justified, but it does provide a way to vary the instant at which halo mergers are deemed to have occurred in the semi-analytic model, allowing us to investigate whether this choice has a large effect on the resulting galaxy population.

Figure 4.11 shows how varying the parameter M_{frac} affects the comparison between the SPH and semi-analytic galaxies. From left to right the columns show results for semi-analytic models with M_{frac} set to 10, 0.75 and 0.5. Setting $M_{\mathrm{frac}} > 1$ prevents subhalos from being considered separate halos even if they have retained all of their original mass; the results obtained with $M_{\mathrm{frac}} = 10$ are identical to those shown in Figure 4.10 (with $N_{\mathrm{SPH}} = 100$) and are shown for comparison.

Reducing M_{frac} to 0.75 has several minor effects on the comparison between SPH and semi-analytic galaxies. Several GALFORM galaxies which are less massive than their SPH counterparts become slightly more massive, so that the overall level of agreement between the models is improved. This occurs because halo mergers are delayed slightly, which gives galaxies more time to accrete cooled gas before they become satellites in another halo.

Setting $M_{\mathrm{frac}} < 1$ also removes a couple of low mass, unmatched GALFORM galaxies. These are objects close to the minimum mass for cooling which, in the simulation, consist of two halos of similar mass in the process of merging. With $M_{\mathrm{frac}} > 1$, the semi-analytic model treats these binary objects as single halos which are just massive enough for cooling to occur. In the SPH simulation, the mass is really shared between two similar subhalos, neither of which is sufficiently well resolved for cooling to be effective. Reducing M_{frac} causes these objects to be treated as separate halos in the semi-analytic model. As in the simulation, these separate semi-analytic halos have insufficient mass for cooling at $z = 1$ and merge onto another, much more massive halo, before they are able to gain sufficient mass.

If M_{frac} is reduced to 0.5, the semi-analytic model is able to produce a counterpart to the most massive, otherwise unmatched, SPH galaxy. The halo where this galaxy formed merged onto the most massive halo in the simulation prior to the onset of cooling at $z = 1$ and consequently the galaxy was unable to form in the semi-analytic model. Delaying the merger allows cooling to occur and results in a galaxy of similar mass to the one seen in the simulation.

Overall, setting $M_{\mathrm{frac}} < 1$ does appear to improve agreement between the models, although the effects are not large. It appears that simply considering halos to be merged as soon as they are joined by the FOF algorithm (as we effectively do with $M_{\mathrm{frac}} > 1$)
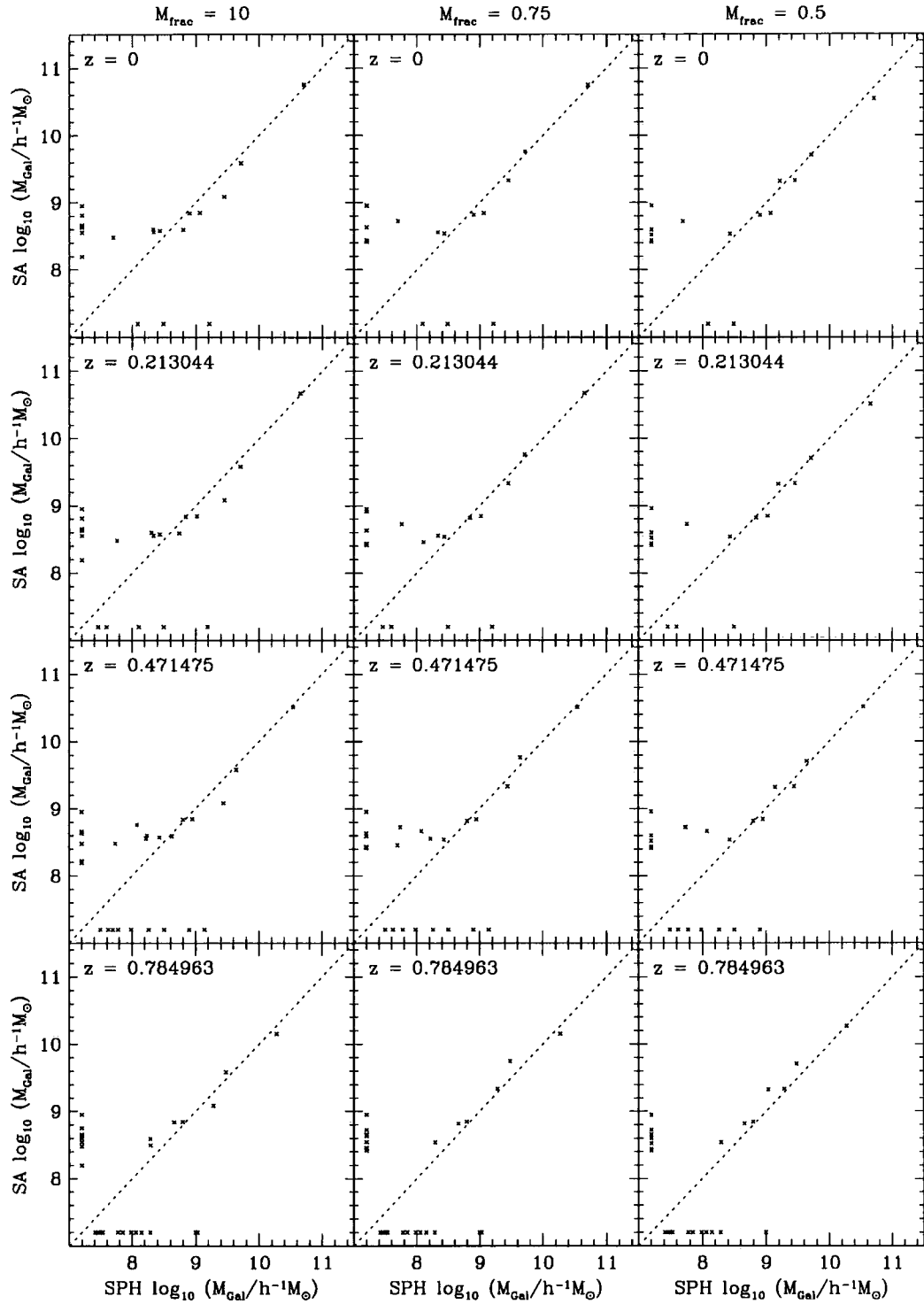
Figure 4.11: Effect of varying the parameter M_{frac} on the comparison between SPH and semi-analytic galaxy masses. Results for $M_{\text{frac}} = 10$ (left), 0.75 (middle) and 0.5 (right) are shown at four different redshifts. Galaxies are matched between the SPH and semi-analytic models using the method described in the text.

stops cooling onto satellite galaxies somewhat earlier in the semi-analytic model than in the simulation. This results in less massive, or even absent, semi-analytic galaxies and this is exacerbated by the sudden onset of cooling at $z = 1$.

4.7 Conclusions

In this Chapter we have compared a simplified, high resolution SPH simulation of the formation of a single galaxy to a similarly simplified semi-analytic model. We found the temperature and mass of the hot halo gas in the simulation prior to the onset of cooling to be approximately consistent with the assumptions used in the GALFORM model. We determined that the small difference in gas temperature between the simulation and the semi-analytic model had little or no effect on the mass of gas which cooled. It is not particularly surprising that the assumed temperatures and masses of hot halo gas are consistent with the simulation, since these assumptions were originally motivated by the results of non-radiative SPH simulations of galaxy clusters.

We developed an improved version of the N-body GALFORM semi-analytic model which allows a more direct comparison between the models than was possible previously. As well as taking halo merger histories from the SPH simulation, this model uses halo substructure information to determine when semi-analytic galaxies should merge. Galaxy masses in the SPH and semi-analytic models can then be compared on a galaxy by galaxy basis.

In poorly resolved halos, the SPH and semi-analytic models behave rather differently, since cooling in SPH becomes inefficient with small numbers of gas particles. We attempted to model the limited mass resolution of the simulation by preventing cooling in halos with fewer than $N_{\rm SPH}$ dark matter particles. Setting $N_{\rm SPH} = 100$ appeared to be the best compromise between removing unmatched semi-analytic galaxies and not preventing the formation of galaxies which *did* have SPH counterparts. However, there were still a number of (relatively low mass) semi-analytic galaxies in halos which contained no SPH galaxy. More sophisticated modelling of the SPH resolution limit may have helped to remove some of these.

There were also a few quite massive SPH galaxies which did not appear in the semi-analytic model. These were found to be due to a combination of the abrupt onset of cooling in the SPH simulation at $z = 1$ and the sudden cessation of cooling onto galaxies which had become satellites following a halo merger event. We attempted to solve this problem by changing the criteria for two halos to be considered merged. We found that by

delaying halo mergers (relative to the instant at which our original halo finding algorithm would have considered the halos to be merged) some of the previously unmatched SPH galaxies could now be matched. This also had a beneficial side effect - the agreement between SPH and GALFORM galaxy masses was slightly improved.

In summary, the SPH simulation and the improved N-body GALFORM model appear to be in good agreement in terms of the state of the hot halo gas in the absence of cooling and the rate at which gas cools onto individual galaxies. However, the physics included in these models is deliberately simplified in order to avoid the worst effects of limited resolution and the extra complication introduced by the addition of stellar feedback.

Chapter 5

Models with Star Formation and Feedback

5.1   Introduction

In the last Chapter, we considered an SPH simulation of the formation of a single galaxy which included only radiative cooling and star formation. This allowed us to investigate differences between SPH and semi-analytic treatments of the cooling of gas within dark matter halos without the extra uncertainty associated with feedback. Simplified simulations like this provide a useful way to gain understanding of particular aspects of the process of galaxy formation. However, the ultimate goal of any galaxy formation model must be to reproduce the population of galaxies seen in the real universe, and ideally predict observations which have yet to be made.

The latest simulations are now able to simultaneously resolve the detailed structure of galaxies and their cosmological context while including the additional physics required to produce realistic galaxies. This is achieved using the "zooming in" technique described in the previous Chapter along with numerical recipes for processes such as star formation, feedback and metal enrichment (e.g. Abadi et al. 2003, Governato et al. 2002, preprint (astro-ph/0207044), Sommer-Larsen et al. 2002).

Here, we examine a set of such simulations in which cooling is allowed at all times and recently formed stars inject energy (both kinetic and thermal) into nearby gas. This is intended to mimic the regulatory effect of supernovae on the rate at which gas is converted into stars. This scheme results in model galaxies which are very similar to observed galaxies in many respects.

These simulations are compared to a semi-analytic model similar to that of Chapter 4 which also includes stellar feedback. However, we make no attempt at first to tune the

semi-analytic feedback prescription to match the SPH algorithm. Instead, we adopt a standard prescription which is known to produce a population with realistic statistical properties when used to fill a large volume with semi-analytic galaxies (Benson et al. 2000). We then modify the semi-analytic model to reproduce the masses of the simulated galaxies, their satellites, and their progenitors as closely as possible. The size and nature of the changes required provide insight into the differences between the SPH simulations and the full semi-analytic model. This approach is intended to provide an indication of the uncertainties present in current numerical models of galaxy formation due to the poorly understood processes of star formation and feedback.

The rest of the Chapter is laid out as follows. In Section 5.2 we describe the SPH simulations. We compare these simulations with the full semi-analytic model in Section 5.3, and with a feedback-free model in Section 5.4. In Section 5.5 we use the semi-analytic model to predict the luminosity function which might be obtained if SPH simulations of many more galaxies could be carried out. We present our conclusions in Section 5.6.

5.2 The Simulations

The simulations used in this Chapter are a set of four SPH simulations of the formation of individual galaxies, provided by Julio Navarro and Mario Abadi. Two of these simulations (which we refer to here as KIA1 and KIA3) are described in detail by Abadi et al. (2003) and Meza et al. (2003).

The simulations were carried out with the GRAPESPH code (Steinmetz 1996), which computes gravitational interactions using specialised hardware. The physical processes modelled include gravitational and pressure forces, hydrodynamical shocks, Compton and radiative cooling, and heating by a photoionising UV background.

These models assume the ΛCDM cosmology with the following parameters: $\Omega_0 = 0.3$, $h = 0.65$, $\Omega_b = 0.019h^{-2}$, $\Lambda_0 = 0.7$ and $\sigma_8 = 0.9$. The dark matter halo containing each galaxy was picked from a simulation of a large volume, and then resimulated at high resolution using methods similar to those described in Chapter 4. However, these models are more realistic than the one we considered previously: cooling is allowed at all redshifts and stellar feedback is included.

Star formation is treated by allowing gas particles to form new star particles under certain conditions. Star particles are created in regions in which the gas is converging and Jeans unstable. The star formation rate, expressed in terms of mass of stars per unit

Name	$N_{\rm DM}$	$m_{\rm DM}/h^{-1}{\rm M}_\odot$	$N_{\rm gas}$	$m_{\rm gas}/h^{-1}{\rm M}_\odot$
KIA1	92 224	4.71×10^7	92 224	8.31×10^6
KIA2	104 768	1.21×10^7	104 768	2.14×10^6
KIA3	105 729	1.21×10^7	105 729	2.14×10^6
KIA5	129 856	1.21×10^7	129 856	2.14×10^6

Table 5.1: Initial numbers ($N_{\rm DM}$ and $N_{\rm gas}$) and masses ($m_{\rm DM}$ and $m_{\rm gas}$) of gas and dark matter particles in the high resolution regions of the four simulations.

volume per unit time, in such regions is given by:

$$\dot{\rho}_\star = \frac{c_\star \rho_{\rm gas}}{\max(\tau_{\rm cool}, \tau_{\rm dyn})} \tag{5.1}$$

where $\rho_{\rm gas}$ is the local gas density, $\tau_{\rm cool}$ and $\tau_{\rm dyn}$ are the cooling and dynamical timescales of the gas respectively, and $c_\star$ is a free parameter. Newly created star particles inject 10^{49} ergs of energy per solar mass of stars formed into the surrounding gas over a period of 3×10^7 years. Most of this energy is used to heat the surrounding gas, but a fraction ϵ_v adds to the kinetic energy of the gas. A similar scheme was used by (Navarro & White 1993). Metal enrichment is treated by assuming that stars contribute material enriched with $1.7{\rm M}_\odot$ of metals per $100{\rm M}_\odot$ of stars formed to the surrounding gas over the same period of time.

The numbers and masses of particles in the four simulations are shown in Table 5.2. Note that the number of gas particles shown here is only correct at early times, before the onset of star formation which gradually transforms gas particles into star particles.

By redshift $z = 0$, in all four simulations much of the gas has been converted into stars. There are 100 000–200 000 star particles in each simulation at this time, with mean masses of approximately $2.5 \times 10^6 h^{-1}{\rm M}_\odot$ (in the KIA1 simulation) and $6.5 \times 10^5 h^{-1}{\rm M}_\odot$ (in the KIA2, KIA3 and KIA5 simulations). There are 40-50 output times for each simulation between redshifts $z = 50$ and $z = 0$.

5.3 Comparison with the Full Semi-analytic Model

5.3.1 Description of the Full Semi-analytic Model

Since these simulations are intended to treat the formation of individual galaxies in as realistic a manner as current computational resources will allow and result in galaxies which resemble those seen in the real universe, we begin by comparing the simulations

to a semi-analytic model which reproduces the properties of the observed local galaxy population reasonably well.

The version of the N-body GALFORM semi-analytic model employed in this chapter is similar to that described in Chapter 4, but with cooling allowed at all redshifts and a feedback prescription included. As before, gas within dark matter halos is assumed to be shock heated to the virial temperature when the halo forms, and any gas which has had time to radiate away its energy and flow to the centre of the halo is added to the disk of the central galaxy. We assume that the gas density profile is given by Equation 2.2, and set the initial core radius $r^0_{core} = 0.66r_{NFW}$. We allow the core radius to increase to maintain the pressure at the virial radius. Cooling is allowed in all dark matter halos containing ten or more dark matter particles.

The merger tree for the dark matter halo of each galaxy is determined from the dark matter component of the simulation, and satellite galaxy positions and galaxy-galaxy mergers are determined using halo substructures. The techniques used to do this are identical to those presented in Chapter 4. We set the parameter M_{frac} in the halo finding algorithm to 0.75 so that halos are considered to merge somewhat later than the FOF algorithm would indicate. Previously, this appeared to slightly improve the level of agreement between the SPH and semi-analytic models, although the effect is not large.

For our initial comparison, we employ the same star formation and feedback prescriptions as in Chapter 2. See Section 2.3.2 for details.

5.3.2 Identifying Galaxies in the Simulation

We identify galaxies in the SPH simulation by applying the FOF algorithm to cool ($T < 10^5 K$) gas and star particles as in Chapter 4. However, in this case the masses of the gas and star particles are not equal, and the mass of an individual gas or star particle may vary over the course of the simulation. It is not immediately obvious whether FOF with a single linking length for all particles will correctly identify galaxies, or what an appropriate linking length would be.

For well resolved objects, the FOF algorithm approximately picks out regions enclosed by a surface of constant density. The linking length corresponding to a particular mass density depends on the cube root of the particle mass. Since the masses of the gas and star particles are generally of the same order of magnitude, this weak dependence of the linking length on the particle mass and the highly over-dense, well defined nature of the simulated galaxies, suggests that it may be reasonable to use a single linking length for

all of the cool gas and star particles.

We therefore use a linking length $b = 0.015$, in terms of the mean separation of gas particles before any star formation occurs, for all particles at all output times. We find that the masses of the resulting groups of particles are not particularly sensitive to the choice of linking length, although setting b to about 0.03 or greater causes the FOF algorithm to join galaxies which, by eye, are clearly separate objects.

5.3.3   Comparison Between the Models

We begin by comparing the total mass of galactic (ie. cold and dense) material in halos in the SPH simulations and the semi-analytic model. SPH galaxies are identified using the FOF algorithm as described above. An SPH galaxy is considered to be "in" a halo if a dark matter particle belonging to the halo is within a linking length ($b = 0.2$ in terms of the mean separation of dark matter particles) of its centre of mass. Only gas and star particles found to be in galaxies by the FOF algorithm are included in this comparison.

The thick lines in Fig. 5.1 show the total mass of the galaxies in the most massive progenitor halo of each of the four simulated galaxies as a function of redshift. The thick solid lines show total galaxy masses from the SPH simulation, and the thick dashed lines show the same quantity derived from the semi-analytic model. There is a much greater mass of galactic material present in the SPH simulation than in the semi-analytic model at redshift $z = 0$ — in all four cases the difference is about a factor of five or more. The difference between the two models is even larger if only the stellar mass (shown by the thin solid and thin dashed lines in the figure) is considered. At high redshifts ($z \simeq 4$) the difference in the total galactic mass is smaller, but there are far fewer stars in the semi-analytic model.

Since we know that the SPH and semi-analytic models generally cool similar quantities of gas (see Chapter 4), these differences must be due to the quite different implementations of star formation and feedback employed in the models. The semi-analytic feedback prescription appears to be much more effective at reheating cold gas and regulating star formation than the prescription used in the simulations. A smaller fraction of the cold, dense gas is converted into stars, and the overall mass of galaxies formed is smaller by almost an order of magnitude at low redshift. This is not entirely unexpected. Most of the energy released as a result of star formation in the simulation is used to increase the temperature of the surrounding gas. However, Navarro & Steinmetz (2000) note that simply injecting thermal energy into the gas is not an efficient way to regulate
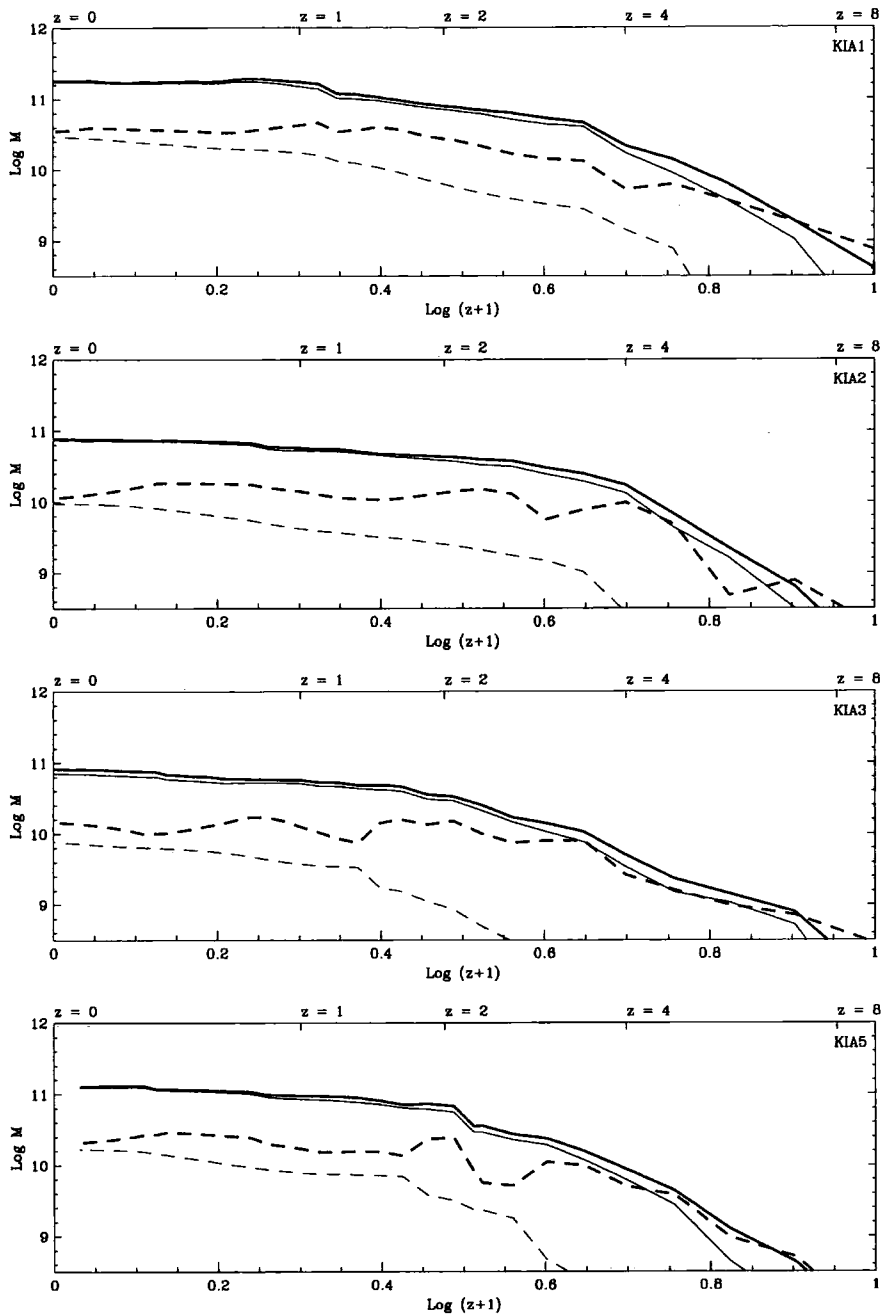
Figure 5.1: Mass of cold, dense gas and stars in the most massive progenitor halos of the four simulated galaxies (KIA1, KIA2, KIA3 and KIA5) as a function of redshift. The thin lines indicate the mass of stars present in the progenitor halos while the thicker lines show the total mass of cold, dense gas and stars. The unbroken lines show results from the SPH simulations, and the dashed lines correspond to the semi-analytic model with feedback included.

star formation in dense environments because the gas in such regions will be able to radiate the energy away almost immediately. Abadi et al. (2003), describing the feedback mechanism employed in the simulations used in this Chapter, say that while the small fraction ($\epsilon_v = 0.05$) of the feedback energy which is added to the kinetic energy of the nearby gas prevents rapid transformation of cold gas into stars, only a minor fraction of the cooled gas is returned to a diffuse, intergalactic state. Consequently, the total mass of material in galaxies in the simulation may be expected to be close to what would be found in the absence of feedback.
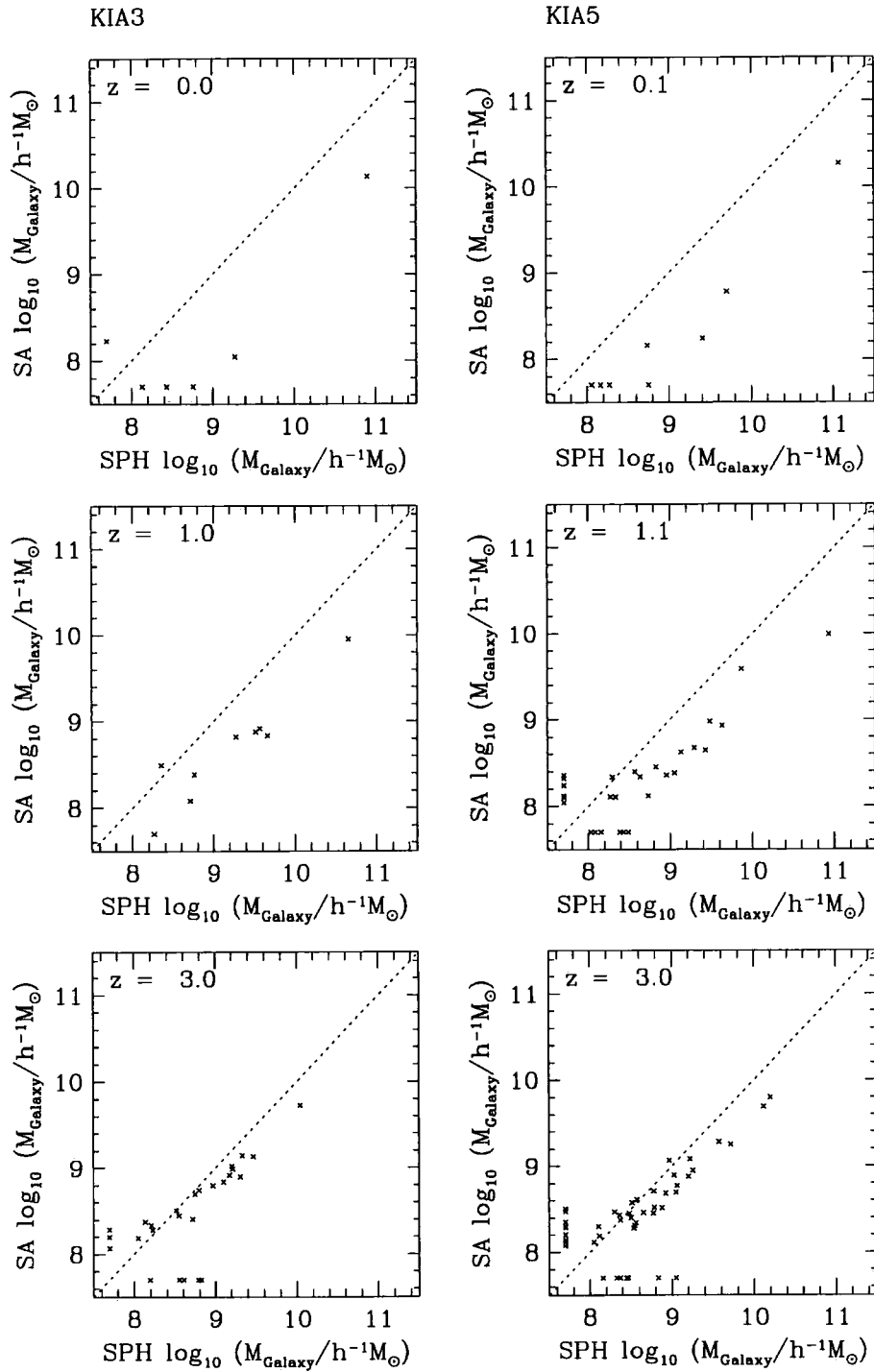
There are two possible explanations for the discrepancy seen in Fig. 5.1. The semi-analytic galaxies may simply be less massive than their SPH counterparts. Alternatively, in the SPH simulation galaxies may occur in halos where no semi-analytic galaxies are able to form. In order to investigate which of these is the case, we compare the masses of individual galaxies between the models and determine whether any galaxies exist in one model but not the other. Fig. 5.2(a) and Fig. 5.2(b) show the results of this comparison for the four simulations. The algorithm described in Section 4.6.3 is used to identify GALFORM galaxies with their SPH counterparts using only the positions of the galaxies. Galaxies present in the semi-analytic model which are not identified with any SPH galaxy are plotted close to the y axis. Galaxies present in the simulation which are not identified with any GALFORM galaxy are plotted close to the x axis. The top, middle and bottom panels in each column show the comparison at redshifts $z = 0$, $z = 1$ and $z = 3$ respectively, and each column shows results from one of the four simulations.

While there are a number of SPH galaxies without semi-analytic counterparts, these are almost all two orders of magnitude less massive than the main galaxy. The most notable exception is at $z = 0$ in the KIA1 simulation, where the second most massive SPH galaxy has no semi-analytic counterpart. This galaxy may have been produced by a merger between galaxies which formed in halos which, in the semi-analytic model, were of low enough mass that feedback prevented the creation of galaxies. The galaxies which are present in both models generally have much lower masses in the semi-analytic model than in the simulations, at least at lower redshifts. The difference is less pronounced, but still clearly present, at $z = 3$. Overall, it appears that the feedback prescription in the semi-analytic model is preventing the formation of small galaxies in low mass halos and greatly reducing the rate at which more massive galaxies can grow, whereas feedback in the simulation is having a much smaller effect on the galaxy masses.
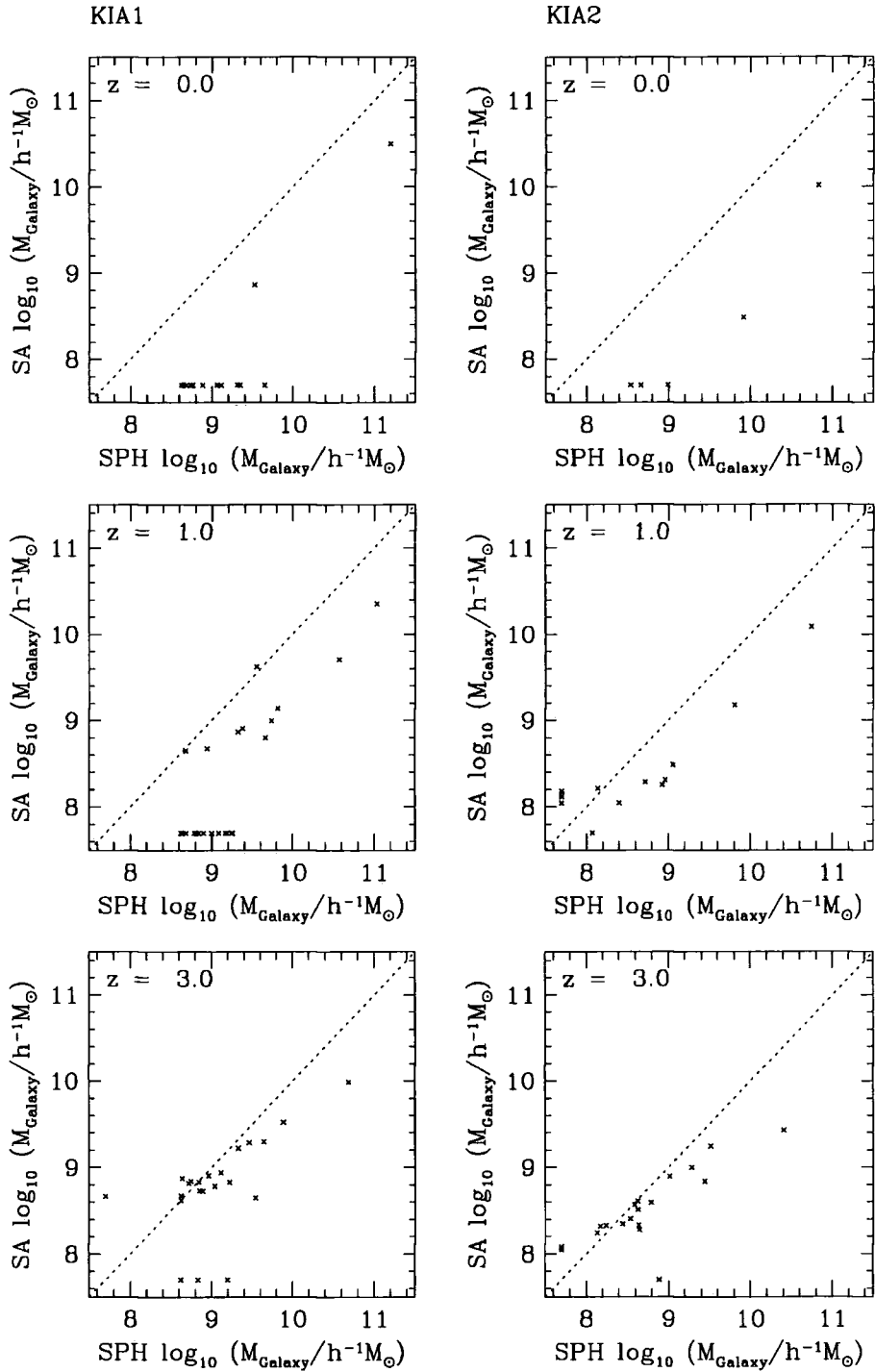
(a) KIA1 and KIA2 simulations

Figure 5.2: Comparison of galaxy masses between the SPH simulations and the full semi-analytic model. Galaxies are matched between the models using their positions only. The masses of galaxies appearing in one model but not the other are plotted as points close to the relevant axis. The top, middle and bottom panels show the comparison at redshifts $z = 0$, $z = 1$ and $z = 3$ respectively.

(b) KIA3 and KIA5 simulations

Figure 5.2: Comparison of galaxy masses between the SPH simulations and the full semi-analytic model (continued)

5.4   Comparison with a Stripped Down Semi-analytic Model

5.4.1   Description of the Model

If the differences seen in Section 5.3 are due to the relatively weak feedback prescription employed in the simulation, semi-analytic models with little or no feedback ought to more closely resemble the simulated galaxies. We now compare the SPH simulation with a semi-analytic model in which feedback is neglected entirely. This may initially appear difficult to justify: the addition of a portion of the supernova energy to the kinetic energy of nearby gas particles is intended to ensure that feedback remains effective even in the presence of efficient radiative cooling. However, as noted above, this type of feedback is primarily effective at preventing the rapid transformation of all available cold, dense, gas into stars. It does not appear to return large masses of galactic gas to the intergalactic medium (Abadi et al. 2003). It will therefore have little direct effect on the total masses of the simulated galaxies.

Feedback will, however, have an indirect effect on the rate at which gas cools through the metallicity of the diffuse halo gas. Recently formed star particles distribute a quantity of metals to their neighbouring gas particles. These particles will tend to be in dense regions where cooling is underway. Increased metallicity can significantly reduce the cooling time of hot gas and hence increase the masses of the resulting galaxies.

In the semi-analytic model, metals are added to the hot halo gas through the reheating of cold, galactic gas which has been enriched by supernovae. Removing feedback from the model ensures that no metals ever reach the hot halo gas. It is therefore necessary to artificially assign a metallicity to the gas so that the cooling rate is not unduly reduced. While it would be possible to carefully match the assigned metallicity to that observed in the simulation, we find that galaxy masses in the semi-analytic model are largely insensitive to the exact choice of metallicity.

If we assume a constant metallicity, Z, for the hot halo gas at all redshifts we obtain very similar galaxy masses for Z between $Z = 0.001Z_\odot$ and $Z = 0.1Z_\odot$, where $Z_\odot$ is solar metallicity. Lower metallicities than this cause a reduction in galaxy masses at redshifts below about three. At higher redshifts the galaxy masses are completely independent of metallicity. Perhaps surprisingly, assigning the hot gas solar metallicity reduces the masses of the most massive semi-analytic galaxies at low redshift by around 50%. This may be because increased cooling at earlier times reduces the mean density of gas in later halos and results in cooling times greater than the age of the halo.

In the analysis below, we set $Z = 0.01Z_\odot$ for all hot gas in the semi-analytic model at all redshifts. As before, we assume gas density profile which has an initial radius $r^0_{\rm core} = 0.66r_{\rm NFW}$. Again, the core radius increases as gas cools in order to maintain the pressure at the virial radius. Cooling is allowed only in halos with a mass of gas greater than $N_{\rm SPH}m_{\rm gas}$, where $m_{\rm gas}$ is the mass of a gas particle before any star formation occurs. In Chapter 4 we found this cooling model to be in reasonable agreement with a high resolution SPH galaxy simulation. This choice of density profile is also the same as that used in the full semi-analytic model of Section 5.3.

We set $N_{\rm SPH} = 75$, since this minimises the number of low mass unmatched semi-analytic galaxies without preventing the formation of semi-analytic galaxies which have counterparts in the SPH simulation. This is a small change from the cooling model used in Chapter 4 (which had $N_{\rm SPH} = 100$), but here we are using a different SPH implementation which may behave slightly differently in very poorly resolved halos. In any case, the choice of $N_{\rm SPH}$ has a negligible effect on galaxies which are not close to the resolution limit of the simulation.

Without feedback, the semi-analytic star formation rate has no effect on the masses of the model galaxies. It does however, affect their luminosities, which will be considered in Section 5.5.1. The star formation rate in the simulation is given by Eqn. 5.1. In the dense regions where stars are likely to form, it will usually be the case that $\tau_{\rm cool} < \tau_{\rm dyn}$ so that the star formation rate per unit mass is inversely proportional to the local dynamical time. In the semi-analytic model the star formation rate is given by:

$$\dot{M}_\star = \frac{M_{\rm cold}}{\tau_\star} \tag{5.2}$$

where $M_{\rm cold}$ is the mass of cold gas in the galactic disk and $\tau_\star$ is the star formation timescale. We may obtain a star formation timescale with a similar form to that used in the SPH simulation if we set

$$\tau_\star = \frac{t_{\rm disk}}{c_\star} \tag{5.3}$$

where $t_{\rm disk}$ is the dynamical time of the galactic disk.

The full semi-analytic model of Section 5.3 assumes that when stars form, a fraction, R, of the stellar mass is instantaneously recycled into the interstellar medium. However, in the simulation stars only return metals to the interstellar medium. We attempt to reproduce this behaviour in the semi-analytic model by setting the recycled mass fraction to $R = 0$ and the yield of metals per solar mass of stars formed, p, to 0.017 — each

$100M_\odot$ of stars formed in the simulation returns $1.7M_\odot$ of metals to the surrounding gas particles.

5.4.2   Comparison Between the Models

For each of the four galaxies, the thick lines in Fig. 5.3 show the total galactic mass in the most massive progenitor halo as a function of redshift, for both the semi-analytic model (dashed lines) and the SPH simulation (solid lines). The dashed and solid thin lines show the mass of stars present in each case.

This semi-analytic model is clearly in much closer agreement with the SPH simulation. For three of the four galaxies, the total mass agrees to within 50% at all redshifts. The exception is the KIA2 galaxy, which is significantly less massive at redshift $z = 2$ in the semi-analytic model than in the simulation. By redshift zero the difference has decreased somewhat.

The stellar masses are also in much better agreement. The star formation prescription in this semi-analytic model appears to convert almost all of the available gas into stars, and at low redshift this seems to be a fair approximation to what happens in the SPH simulations. At higher redshifts, the simulations contain more galactic gas than is present in the semi-analytic model. This is not a particularly significant result however. It may not be possible to find a semi-analytic star formation formula which is exactly equivalent to the particle-based SPH star formation algorithm, and, in the absence of feedback, the semi-analytic star formation rate may be adjusted arbitrarily without affecting the total galaxy masses.

The masses of individual galaxies in the SPH and semi-analytic models are compared in Fig. 5.4(a) (KIA1 and KIA2 simulations) and Fig. 5.4(b) (KIA3 and KIA5 simulations). GALFORM galaxies are identified with objects in the SPH simulations using their positions as before. Again, the level of agreement between the models is greatly improved. The masses of the semi-analytic galaxies have increased, and galaxies are now able to form in almost all locations where SPH galaxies are present. There are, however, a few semi-analytic galaxies close to the 75 particle threshold for cooling which are not matched to SPH galaxies. The formation of these objects was conveniently prevented by feedback in the full semi-analytic treatment, but they are most likely a consequence of the simplistic way in which we model the limited mass resolution of the simulation. It is perhaps not surprising that the behaviour of the SPH algorithm in poorly resolved halos cannot be exactly described by simply preventing cooling below some halo mass.
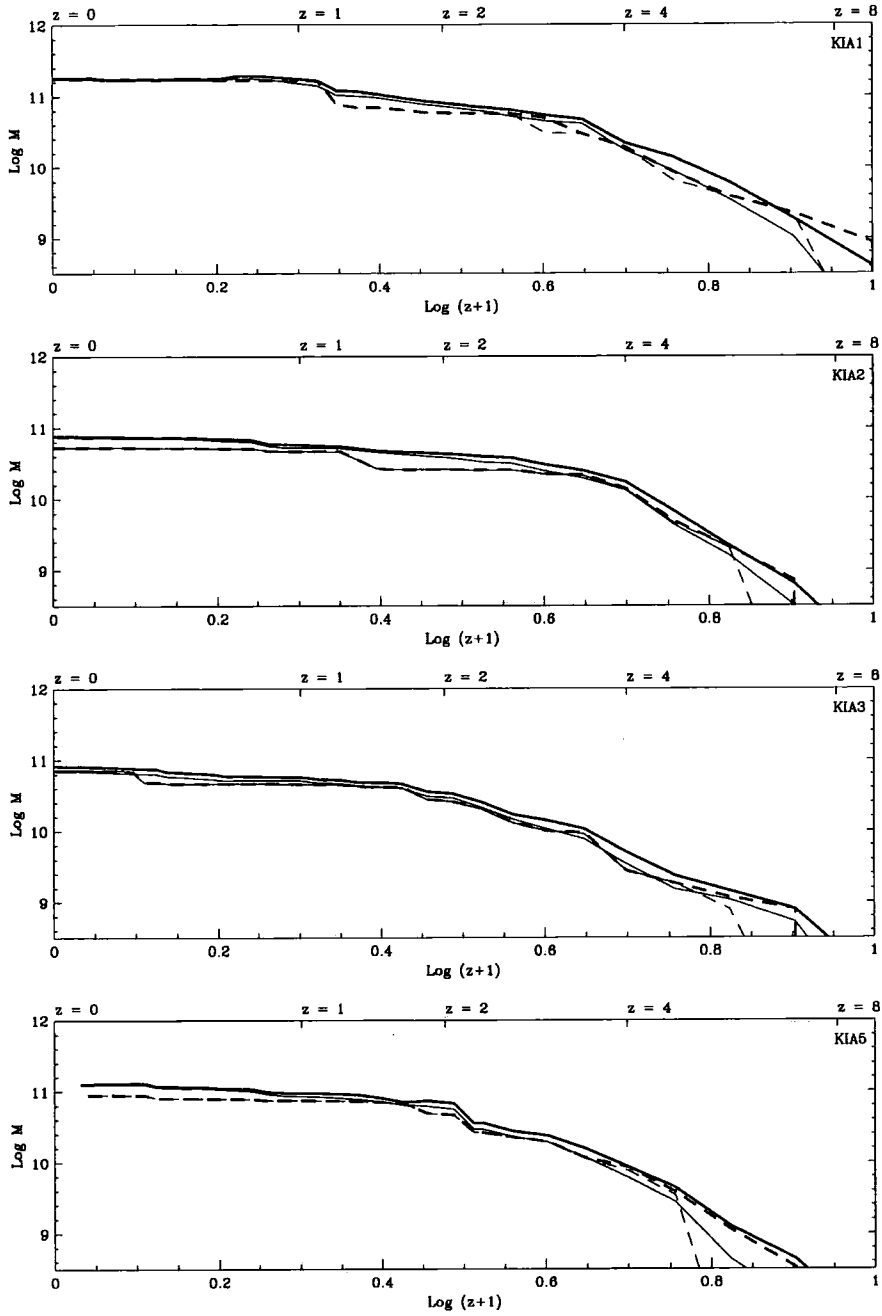
Figure 5.3: Mass of cold, dense gas and stars in the most massive progenitor halos of the four simulated galaxies (KIA1, KIA2, KIA3 and KIA5) as a function of redshift. The thin lines indicate the mass of stars present in the progenitor halos while the thicker lines show the total mass of cold, dense gas and stars. The unbroken lines show results from the SPH simulations, and the dashed lines correspond to the semi-analytic model with an increased star formation rate but without feedback.
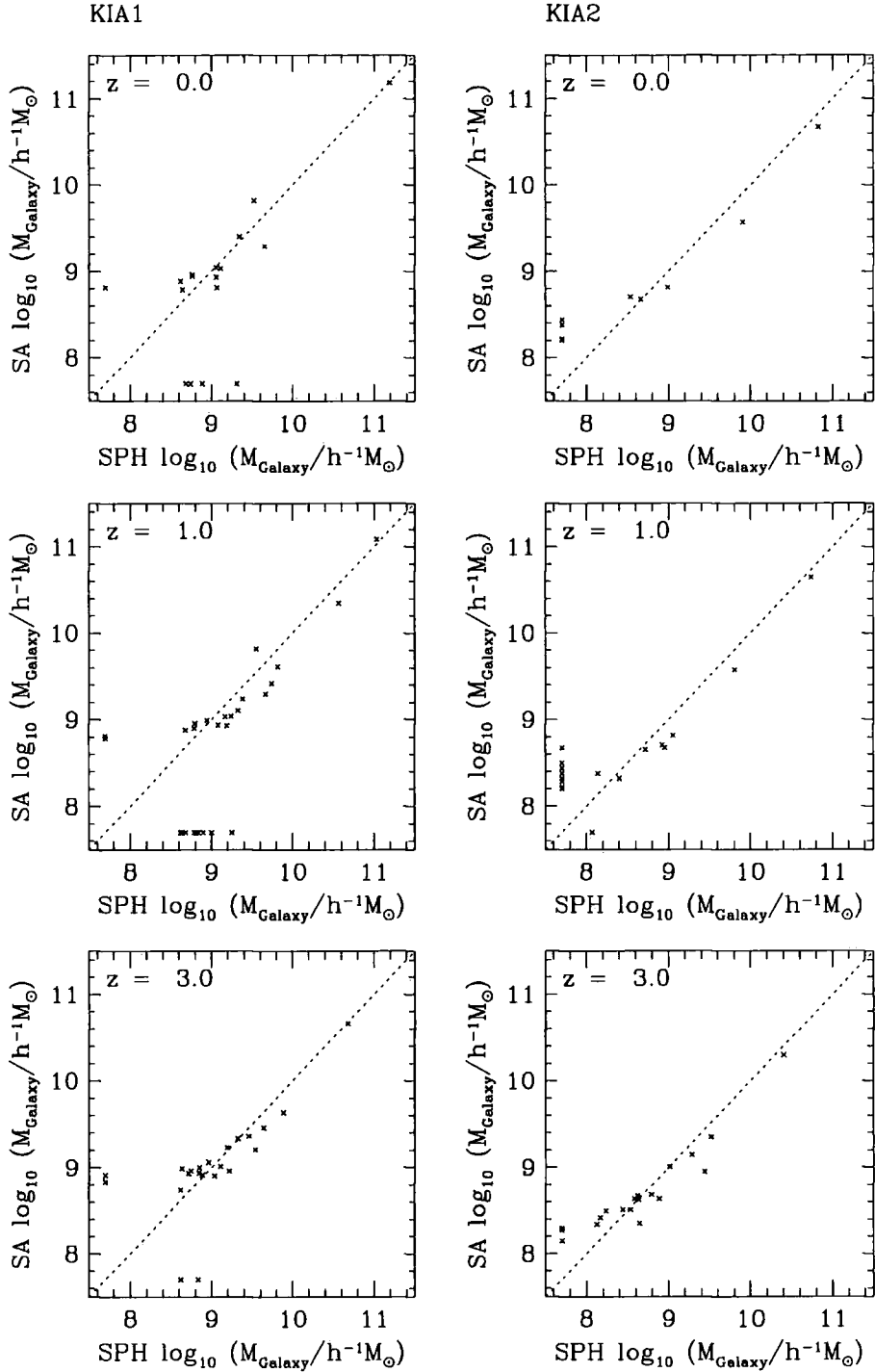
KIA1   KIA2

(a) KIA1 and KIA2 simulations

Figure 5.4: Comparison of galaxy masses between the SPH simulations and the stripped down semi-analytic model. Galaxies are matched between the models using their positions only. The masses of galaxies appearing in one model but not the other are plotted as points close to the relevant axis. The top, middle and bottom panels show the comparison at redshifts $z = 0$, $z = 1$ and $z = 3$ respectively.

(b) KIA3 and KIA5 simulations

Figure 5.4: Comparison of galaxy masses between the SPH simulations and the stripped down semi-analytic model (continued)

Galaxy masses in the SPH simulations are clearly more closely reproduced by a semi-analytic model without feedback. The differences between models with and without feedback are much greater than the small uncertainties due to our choice of metallicity, cooling threshold N_{SPH}, and FOF linking length used for galaxy identification. From the results presented in Chapter 4 we know that the semi-analytic and SPH treatments of cooling are in approximate agreement. The SPH feedback algorithm is therefore having little effect on the mass of material which is incorporated into galaxies.

5.4.3 Angular Momentum of the Model Galaxies

Abadi et al. (2003) show that the KIA3 SPH galaxy has significantly lower specific angular momentum than observed late type spirals with similar rotational velocities. It is suggested that significant changes to the star formation algorithm to prevent large quantities of stars forming at high redshift may be needed to reconcile the simulation with observations. The KIA5 galaxy suffers from the same problem.

For each galaxy, the stripped down semi-analytic model predicts the circular velocity and scale radius of the disk. We find that the semi-analytic versions of the KIA3 and KIA5 galaxies have much higher disk circular velocities and much smaller scale radii than the SPH simulations. The magnitudes of these differences are such that the semi-analytic disks appear to contain even less angular momentum than the simulated objects.

There are several possible reasons why the semi-analytic models may generate galaxies with quite different disk velocities from those found in the simulation. The semi-analytic model makes a number of assumptions in order to determine the angular momentum of the galactic disks. For example, it assumes that initially the angular momentum of the gas increases linearly with radius, that the angular momentum of collapsing halo gas is conserved, and that accretion of satellite galaxies in minor mergers does not affect the specific angular momentum of the galactic disk. These assumptions may not hold in the simulation.

Secondly, the angular momentum content of the SPH and semi-analytic model galaxies is sensitive to the feedback prescription used. Since the feedback in the KIA1-KIA5 galaxy simulations appears to have little effect on the mass of gas which collapses and forms stars, we have modelled the SPH simulations using a semi-analytic scheme which neglects feedback entirely. In terms of galaxy masses, this works very well. However, the SPH feedback implementation may be having some effect on galaxy angular momenta. For example, the small amount of material which *is* ejected may preferentially be that with

the lowest angular momentum.

Finally, the bulge to disk ratios of the SPH galaxies are not the same as those in the semi-analytic model. For example, the ratio of bulge luminosity to total luminosity of the KIA3 galaxy (in the b_J-band) is about 20% in the semi-analytic model and around 50% in the simulation. The circular velocity of the disk will depend on its mass as well as on the specific angular momentum of the gas which forms it.

The angular momenta, sizes and circular velocities of model disk galaxies pose significant problems. SPH simulations of galaxy formation typically have difficulty in reproducing observed disk sizes. The gas which collapses onto galaxies in these simulations generally does not retain its angular momentum, resulting in the formation of smaller disks than are observed (e.g. Navarro & Benz 1991, Navarro & White 1994, Steinmetz & Navarro 1999). Rapid cooling at early times creates a clumpy gas distribution in forming halos which allows angular momentum to be lost to the dark matter through dynamical friction.

Semi-analytic models are able to avoid this difficulty and produce more realistic disks by assuming that the specific angular momentum of the gas is conserved. The justification for this is that effective stellar feedback will maintain the intergalactic halo gas in a diffuse state, thereby greatly reducing the effects of dynamical friction. However, these models have difficulty in simultaneously matching the bright end of the luminosity function and the Tully-Fisher relation. This is a long standing problem in semi-analytic modelling of galaxy formation (e.g. White & Frenk 1991, Kauffmann et al. 1993, Cole et al. 1994, Heyl et al. 1995).

To investigate these issues, it would be useful to be able to directly compare the angular momenta of the SPH and semi-analytic galaxies. Differences between them could indicate unrealistic aspects of the SPH simulations or failures of the assumptions made in the semi-analytic model. In order to do this, semi-analytic dark matter halos would have to be assigned spin parameters consistent with the dark matter component of the simulation. The sensitivity of disk angular momenta to the feedback prescription used means that it would also be necessary to include much more sophisticated modelling of the SPH feedback algorithm in the semi-analytic model.

Given the simple nature of our attempt to model the SPH simulations using N-body GALFORM, it is not feasible to examine these issues here. This is, however, a possible direction for future work.

5.5 Simulating a Large Volume

We now use semi-analytic models incorporating the same modelling of cooling, star formation and feedback processes as those described in Sections 5.3 and 5.4 to simulate a representative volume of the universe and derive the statistical properties of the resulting galaxy populations. We will refer to the model including feedback as the Full Semi-Analytic (FSA) model, and to the model designed to better match the SPH simulations as the Stripped Down Semi-Analytic (SDSA) model.

Dark matter halo merger trees for these models are obtained using the same Monte Carlo algorithm as was used in Chapter 2. See Cole et al. (2000) for details. The minimum dark matter mass for a progenitor halo is set equal to ten times the mass of one high resolution dark matter particle from the KIA1 simulation. Realisations of halos on a grid of masses running from about 10^8 to $10^{15}h^{-1}M_\odot$ at redshift zero are generated and used to populate a volume of $10^6 h^{-3}\text{Mpc}^3$. The mass function determined from N-body simulations by Jenkins et al. (2001) is used to determine the number of halos required of each mass. Since no positional information is available for galaxies in these halos, galaxy-galaxy mergers are treated using the dynamical friction argument, also employed in Chapters 2 and 3 and described by Cole et al. (2000).

5.5.1 Luminosity Functions

Fig. 5.5 shows luminosity functions derived from the FSA model. This model is in fair agreement with observations of the local b_J-band (Zucca et al. 1997, Norberg et al. 2002, Ratcliffe et al. 1998, Loveday et al. 1992) and K-band (Glazebrook et al. 1995, Gardner et al. 1997, Mobasher et al. 1993, Cole et al. 2001) luminosity functions, when modelling of the effects of dust is included.

The dotted lines in Fig. 5.6 show the luminosity functions predicted by the SDSA model for a $10^6 h^{-3}\text{Mpc}^3$ volume. This model is much less successful at reproducing observed galaxy luminosities. In the b_J-band there are around an order of magnitude too many galaxies at very bright and very faint magnitudes. The model luminosity function approaches the observational data most closely at magnitudes of around -19, but even here there are twice as many galaxies as are seen in the real universe. The K-band luminosity function looks very similar, with too many galaxies at all luminosities and an excess of extremely bright objects. This is due to the transformation of almost all of the available baryons into stars in this model. If we improve the mass resolution of the model by
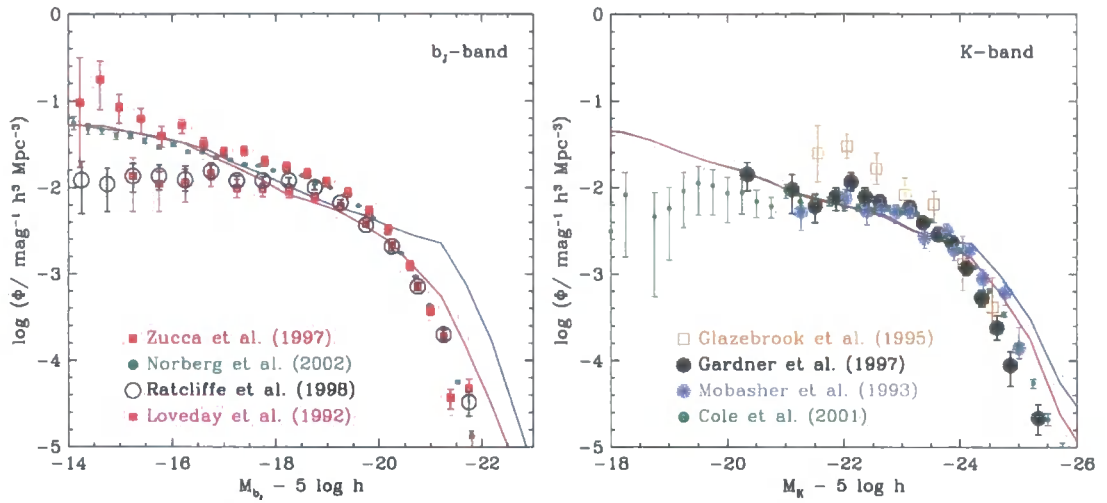
Figure 5.5: b$_J$ and K-band luminosity functions (left and right panels respectively), for the present day population of galaxies in a volume of $10^6 h^{-3} \text{Mpc}^3$ as predicted by the FSA model. The lines without error bars are output from the model. Model luminosity functions with and without a treatment of the effects of dust are included. Points with error bars are observational data.
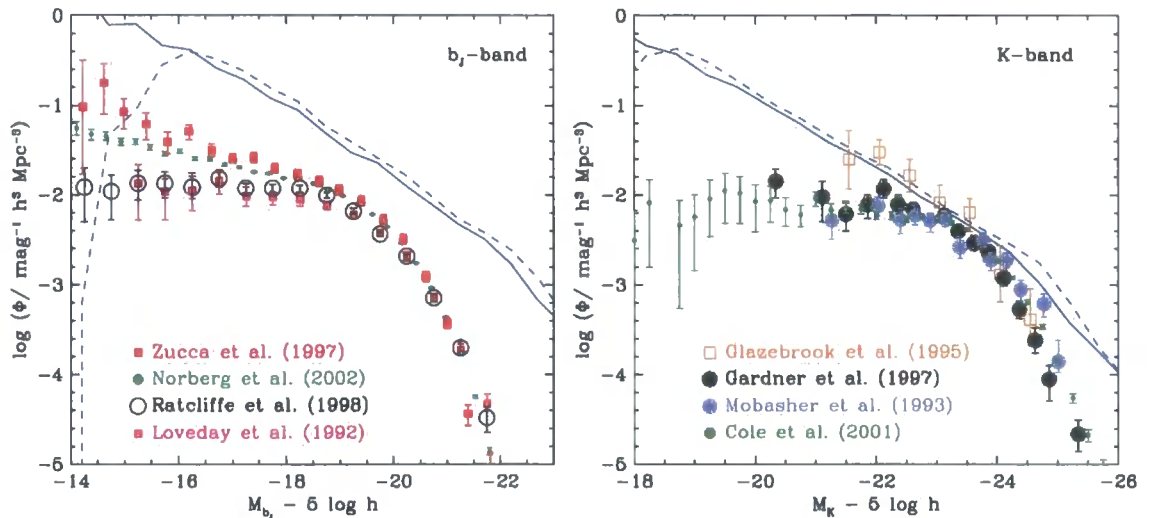
Figure 5.6: b$_J$ and K-band luminosity functions (left and top right respectively) for the present day population of galaxies in a volume of $10^6 h^{-3} \text{Mpc}^3$ as predicted by the SDSA model. The lines without error bars are output from the model. The solid and dashed lines correspond to models with $N_{\text{SPH}} = 10$ and $N_{\text{SPH}} = 75$ respectively. Dust extinction is not included. The same observational data as in Fig. 5.5 are shown here.

reducing the cooling threshold parameter, N_{SPH}, from 75 to 10, we find that marginally more faint galaxies are produced and the abundance of brighter objects falls slightly. This is not unexpected, because without feedback gas cools extremely rapidly in small halos at high redshift and the total mass of cooled material becomes dependent on the mass resolution of the calculation. Varying the mass resolution in this range has little effect on the full semi-analytic model because feedback inhibits the formation of galaxies in low mass halos.

From the results of Section 5.4, we know that the cooling and star formation prescriptions of the SDSA model reproduce the galaxy masses seen in the simulation much more closely than the prescriptions used in the FSA model. Fig. 5.6 therefore gives some indication of the luminosity function which would be obtained if sufficient computational resources were available to carry out SPH simulations of a large volume with the same mass resolution and model assumptions as the galaxy simulations we consider here.

This is something of an extrapolation of the semi-analytic model. The SDSA model contains halos at $z = 0$ with masses both much greater and much smaller than the four simulated halos against which the N-body GALFORM model has been tested. However, we find reasonable agreement with the SPH simulations in progenitor halos at redshifts $z > 0$, so the model may be expected to reproduce the behaviour of a large SPH simulation for the less massive halos. It cannot be guaranteed that this agreement extends to more massive halos such as clusters of galaxies, but such halos are less common and have a smaller influence on the overall galaxy luminosity function.

It seems reasonable to conclude that a large volume SPH simulation with the same star formation and feedback prescriptions as the KIA1-KIA5 galaxy simulations will convert halo gas into stars too efficiently and over predict the abundance of very faint and very bright galaxies.

5.6 Conclusions

In this Chapter we have examined four high resolution SPH simulations of the formation of individual galaxies. These simulations include plausible treatments of star formation and feedback and produce galaxies which strongly resemble galaxies seen in the real universe. The N-body GALFORM model was used to generate semi-analytic realisations of these galaxies using prescriptions for cooling, star formation and feedback which, when applied to a large volume, result in a population of galaxies with realistic statistical

properties. These properties include the local luminosity function, Tully-Fisher relation and distribution of disk sizes.

We find significant differences between these models. In the SPH simulations, almost all of the baryons in the dark matter halo of each galaxy are converted into stars, whereas in the semi-analytic model large amounts of hot halo gas remain at $z = 0$. The SPH feedback algorithm appears to have little effect on the rate at which gas is incorporated into galaxies.

We then carried out the same comparison with a similar semi-analytic model in which feedback was neglected entirely. The model was able to closely reproduce the masses of individual SPH galaxies and their progenitors at redshifts between $z = 0$ and $z \simeq 3$. There were uncertainties in this comparison due to the limited mass resolution of the simulation and choice of metallicity for the hot halo gas, but these were much smaller than the differences between models with and without feedback.

Two of the SPH simulations form disk galaxies. We found that these also formed disks in the feedback-free semi-analytic model, but with much higher circular velocities and smaller scale radii. Both the SPH and semi-analytic objects appear to have less angular momentum than observed disk galaxies. However, the angular momentum of the galaxies is sensitive to the feedback prescription employed. Simply neglecting feedback in the semi-analytic model closely reproduces the SPH galaxy masses, but a more sophisticated approach would be required to investigate the build up of angular momentum.

The semi-analytic model was then used to calculate the local galaxy luminosity function with and without feedback. In this case, halo merger histories were obtained using the Monte-Carlo algorithm of Cole et al. (2000). Without feedback, too many galaxies of all luminosities are formed. The discrepancy between model and observed luminosity functions is greatest at very bright and very faint magnitudes. This model uses the cooling and star formation prescriptions which most closely match the behaviour of the SPH simulations. It is therefore probable that if simulations similar to the KIA1-KIA5 simulations could be carried out in a much larger volume, the resulting galaxy luminosity function would be quite unrealistic.

Chapter 6

Conclusions

6.1 The N-body GALFORM Model

We have developed a semi-analytic galaxy formation model, N-body GALFORM, which uses the methods of Cole et al. (2000) to populate dark matter halos in an N-body simulation with semi-analytic galaxies. In this model, halo merger histories are determined from the simulation. We have shown that the galaxy populations predicted by this model closely resemble those predicted by the model of Cole et al. (2000) when the effects of limited mass resolution are accounted for. The remaining differences are due to the distribution of progenitor masses in the Monte-Carlo generated merger trees of the Cole et al. model, which does not agree exactly with the distribution found in N-body simulations.

6.2 Radiative Cooling in SPH and Semi-analytic Galaxy Formation Models

SPH and semi-analytic calculations of the mass of gas which cooled in dark matter halos in a $50^3 h^{-3} \mathrm{Mpc}^3$ simulation volume have been compared using the N-body GALFORM model. In order to simplify the problem, star formation was neglected. At redshift z=0, the cooled gas mass in well-resolved halos agreed remarkably well, and this agreement can be improved even further with minor changes to the semi–analytic cooling prescription. At high redshift, resolution effects in the simulation become increasingly important and, as a result, more gas cools in low mass halos in the SPH simulation than in the semi-analytic model. The cold gas mass function of individual galaxies in the two treatments at z=0 also agrees very well and, when the effects of mergers are accounted for, the masses of individual galaxies and their 2-point correlation functions are also in excellent agreement.

We have carried out a more detailed comparison between the N-body GALFORM model and a simplified, high resolution simulation of the formation of a single galaxy. While this simulation includes star formation, there is no attempt to model its effects on the remaining gas. In order to minimise resolution effects, radiative cooling is only allowed to

occur at redshifts $z < 1$. This prevents the formation of galaxies in very poorly resolved halos at high redshift, and allows us to investigate some of the assumptions made in the semi-analytic model regarding the state of the gas before any cooling occurs. We find that the temperature and mass of the gas in the simulated halos at $z = 1$ are approximately consistent with the assumptions of the semi-analytic model, at least for halos of more than around 100 particles.

We have examined the masses of individual galaxies in the SPH and semi-analytic models, and found that almost all of the well resolved galaxies present in one model also appear in the other with similar masses. One or two massive SPH galaxies without semi-analytic counterparts led us to explore the effect of varying the instant at which two halos are considered to have merged. This is important because, in the GALFORM model, the accretion of gas onto a galaxy ceases as soon as its parent halo merges with a more massive object. It was found that delaying the point at which this occurs improves agreement between the models by removing some unmatched galaxies and tightening the correlation between individual galaxy masses.

These results confirm and extend the earlier conclusions of Benson, Pearce, Frenk, Baugh & Jenkins (2001) that SPH simulations and semi-analytic models give consistent results for the evolution of cooling galactic gas. While Benson et al. were limited to a statistical comparison, we have been able to demonstrate that this agreement holds on a halo by halo and galaxy by galaxy basis. Our results, along with those of Yoshida et al. (2002), establish the combined N-body/semi-analytic approach as a viable, and less computationally intensive, alternative to full hydrodynamical simulations for some applications.

6.3 Comparison between Full SPH and Semi-analytic Models

We also carried out a comparison between the N-body GALFORM model and a set of much more realistic SPH simulations. Both the semi-analytic model and the SPH simulations included radiative cooling (at all redshifts), star formation, and feedback due to supernovae. The prescriptions used in the semi-analytic model were similar to those used by Cole et al. (2000), and result in a population of galaxies with a realistic luminosity function, Tully-Fisher relation, and distribution of disk sizes. The algorithms employed in SPH simulations of galaxy formation cannot be directly tested against this type of ob-

servational data, because it is not practical to simulate a large enough sample of galaxies with acceptable resolution. However, the star formation and feedback algorithms used in the hydrodynamic simulations we considered here have been shown to produce individual galaxies which bear a strong resemblance to observed galaxies — see, for example, Meza et al. (2003).

We were therefore directly comparing complete, state of the art SPH and semi-analytic models of galaxy formation in order to find differences due to our uncertain knowledge of the physical processes involved. This is in contrast to the previous Chapters, where we investigated different numerical treatments of a single, relatively well understood process, i.e. radiative cooling.

We have found that there are very significant differences between the SPH simulations and the N-body GALFORM model. The SPH galaxies are much more massive than those predicted to form in the same dark matter halos by the full semi-analytic model. This discrepancy must be due to the quite different star formation and feedback algorithms employed. In particular, we have confirmed that, unlike the semi-analytic feedback prescription, the SPH feedback scheme has little effect on the rate at which gas cools. Consequently, a semi-analytic model adjusted to reproduce the behaviour of the SPH simulations produces a luminosity function with a large excess of galaxies at very faint and very bright magnitudes.

6.4   Directions for Future Work

In this thesis we have shown that two currently popular numerical techniques used to treat the cooling of diffuse gas in dark matter halos give consistent results and are therefore likely to be reasonably reliable. We have also demonstrated that the dominant uncertainty in modern galaxy formation models is the treatment of star formation and feedback. This is clearly an area in which our understanding is far from complete.

The approach adopted in Chapter 5, of adapting the semi-analytic model to mimic an SPH simulation, could be used to provide an indication of the effect of various feedback schemes on SPH simulations of galaxy formation. The low computational cost associated with semi-analytic modelling would allow a more thorough investigation of the parameter space associated with each scheme. The ultimate aim of such an investigation would be to identify physically reasonable SPH star formation and feedback algorithms such that the properties of individual galaxies and the statistical properties of the model galaxy

population were both in agreement with observations. This is a necessary condition if the simulations are to reflect what happens in the real Universe. However, implementing equivalent star formation and feedback algorithms in both models would be a non-trivial task. Detailed comparisons such as those in Chapter 5 would be required to ascertain that the SPH and semi-analytic implementations genuinely were equivalent.

There are a number of assumptions in the GALFORM model relating to the build-up of angular momentum of the semi-analytic galaxies — for example, it is assumed that halo gas retains its angular momentum as it collapses and that this determines the size of the resulting disk. These assumptions are plausible, physically motivated and lead to realistic galaxy sizes. Nevertheless, they have still not been tested in detail. This is largely because the model could only be directly tested against hydrodynamic simulations, which can be unreliable in this respect due to numerical problems and the possible neglect of important physical processes. Indeed, in SPH galaxy simulations artificial angular momentum losses typically lead to the formation of galaxies with much smaller disks than are observed. Better understanding of such problems (see, for example, Sommer-Larsen & Dolgov 2001, Okamoto et al. 2003) may now make such a comparison worthwhile.

Finally, the combined N-body/semi-analytic approach provides a way to include a realistic population of galaxies with a wide range of known properties in N-body simulations of volumes large enough that full hydrodynamic calculations would be impractical. This technique could, for example, be applied to the "Millenium" simulation planned by the Virgo Consortium. Such a model could be tested against large galaxy redshift surveys such as the 2dF Galaxy Redshift Survey or the Sloan Digital Sky Survey. Detailed and realistic theoretical models of large volumes of the Universe will also be useful for testing the procedures used to analyse observational data.

Bibliography

Abadi M G, Navarro J F, Steinmetz M & Eke V R 2003 ApJ **591**, 499.

Barnes J & Efstathiou G 1987 ApJ **319**, 575.

Baugh C M, Benson A J, Cole S, Frenk C S & Lacey C G 1999 MNRAS **305**, L21.

Baugh C M, Cole S & Frenk C S 1996 MNRAS **283**, 1361.

Baugh C M, Cole S, Frenk C S & Lacey C G 1998 ApJ **498**, 504.

Bennett C L, Banday A J, Gorski K M, Hinshaw G, Jackson P, Keegstra P, Kogut A, Smoot G F, Wilkinson D T & Wright E L 1996 ApJ **464**, L1.

Bennett C L, Halpern M, Hinshaw G, Jarosik N, Kogut A, Limon M, Meyer S S, Page L, Spergel D N, Tucker G S, Wollack E, Wright E L, Barnes C, Greason M R, Hill R S, Komatsu E, Nolta M R, Odegard N, Peiris H V, Verde L & Weiland J L 2003 ApJS **148**, 1.

Benson A J, Cole S, Frenk C S, Baugh C M & Lacey C G 2000 MNRAS **311**, 793.

Benson A J, Frenk C S, Baugh C M, Cole S & Lacey C G 2001 MNRAS **327**, 1041.

Benson A J, Pearce F R, Frenk C S, Baugh C M & Jenkins A 2001 MNRAS **320**, 261.

Binney J 1977 ApJ **215**, 483.

Birkinshaw M 1979 MNRAS **187**, 847.

Bond J R, Cole S, Efstathiou G & Kaiser N 1991 ApJ **379**, 440.

Bond J R, Efstathiou G & Silk J 1980 *Physical Review Letters* **45**, 1980.

Bower R G 1991 MNRAS **248**, 332.

Bruzual A. G & Charlot S 1993 ApJ **405**, 538.

Burbidge E M, Burbidge G R, Fowler W A & Hoyle F 1957 *Reviews of Modern Physics* **29**, 547.

Cen R & Ostriker J P 2000 ApJ **538**, 83.

Cole S 1991 ApJ **367**, 45.

Cole S, Aragon-Salamanca A, Frenk C S, Navarro J F & Zepf S E 1994 MNRAS **271**, 781.

Cole S & Lacey C 1996 MNRAS **281**, 716.

Cole S, Lacey C G, Baugh C M & Frenk C S 2000 MNRAS **319**, 168.

Cole S, Norberg P, Baugh C M, Frenk C S, Bland-Hawthorn J, Bridges T, Cannon R, Colless M, Collins C, Couch W, Cross N, Dalton G, De Propris R, Driver S P, Efstathiou G, Ellis R S, Glazebrook K, Jackson C, Lahav O, Lewis I, Lumsden S, Maddox S, Madgwick D, Peacock J A, Peterson B A, Sutherland W & Taylor K 2001 MNRAS **326**, 255.

Colless M & the 2dFGRS team 2003, preprint (astro-ph/0306581).

Couchman H M P, Thomas P A & Pearce F R 1995 ApJ **452**, 797.

Davis M, Efstathiou G, Frenk C S & White S D M 1985 ApJ **292**, 371.

Eke V R, Cole S & Frenk C S 1996 MNRAS **282**, 263.

Eke V R, Navarro J F & Frenk C S 1998 ApJ **503**, 569.

Evrard A E & Henry J P 1991 ApJ **383**, 95.

Evrard A E, Summers F J & Davis M 1994 ApJ **422**, 11.

Faber S M & Gallagher J S 1979 ARA&A **17**, 135.

Ferrara A, Bianchi S, Cimatti A & Giovanardi C 1999 ApJS **123**, 437.

Freedman W L, Madore B F, Gibson B K, Ferrarese L, Kelson D D, Sakai S, Mould J R, Kennicutt R C, Ford H C, Graham J A, Huchra J P, Hughes S M G, Illingworth G D, Macri L M & Stetson P B 2001 ApJ **553**, 47.

Frenk C S, Evrard A E, White S D M & Summers F J 1996 ApJ **472**, 460.

Frenk C S, White S D M, Bode P, Bond J R, Bryan G L, Cen R, Couchman H M P, Evrard A E, Gnedin N, Jenkins A, Khokhlov A M, Klypin A, Navarro J F, Norman M L, Ostriker J P, Owen J M, Pearce F R, Pen U L, Steinmetz M, Thomas P A, Villumsen J V, Wadsley J W, Warren M S, Xu G & Yepes G 1999 ApJ **525**, 554.

Gardner J P, Sharples R M, Frenk C S & Carrasco B E 1997 ApJ **480**, L99.

Gingold R A & Monaghan J J 1977 MNRAS **181**, 375.

Glazebrook K, Peacock J A, Miller L & Collins C A 1995 MNRAS **275**, 169.

Governato F, Babul A, Quinn T, Tozzi P, Baugh C M, Katz N & Lake G 1999 MNRAS **307**, 949.

Governato F, Baugh C M, Frenk C S, Cole S, Lacey C G, Quinn T & Stadel J 1998 Nature **392**, 359.

Governato F, Mayer L, Wadsley J, Gardner J, Willman B, Hayashi E, Quinn T, Stadel J & Lake G 2002, preprint (astro-ph/0207044).

Gross M A K, Somerville R S, Primack J R, Holtzman J & Klypin A 1998 MNRAS **301**, 81.

Guth A H 1981 Phys. Rev. D **23**, 347.

Heyl J S, Cole S, Frenk C S & Navarro J F 1995 MNRAS **274**, 755.

Hubble E 1929 *Proceedings of the National Academy of Science* **15**, 168.

Hubble E P 1926 ApJ **64**, 321.

Jenkins A, Frenk C S, Pearce F R, Thomas P A, Colberg J M, White S D M, Couchman H M P, Peacock J A, Efstathiou G & Nelson A H 1998 ApJ **499**, 20.

Jenkins A, Frenk C S, White S D M, Colberg J M, Cole S, Evrard A E, Couchman H M P & Yoshida N 2001 MNRAS **321**, 372.

Katz N, Hernquist L & Weinberg D H 1992 ApJ **399**, L109.

Katz N, Keres D, Dave R & Weinberg D H 2003 *in* 'ASSL Vol. 281: The IGM/Galaxy Connection. The Distribution of Baryons at z=0' p. 185.

Katz N, Weinberg D H & Hernquist L 1996 ApJS **105**, 19.

Kauffmann G 1996 MNRAS **281**, 475.

Kauffmann G & Charlot S 1998 MNRAS **297**, L23.

Kauffmann G, Colberg J M, Diaferio A & White S D M 1999*a* MNRAS **303**, 188.

Kauffmann G, Colberg J M, Diaferio A & White S D M 1999*b* MNRAS **307**, 529.

Kauffmann G & Haehnelt M 2000 MNRAS **311**, 576.

Kauffmann G, Nusser A & Steinmetz M 1997 MNRAS **286**, 795.

Kauffmann G, White S D M & Guiderdoni B 1993 MNRAS **264**, 201.

Kay S T & Bower R G 1999 MNRAS **308**, 664.

Kennicutt R C 1983 ApJ **272**, 54.

Kennicutt R C 1998 ARA&A **36**, 189.

Kurki-Suonio H 2002 *Space Science Reviews* **100**, 249.

Lacey C, Baugh C, Frenk C, Cole S, Bressan S, Granato G & Silva L 2002 *Rev.Mex.AA Serie de Conferencias*, in preparation .

Lacey C & Cole S 1993 MNRAS **262**, 627.

Lacey C & Cole S 1994 MNRAS **271**, 676.

Lacey C & Silk J 1991 ApJ **381**, 14.

Lifshitz E 1946 *J.Phys. USSR* **10**, 116.

Loveday J, Peterson B A, Efstathiou G & Maddox S J 1992 ApJ **390**, 338.

Lucy L B 1977 AJ **82**, 1013.

Mather J C, Cheng E S, Cottingham D A, Eplee R E, Fixsen D J, Hewagama T, Isaacman R B, Jensen K A, Meyer S S, Noerdlinger P D, Read S M, Rosen L P, Shafer R A, Wright E L, Bennett C L, Boggess N W, Hauser M G, Kelsall T, Moseley S H, Silverberg R F, Smoot G F, Weiss R & Wilkinson D T 1994 ApJ **420**, 439.

Meza A, Navarro J F, Steinmetz M & Eke V R 2003 ApJ **590**, 619.

Mo H J & White S D M 2002 MNRAS **336**, 112.

Mobasher B, Sharples R M & Ellis R S 1993 MNRAS **263**, 560.

Navarro J F & Benz W 1991 ApJ **380**, 320.

Navarro J F, Frenk C S & White S D M 1995 MNRAS **275**, 720.

Navarro J F, Frenk C S & White S D M 1996 ApJ **462**, 563.

Navarro J F, Frenk C S & White S D M 1997 ApJ **490**, 493.

Navarro J F & Steinmetz M 2000 ApJ **538**, 477.

Navarro J F & White S D M 1993 MNRAS **265**, 271.

Navarro J F & White S D M 1994 MNRAS **267**, 401.

Norberg P, Cole S, Baugh C M, Frenk C S, Baldry I, Bland-Hawthorn J, Bridges T, Cannon R, Colless M, Collins C, Couch W, Cross N J G, Dalton G, De Propris R, Driver S P, Efstathiou G, Ellis R S, Glazebrook K, Jackson C, Lahav O, Lewis I, Lumsden S, Maddox S, Madgwick D, Peacock J A, Peterson B A, Sutherland W & Taylor K 2002 MNRAS **336**, 907.

Ofek E O & Maoz D 2003 ApJ **594**, 101.

Okamoto T, Jenkins A, Eke V R, Quilis V & Frenk C S 2003 MNRAS **345**, 429.

Pearce F R & Couchman H M P 1997 *New Astronomy* **2**, 411.

Pearce F R, Jenkins A, Frenk C S, Colberg J M, White S D M, Thomas P A, Couchman H M P, Peacock J A, Efstathiou G & The Virgo Consortium 1999 ApJ **521**, L99.

Pearce F R, Jenkins A, Frenk C S, White S D M, Thomas P A, Couchman H M P, Peacock J A & Efstathiou G 2001 MNRAS **326**, 649.

Press W H & Schechter P 1974 ApJ **187**, 425.

Ratcliffe A, Shanks T, Parker Q A & Fong R 1998 MNRAS **293**, 197.

Rees M J & Ostriker J P 1977 MNRAS **179**, 541.

Salpeter E E 1955 ApJ **121**, 161.

Schmidt B P, Kirshner R P & Eastman R G 1992 ApJ **395**, 366.

Sheth R K, Mo H J & Tormen G 2001 MNRAS **323**, 1.

Silk J 1977 ApJ **211**, 638.

Smith S 1936 ApJ **83**, 23.

Somerville R S & Primack J R 1999 MNRAS **310**, 1087.

Sommer-Larsen J & Dolgov A 2001 ApJ **551**, 608.

Sommer-Larsen J, Götz M & Portinari L 2002 Ap&SS **281**, 519.

Springel V & Hernquist L 2002 MNRAS **333**, 649.

Springel V, White S D M, Tormen G & Kauffmann G 2001 MNRAS **328**, 726.

Springel V, Yoshida N & White S D M 2001 *New Astronomy* **6**, 79.

Steinmetz M 1996 MNRAS **278**, 1005.

Steinmetz M & Muller E 1995 MNRAS **276**, 549.

Steinmetz M & Navarro J F 1999 ApJ **513**, 555.

Sutherland R S & Dopita M A 1993 ApJS **88**, 253.

Tonry J L, Schmidt B P, Barris B, Candia P, Challis P, Clocchiatti A, Coil A L, Filippenko
    A V, Garnavich P, Hogan C, Holland S T, Jha S, Kirshner R P, Krisciunas K,
    Leibundgut B, Li W, Matheson T, Phillips M M, Riess A G, Schommer R, Smith
    R C, Sollerman J, Spyromilio J, Stubbs C W & Suntzeff N B 2003 ApJ **594**, 1–24.

Tormen G 1997 MNRAS **290**, 411.

Tormen G 1998 MNRAS **297**, 648.

Tormen G, Bouchet F R & White S D M 1997 MNRAS **286**, 865.

Tully R B & Fisher J R 1977 A&A **54**, 661.

van Kampen E, Jimenez R & Peacock J A 1999 MNRAS **310**, 43.

Wagoner R V, Fowler W A & Hoyle F 1967 ApJ **148**, 3.

Warren M S, Quinn P J, Salmon J K & Zurek W H 1992 ApJ **399**, 405.

Wechsler R H, Somerville R S, Bullock J S, Kolatt T S, Primack J R, Blumenthal G R
    & Dekel A 2001 ApJ **554**, 85.

White S D M & Frenk C S 1991 ApJ **379**, 52.

White S D M, Frenk C S & Davis M 1983 ApJ **274**, L1.

White S D M, Frenk C S, Davis M & Efstathiou G 1987 ApJ **313**, 505.

White S D M & Rees M J 1978 MNRAS **183**, 341.

Wu K K S, Fabian A C & Nulsen P E J 2000 MNRAS **318**, 889.

Yoshida N, Stoehr F, Springel V & White S D M 2002 MNRAS **335**, 762.

Zucca E, Zamorani G, Vettolani G, Cappi A, Merighi R, Mignoli M, Stirpe G M, MacGillivray H, Collins C, Balkowski C, Cayatte V, Maurogordato S, Proust D, Chincarini G, Guzzo L, Maccagni D, Scaramella R, Blanchard A & Ramella M 1997 A&A **326**, 477.

Zwicky F 1933 *Helvetica Phys. Acta* **6**, 110.